NTNU – Trondheim
Norwegian University of
Science and Technology

Investigation of Fundamental Properties of Catalysts for Direct and Indirect Synthesis of DME

Kamilla Opheim Risa

Chemical Engineering and Biotechnology
Submission date: June 2014
Supervisor: Hilde Johnsen Venvik, IKP
Co-supervisor: Farbod Dadgar, IKP

Norwegian University of Science and Technology
Department of Chemical Engineering

Problem Statement

Dimethyl ether (DME), CH_3OCH_3, is the simplest ether and a possible clean and economical fuel for the future, with the characteristics of a sulfur free diesel fuel with low particulate emissions and high cetane number. The properties of DME are similar to those of LPG and it can hence be used for power generation as well as residential heating and cooking.

DME is currently produced in a two-step process; a methanol synthesis step followed by the methanol dehydration reaction. DME production directly from syngas is thermodynamically more favorable than from methanol and the direct DME synthesis should thus be more economic, provided a suitable catalyst is identified and combined with the appropriate reactor technology.

At NTNU, we have successfully applied so-called microstructured reactors with integrated heat exchange, for the direct synthesis of DME over physical mixtures of a Cu-based methanol synthesis catalysts and an acidic methanol dehydration catalyst (γ alumina, H-ZSM-5).

The aim of the project was originally to relate the activity and stability of different methanol synthesis and dehydration catalysts in separate reactions to the direct synthesis. However, the characterization of the acidic catalysts turned out to be very interesting and quite challenging. The aim of the project was therefore shifted to focus more on the characterization of catalysts relevant for direct DME synthesis, especially the acidic catalysts, than originally intended. The project is part of a collaboration with SINTEF Materials and Chemistry.

Declaration of Compliance

I declare that this is an independent work according to the exam regulations of the Norwegian University of Science and Technology (NTNU).

Place and date:

Trondheim, 16.6.2014

Signature:

Kamilla O. Rø

Sammendrag

Dimetyl eter (DME) har vist potensial som et miljøvennlig drivstoff. Den største fordelen med å bruke DME som drivstoff ligger i den rene forbrenningen; utslipp av sot og partikler, NO_x og SO_x er betraktelig redusert i forhold til utslipp forbundet med diesel forbrenning. DME blir i dag produsert via en to-stegs prosess der metanol syntese etterfølges av metanol dehydrering. DME produksjon fra syntesegass representerer en mer termodynamisk gunstig synteserute og burde derfor være mer økonomisk.

Katalysatorer som er relevant for DME produksjon har blitt undersøkt i denne oppgaven. Målet med prosjektet var å relatere aktiviteten og stabiliteten til relevante katalysatorer i separate reaksjoner til produksjon av DME direkte fra syntesegass. Karakterisering av syre egenskapene til dehydreringskatalysatorene ble imidlertid funnet å være veldig interessante og ganske krevende. Dette temaet ble derfor viet mer oppmerksomhet enn planlagt.

Noen av resultatene som er vist i denne oppgaven kommer fra et prosjekt med samme tema, som ble utført høsten 2013. Disse resultatene er inkludert i et forsøk på å presentere et så komplett bilde som mulig.

En $Cu/ZnO/Al_2O_3$ katalysator ble syntetisert, karakterisert og testet. Det ble funnet at natrium konsentrasjonen var langt høyere enn den tillatte grenseverdien. Høye konsentrasjoner av natrium kan forgifte katalysatoren og dermed påvirke katalysatorens aktivitet. Det faktum at høye natrium konsentrasjoner ble funnet, indikerer at katalysator-forløperen ikke ble vasket tilstrekkelig før tørking og kalsinering. Det er derfor sannsynlig at også nitrat-rester ble fjernet i utilstrekkelig grad. Nitrat-rester har blitt påvist til å promotere metall agglomerasjon under kalsinering. Dette kan i så fall ha påvirket både aktiviteten og stabiliteten til katalysatoren.

Både BET overflateareal og kobber dispersjon for den syntetiserte katalysatoren ble bestemt til å være lave sammenlignet med andre lignende katalysatorer. Den hjemmelagede katalysatoren viste også lav aktivitet, i tillegg til hurtig deaktivering, sammenlignet med den kommersielle katalysatoren. Metallpartikkel vekst kan forklare de lave overflatearealene, men også natrium kan være en faktor her. Både tilstedeværelsen av natrium og den lave dispersjonen er faktorer som kan forklare den lave aktiviteten. Metall agglomerasjon under kalsinering kan også ha ført til lav stabilitet, da inter-partikkel avstand har vist seg å være en viktig faktor for sintring.

Det er vanlig at kobberbaserte katalysatorer mister noe aktivitet i løpet av de første 1000 operasjonstimene på grunn av sintring. Den kommersielle katalysatoren ble observert til å kontinuerlig miste aktivitet i løpet av en tidsperiode på 14 dager. Temperatur profiler over katalysatorsjiktet, målt ved forskjellige tidspunkter, støttet opp under sintring som deaktiveringsmekanisme.

Kinetikken til metanol syntesen ble undersøkt ved å variere temperaturen i katalysatorsjiktet. Det ble observert at CO omsetningen økte som funksjon av temperaturen før omsetningen flatet ut nær likevektsomsetningen. Aktiveringsenergien ble bestemt til å være ca. 54 kJ/mol, i forholdsvis god overenstemmelse med litteraturen.

De sure dehydreringskatalysatorene ble karakterisert ved temperatur-programmert desorpsjon (TPD) med ammoniakk og/eller isopropylamin. Konsentrasjonen av sure punkter ble funnet til å være godt korrelert med innholdet av aluminium i zeolitt katalysatorene. Zeolittene ble funnet til å ha to hovedgrupper med sure punkter, i god overenstemmelse med litteratur. Bidrag fra både Brønsted- og Lewis-syre punkter ble funnet i begge gruppene med sure punkter.

Ion-utbyttete zeolitter ble syntetisert. Protoner assosiert med Brønsted-syre punkter ble forsøkt byttet ut med natrium, for å redusere konsentrasjonen av Brønsted-syre punkter. ICP-MS analyser ble utført for å bestemme i hvor stor grad protoner var byttet ut med natriumioner. Resultatene av disse analysene ble imidlertid sett bort fra, da resultatene ble ansett å være upålitelige.

Surheten til de ion-utbyttete zeolittene ble også undersøkt. To hoved grupper av sure punkter ble observert også for disse zeolittene. Selv om disse resultatene er noe usikre på grunn av den ukjente graden av ion-utbytting, så det ble funnet at natrium i hovedsak hadde erstattet protoner assosiert med sterke Brønsted-syre punkter. Dette er i god overenstemmelse med litteratur.

Adsorpsjonskalorimetri med ammoniakk ble også forsøkt for en av zeolitt katalysatorene. Det viste seg å være krevende å utvikle en god eksperimentell prosedyre for disse eksperimentene, men kvalitativt rimelige resultater ble oppnådd.

Abstract

Dimethyl ether (DME) has potential as an environmentally friendly fuel. The main advantage of DME as a fuel lies in its clean combustion; the emissions of soot and particulate matter, as well as NO_x and SO_x are significantly reduced compared to emissions from diesel combustion. DME is produced in a two-step process today, where methanol synthesis is followed by methanol dehydration. The production of DME directly from synthesis gas represents a more thermodynamically favorable synthesis route, and should thus be more economic.

In this thesis, catalysts relevant for DME production have been investigated. The goal of this project was to relate the activity and the stability of relevant catalysts in separate reactions to production of DME directly from synthesis gas. The acidity of the dehydration catalysts was however found to be very interesting, and quite challenging. The aim of the project was therefore shifted to focus more on catalyst characterization, especially the acidic catalysts, than originally intended.

Some of the results included in this thesis are taken from a project on the same topic, which was conducted during the fall of 2013. These results are included in an attempt to present a more complete picture.

A $Cu/ZnO/Al_2O_3$ catalyst was synthesized, characterized and tested. Both batches of catalyst were found to have sodium concentrations well above the acceptable limit. Sodium is considered a catalyst poison, which can affect the activity of the catalyst. The high concentration of sodium indicates that the catalyst precursor was insufficiently washed prior to drying and calcination. It is therefore likely that also nitrate residues were inadequately removed. Nitrate residues have been shown to promote metal agglomeration during calcination. Metal agglomeration may have affected both the activity and the stability of the catalyst.

Both the BET surface area and the copper dispersion of the synthesized catalyst were found to be low compared to similar catalysts. Low activity was observed, and the catalyst deactivated rapidly, compared to the commercial catalyst. Metal particle growth may explain the low BET surface area as well as the low dispersion, but sodium may also be a factor. Both the presence of sodium and the low dispersion of copper may explain the low activity of the catalyst. Metal agglomeration during calcination may also have led to the poor stability, as interparticle distance have been shown to be an important factor for sintering.

It is common for copper based catalysts to loose some activity during the first 1000 hours of operation due to sintering. The commercial catalyst was seen to continuously loose activity over a time period of 14 days. Temperature profiles of the catalyst bed measured at different points in time supported sintering as deactivation mechanism.

The kinetics of the methanol synthesis was investigated by varying the temperature of the catalyst bed. The CO conversion increased as a function of temperature

before it leveled off near the equilibrium conversion. The apparent activation energy was found to be about 54 kJ/mol, in reasonable agreement with literature.

The acidic dehydration catalysts were investigated by temperature-programmed desorption (TPD) with ammonia and/or isopropylamine. The acid site concentration was found to be well correlated with the aluminium content for the zeolites. The zeolites were found to have two main groups of acid sites, in good agreement with literature. Both groups of acid sites were found to have contributions of both Brønsted and Lewis acid sites.

Batches of ion-exchanged zeolites were prepared. Protons associated with Brønsted acid sites were attempted to be replaced with sodium ions, to reduce the amount of Brønsted acid sites. The zeolites were analyzed by ICP-MS to determine the extent of ion-exchange, but the results seemed unreliable and were therefore disregarded.

The acidity of the ion-exchanged zeolites was also investigated. Two main groups of acid sites were found also for these zeolites. Even though the results are somewhat uncertain due to the unknown extent of ion-exchange, it was found that sodium had predominantly replaced protons associated with strong Brønsted acid sites. This is in good agreement with literature.

Adsorption calorimetry with ammonia was attempted for one of the zeolites. Establishing the experimental protocol turned out to be challenging, but qualitatively reasonable results were achieved.

Preface

This master thesis was written as a continuation of the specialization project TKP4510 Catalysis and Petrochemistry, with the title 'Investigations into Catalysts Relevant for Dimethyl Ether Synthesis'. The specialization project and this thesis was written at the Department of Chemical Engineering at the Norwegian University of Science and Technology.

First of all I want to thank my supervisor Hilde J. Venvik for the helpful discussions and for guidance and encouragement. I also want to thank my co-supervisor Farbod Dadgar for assistance with laboratory work and helpful discussions. I am also grateful to Eleni Patanou for her help with the calorimetry setup and for enthusiastic discussions.

Finally I would like to thank Helge Rud Jordal, for his support and patience during these last few weeks.

Contents

Nomenclature

List of Abbreviations

BET	Brunauer-Emmet-Teller
DME	Dimethyl ether
FID	Flame ionization detector
GC	Gas chromatograph
H-ZSM-5 Y	Hydrogen form of ZSM-5, molar $SiO_2 : Al_2O_3$ ratio Y
ICP	Inductively coupled plasma
IR	Infrared spectrometry
LNG	Liquefied natural gas
LPG	Liquefied petroleum gas
MAS	Magic spinning angle
MFC	Mass flow controller
MS	Mass spectrometry
Na(X),H-ZSM-5	ZSM-5 with X % exchange of hydrogen with sodium
NMR	Nuclear magnetic resonance
NO_x	Nitrogen oxides
PFD	Process flow diagram
SO_x	Sulphur oxides
syngas	Synthesis gas
TCD	Thermal conductivity detector
TGA	Thermogravimetric analysis
TOF	Turnover frequency
TPD	Temperature-programmed desorption
UOP	Universal Oil Products
WABT	Weighted average bed temperature
XRD	X-ray diffraction

List of Figures

List of Tables

Chapter 1

Introduction

The world's energy demand is expected to continue to increase as the world's population grows, and as developing countries improve their standard of living. At the same time, there is increasing focus on reducing emissions and being more environmentally friendly.

Dimethyl ether (DME) is a colorless, non-toxic and non-carcinogenic gas which is receiving attention as a more environmentally friendly fuel [1, 2, 3], even though its use does not necessarily imply a reduction in CO_2 emissions. The benefits of DME includes low emissions of soot and particulate matter, NO_x and SO_x [1, 2, 4, 5, 6]. Additionally, DME can be produced from biomass derived synthesis gas [1]. Biomass is a sustainable resource, provided that the biomass is renewed. Moreover, biomass can be considered a carbon neutral energy resource, if sustainable harvesting is ensured [7, 8].

DME is primarily used as an aerosol propellant today, but it can potentially be used in many other applications due to its similarity to liquefied petroleum gas (LPG) [1, 2, 9]. Applications include fuel (diesel engines), power production, residential heating and cooking (town gas) and fuel cells [1, 10, 11].

DME can be used as a substitution to diesel because of its high cetane number [1, 5, 6]. Challenges related to using DME as a fuel in diesel engines are related to the physical properties of DME; DME has poor lubrication characteristics and low viscosity which increases the wear on the engine. Additionally, a larger fuel tank is probably needed since DME is less dense than diesel [1, 5].

DME is also an interesting alternative to liquefied natural gas (LNG), as DME can be distributed and stored using the same kind of technology as for LPG, due to its similar physical properties [12]. The need for costly LNG tanker and terminals can therefore be eliminated [2, 12]. An analysis conducted by Kikkawa & Aioki [12], showed that DME is more economical favorable than LNG for transportation distances greater than 5000 - 7000 km.

The conventional method for DME production today is a two-step technology, which involves a methanol synthesis step followed by a methanol dehydration step [1]. An alternative to this synthesis route is to produce DME directly from synthesis gas [1, 2, 6, 13]. Producing DME directly from synthesis gas has two major advantages; the first advantage is higher carbon conversion per pass, due to an equilibrium shift in the methanol synthesis. The other advantage of direct synthesis of DME is a simplified process and a greater flexibility in syngas composition, meaning that syngas derived from coal or biomass can be used more easily.

The catalyst system used for direct synthesis of DME consists of a methanol synthesis function, and a methanol dehydration function. The two catalytically active sites may be combined in a number of different ways. The simplest and most common approach is to physically mix a methanol synthesis catalyst with a methanol dehydration catalyst [1, 14]. The acidic methanol dehydration catalyst has received much attention lately, as it is not yet known how the acidity of the catalyst affects the activity.

The aim of this project work was originally to relate the activity and stability of the relevant catalysts in separate reactions to direct DME synthesis. The focus was however split into two areas; one area focusing on the methanol synthesis and the $Cu/ZnO/Al_2O_3$ catalyst, and one area focused on the modification and the characterization of acidity in the methanol dehydration catalysts. Modification of zeolite acidity by ion-exchange, and temperature-programmed desorption experiments, were performed as a collaboration between my co-supervisor, F. Dadgar and myself.

This project was a collaboration with SINTEF Materials and Chemistry, and is a continuation of the specialization project, TKP4510, conducted during the fall of 2013. For this reason, some of the results obtained in the specialization project are included in this thesis, in order to present a more complete picture.

Chapter 2

Theory and Background Information

The first two sections of this chapter include theory and background information related to the indirect and direct synthesis of DME, and the catalysts involved. Zeolites are treated in detail in section 2.3, while section 2.4 contains theory and background information regarding characterization methods.

2.1 Indirect Synthesis of Dimethyl Ether

The indirect synthesis of DME is the more conventional route today [1]. The indirect synthesis proceeds via two steps; methanol synthesis from synthesis gas (syngas) followed by methanol dehydration. The production capacity of the plant is rather low for this synthesis route. The results is a fairly high price, making DME less than ideal as a fuel [1].

2.1.1 Methanol Synthesis

Large-scale methanol synthesis is an established industrial process with a long history [1]. Nevertheless, there are still challenges related to this process [15]. The thermodynamics of the reaction favors low temperatures, so developing a catalyst that is active at low temperature is of great interest [15, 16]. Furthermore, the thermal stability of the copper particles on the catalyst is an important issue; even though the catalyst lifetime is about 3-4 years in large-scale plants, about one third of the activity is lost during the first 1000 hours of operation due to sintering of the copper particles [15].

The following reactions are involved in methanol synthesis:

$$CO_2 + 3H_2 \rightleftharpoons CH_3OH + H_2O \tag{2.1a}$$
$$CO + H_2O \rightleftharpoons CO_2 + H_2 \tag{2.1b}$$
$$CO + 2H_2 \rightleftharpoons CH_3OH \tag{2.1c}$$

Note that these three reactions are not independent, reaction 2.1c can be considered as a combination of 2.1a and the water gas shift reaction, 2.1b. All three reactions are exothermic, and reaction 2.1c and 2.1a involves a reduction in the number of molecules. The methanol synthesis is thus favored by low temperature and high pressure. The effect of temperature and pressure on the equilibrium conversion of CO in methanol synthesis is illustrated in figure 2.1. The temperature and pressure dependency presented in figure 2.1 is for a syngas composition with H_2:CO ratio of 2.

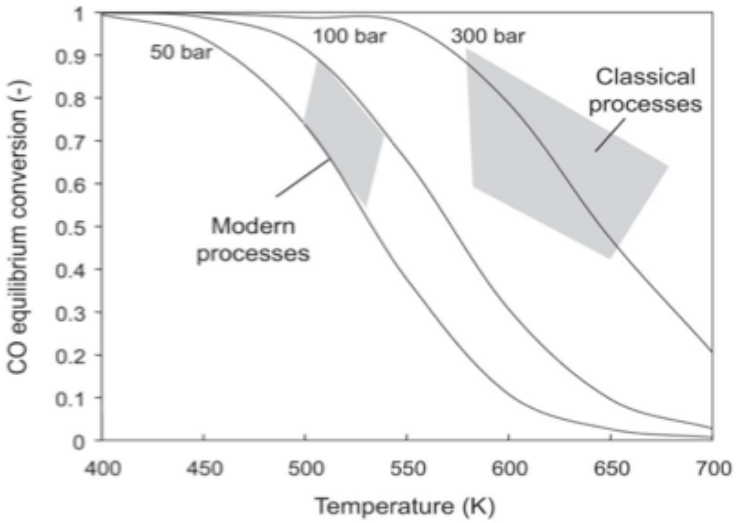

Figure 2.1: *Equilibrium CO conversion in methanol synthesis based on hydrogenation of CO to form methanol and the water-gas-shift reaction, taken from [16]. The curves show the equilibrium CO conversion as a function of temperature and pressure for syngas with H_2:CO = 2*

The CO conversion is also dependent on the composition of the syngas. The optimum syngas composition is found to be: $M = {}^{(H_2 - CO_2)}/_{(CO + CO_2)} \approx 2$ [15]. Typical process conditions of the methanol synthesis today are moderate pressure (50 - 100 bar) and low temperature (500 - 540 K) [16].

Catalyst selectivity is a key issue for methanol synthesis, as there are many possible side reactions [15, 16, 17]. The most commonly applied catalyst today is the Cu/ZnO catalyst supported on alumina [1, 15]. The selectivity of this catalyst is

over 99 % [16]. There is some controversy related to the role of ZnO in the catalyst [18]. Some researches claim that ZnO acts only as a support for the copper particles, as a linear relationship between copper surface area and methanol synthesis activity has been shown. On the other hand, some researchers claim that Zn may act as a chemical promoter by stabilizing the active Cu^+ sites [18, 19, 20].

The original catalyst for methanol synthesis was a $ZnO - Cr_2O_3$ system which was only active at high pressure. This catalyst was in use until the late 1960s, even though more active catalysts had been identified. These catalysts were not used due to their vulnerability to poisons such as sulfur present in the syngas feed [16]. Sodium acts as a catalyst poison for the Cu/ZnO catalyst used today [20].

The most common synthesis procedure for the catalyst used today is coprecipitation using metal nitrates and an alkaline agent such as $NaCO_3$. As the presence of nitrate residues during calcination is assumed to promote metal agglomeration, and since sodium is considered a catalyst poison, it is crucial to wash the catalyst precursor extensively to remove nitrate residues and sodium [20].

As mentioned previously, the assumed deactivation mechanism for the $Cu/ZnO/Al_2O_3$ catalyst is sintering. Both Cu particle size distribution and interparticle spacing is thought to affect the rate of sintering. Equally sized particles with maximal interparticle distance have been shown to drastically reduce the rate of deactivation for Cu/ZnO catalysts supported on silica [19].

The mechanism for methanol synthesis is quite complicated as several reactions are involved and coupled, and it has been an issue subjected to extensive discussion. The core of the discussion is whether methanol is formed by CO or by CO_2. Today there is an agreement that methanol is mainly formed from CO_2 over copper based catalyst systems under industrial conditions [15, 17]. Vanden Bussche and Froment [21] proposed a steady-state kinetic model for methanol synthesis and the water gas shift reaction that is presented in equation 2.3 below. This model is based on the assumption that the main source of carbon in methanol is from carbon dioxide as presented in equation 2.2.

$$CO + H_2O \rightleftharpoons CO_2 + H_2 \rightleftharpoons CH_3OH + H_2O \tag{2.2}$$

$$r_{MeOH} = K' \cdot p_{CO_2} \cdot p_{H_2} \cdot \left(1 - K'' \cdot \frac{p_{H_2O} \cdot p_{CH_3OH}}{p_{H_2}^3 \cdot p_{CO_2}}\right) \beta \tag{2.3}$$

The K' and K" represents the reaction constants and equilibrium constants of the various elementary reactions involved. The kinetic model is quite complicated, but it is clear that the reaction rate is affected by both the partial pressure of CO_2, H_2 and CH_3OH. Note that the reaction rate is not affected by CO concentration.

2.1.2 Methanol Dehydration

The methanol dehydration process has been applied industrially for several years. The process is quite simple and requires low capital investments [1]. Companies like Haldor Topsøe, Lurgi and Mitsubshi Gas Chemical offers technology for DME production from methanol [1].

The overall reaction for methanol dehydration is given in equation 2.4 below:

$$2CH_3OH \rightarrow CH_3OCH_3 + H_2O \tag{2.4}$$

This reaction is slightly exothermic and requires an acidic catalyst. The most common catalysts are γ alumina and the ZSM-5 zeolite. Typical process conditions are low pressure, 10 - 25 bar, and low temperature, 250 °C [1].

2.2 Direct Synthesis of DME

It is possible to produce DME directly from synthesis gas. The reactions involved are 2.1 and 2.4 as shown below [1, 6, 14]:

$$\begin{aligned} CO + 2H_2 &\rightleftharpoons CH_3OH \\ CO_2 + 3H_2 &\rightleftharpoons CH_3OH + H_2O \\ 2CH_3OH &\rightleftharpoons CH_3OCH_3 + H_2O \\ H_2O + CO &\rightleftharpoons H_2 + CO_2 \end{aligned}$$

The overall reactions are as shown in equation 2.6 [1]:

$$3CO + 3H_2 \rightleftharpoons CH_3OCH_3 + CO_2 \tag{2.6a}$$
$$2CO + 4H_2 \rightleftharpoons CH_3OCH_3 + H_2O \tag{2.6b}$$

This synthesis route is more attractive both economically and thermodynamically speaking [1, 4, 6, 13, 22]. In the indirect synthesis route, the conversion of syngas to methanol is limited by the thermodynamic equilibrium, thus requiring high pressure and low temperature to achieve a reasonable per-pass CO conversion. When the methanol synthesis and methanol dehydration reactions are combined in the same reactor, a synergistic effect arises; methanol formed by reactions 2.1c and 2.1a are consumed by reaction 2.4, shifting the equilibrium to the right and allowing for a higher per-pass CO conversion. In addition, the water formed by reaction 2.1a and 2.4, shifts the equilibrium of the water-gas-shift reaction towards producing more H_2 and CO_2 [1, 2, 6, 13]. This effect is illustrated in figure 2.2, taken from [2].

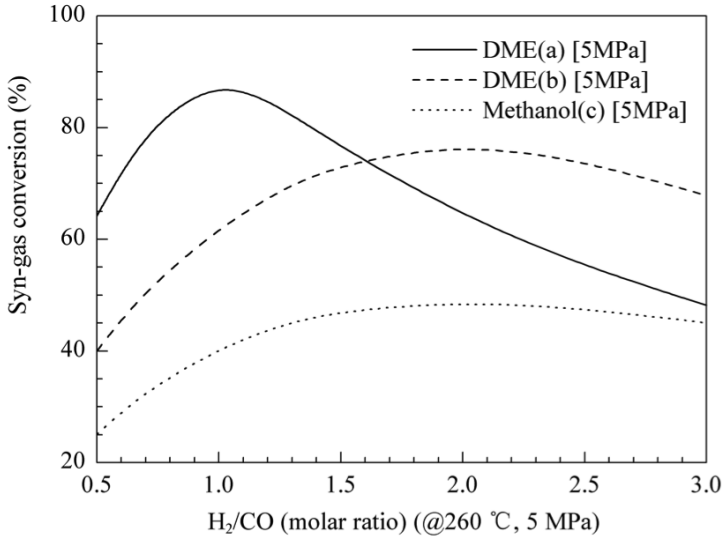

Figure 2.2: *Syngas conversion in methanol synthesis and direct synthesis of DME, taken from [2]. (a) represents the overall reaction given in equation 2.6a while (b) represents the overall reaction given in equation 2.6b*

It is clearly seen that the syngas conversion is significantly higher in the direct synthesis of DME, curve (a) and (b), compared to methanol synthesis, curve (c).

Research into the direct DME synthesis is still ongoing, but most groups reports process conditions of low temperatures and medium pressure, typically 250 - 260 °C and 40 - 50 bar [6, 10, 13, 22].

The catalyst system used for direct DME synthesis must have active sites for methanol synthesis as well as methanol dehydration [9, 10, 11, 14]. Different strategies for combing the two types of active sites have been tried, and there is ongoing research on this area. It is expected that the method used for combining the two active sites will impact the catalytic performance of the catalyst [3, 13].

Although theory suggests that bifunctional catalysts perform better when the two active sites are in close contact, this does not seem to be the case for direct DME synthesis [3, 10, 13, 14]. Evidence suggests that the two types of active sites interact in a destructive manner [3, 6, 10, 13, 14]. These interactions have been shown to include a partial exchange of zeolite protons with Cu ions, leading to a decrease in acid site concentration [3].

Methods where the active sites for the methanol synthesis and methanol dehydration are formed in separate stages and subsequently mixed seems to produce the most efficient catalysts [14]. There are however several methods used for mixing the two catalysts, e.g. coprecipitation-impregnation, coprecipitation-sedimentation,

sol-gel impregnation and physical mixtures. The most widely applied method is the physical mixing of the two catalysts due to its simplicity [1, 14]. A study by Garcia-Trenco and Martinez [6] showed that the catalytic behavior is influenced by the mixing method. When the two catalysts were mixed by mixing pre-pelletized catalysts, the catalytic performance (stability) was better than when the two catalysts were mixed by grinding the two powders together followed by pelletizing of the homogenous mixture.

The methanol dehydration function of the hybrid catalyst system has received much attention. It is generally agreed upon that zeolites are more suitable than γ alumina [6, 14]. Zeolites offer higher activity at lower temperature, which is thermodynamically favorable for methanol synthesis step. Furthermore, water adsorbs strongly on the Lewis acid sites of γ alumina, inhibiting methanol dehydration. This effect is less significant for zeolites as they are more hydrophobic and have predominantly Brønsted acid sites [6].

The most commonly used zeolite for direct DME synthesis is H-ZSM-5, although other zeolites are also used [1]. The acidic properties of the zeolite have received much attention and is expected to affect the catalytic performance, although the literature is somewhat confusing and contradictory on this area [6]. This can partly be explained by the fact that characterization of acidity in solid acids is not a straightforward matter, and partly due to the fact that the direct synthesis of DME is more complicated than the methanol dehydration by itself, thus making it hard to draw general conclusions from methanol dehydration studies [6].

The acidity of zeolites is rather complicated, and several aspects must be considered; the type of acid site (Lewis or Brønsted acid site), the strength of the acid sites, acid site density and the distribution of acid sites of different strengths. Some studies suggests that Lewis acid-base pairs are the major active sites for methanol dehydration, whereas strong Brønsted acid sites promotes the conversion of DME to hydrocarbons, and other studies suggests the opposite [6].

Both Lewis and Brønsted acid sites may be present in a zeolite simultaneously. It is therefore necessary to use characterization methods which can distinguish Lewis acid sites from Brønsted acid sites. This may be difficult as the two types of acid sites can interact with each other [23]. In addition, there exists a range of acidic strength within a given acid site type, as the acidity of a given acid site may be affected by neighboring atoms, by its location, and by the aluminium content, making acidity characterization complicated. The issue of zeolite acidity is addressed in more detail in section 2.3.

2.3 Zeolites

Zeolites consist of microporous, crystalline aluminium silicates. More than 600 types of zeolites are known today [17]. The building blocks of zeolites are SiO_4 and

AlO_4 tetrahedra. Silicon and aluminium are bound via oxygen bridges, as shown in figure 2.3.

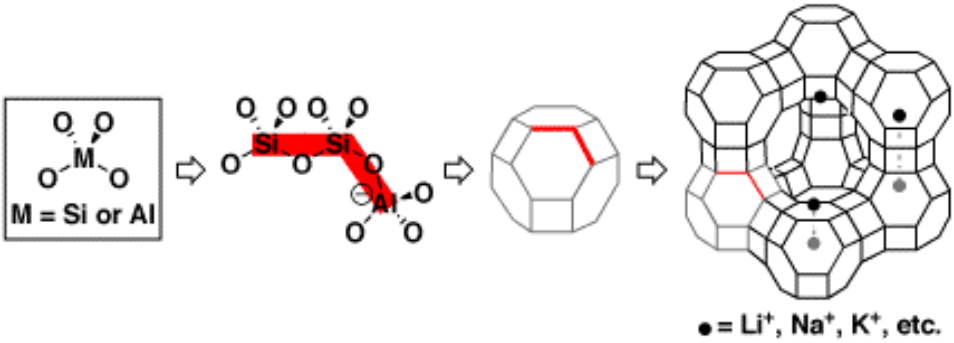

Figure 2.3: *Zeolite structure, from a single tetrahedron to the framework structure of a faujasite class zeolite. Taken from the homepage of prof. Thomas Poon [24].*

Each aluminium atom in the zeolite structure is associated with a negative charge as shown in figure 2.3. Cations are required to compensate for this negative charge. If the charge-compensating cation is a proton, the oxygen bridge binding aluminium to silicon becomes protonated, creating a Brønsted acid site [17, 23, 25, 26].

The zeolite used for the methanol dehydration reaction is the ZSM-5 zeolite. The pore structure of the ZSM-5 zeolite is complex; it consists of straight and sinusoidal channels that are perpendicular to each other [17]. Figure 2.4 shows the structure of the ZSM-5 zeolite and was taken from the database of the International Zeolite Association (IZA) [27].

Zeolites are widely used as catalysts because of their acidic properties and because of their ability to act as molecular sieves (shape selectivity). The acidity of zeolites is a rather complex matter, as both the number of acidic sites (acid site concentration) and the strength of the acidic sites must be considered. The local environment, i.e. the neighboring atoms and the geometry of the acid site, should also be considered. Furthermore, the measurement of acidic strength is not a straightforward matter for solid acids [23].

Both Brønsted acid sites and Lewis acid sites may be present in zeolites [23, 25, 26]. A Brønsted acid is a proton donor, while a Lewis acid is an electron acceptor [23]. Brønsted acid sites in zeolites arise when the oxygen bridge between aluminium and silicon is protonated.

Lewis acid sites may be introduced to zeolites in a number of ways. If a zeolite is heated sufficiently, dehydroxylation of Brønsted acid sites may occur, creating structural Lewis sites. Mild steaming of the zeolite can cause aluminium to dislodge from its regular framework position, thus creating extra-framework aluminium species [23]. Extra-framework aluminium species may act as Lewis acid sites, and can also interact with nearby Brønsted acid sites, making them more

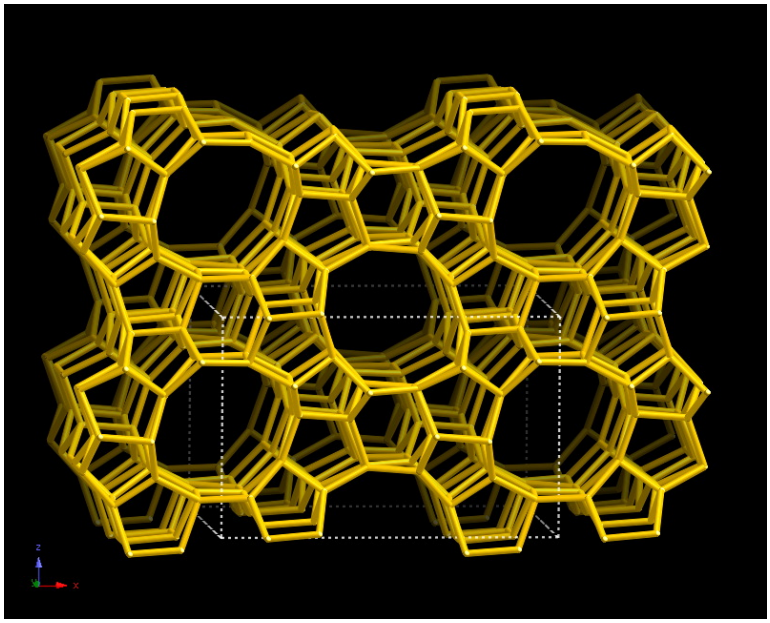

Figure 2.4: *The structure of the ZSM-5 zeolite (MFI type framework). The figure is taken from the database of the International Zeolite Association (IZA) [27].*

acidic. Lewis acidity may also be introduced by ion-exchange of polyvalent cations or multiply-charged species [23].

Thus far we have covered different types of acid sites in zeolite. The acidic properties of one type of acid site, e.g. a protonated oxygen bridge, may not be the same for all sites of that type. The acidic strength of the site depends on the structure of the zeolite, the aluminium content and distribution, and on the local environment of the site defined by the zeolite channels and/or cages geometry. In addition, Lewis and Brønsted acid sites may interact with each other and thus affect acidic strength of the sites involved [23].

There are different strategies for measuring acid strength. For water soluble acids, the acid strength is measured by the dissociation constant of that acid in water. For solid acids however, it is more complicated, and no universal scale of acid strength exists as of yet [23]. For solid acids, both the amount of acid sites (concentration) and the strength of the individual sites must be considered, whereas for acids in aqueous solutions, these parameters are mingled [23]. For example, a 1 M solution of HCl is more acidic than a 0.01 M solution of HCl. The acid is the same, but the concentration is not. As another example, a 1 M solution of HCl is more acidic than a 1 M solution of acetic acid. The concentration is the same, but the acid is not. HCl dissolves completely in water, whereas acetic acid only partially dissolves, thus creating fewer H_3O^+ ions.

For zeolites a distribution of intrinsic acid strengths may exist depending on local, chemical, structural and topological features [23]. Acid strength characterization methods thus need to take into account the absolute or relative amounts of sites possessing a given acid strength. Distinguishing between Lewis and Brønsted acid sites is necessary, but may be complicated by their interactions. It is also relevant to identify the location of the acid sites in the zeolite, as acidic sites located within narrow channels may not be accessible for reactants [23].

The most common way to characterize acidic strength of zeolites is by measuring the adsorption or desorption energy of probe molecules [23]. Adsorption calorimetry is used to measure the heat of adsorption by introducing doses of the probe molecule at increasing vapor pressure to titrate the acid sites from highest to lowest strength [23, 28]. Adsorption calorimetry is described in more detail in section 2.4.5. Temperature-programmed desorption (TPD) is a commonly applied method for measuring acidity. In this method, the zeolite is saturated with the probe molecule at low temperature, and the temperature is then gradually increased. Desorption will then occur at sites of low acid strength at low temperature, and as the temperature is increased, desorption from sites of higher acid strength will occur [28]. TPD is described in more detail in section 2.4.4. Other characterization methods include infrared spectroscopy (IR), solid-state magic angle spinning (MAS) nuclear magnetic resonance (NMR) spectroscopy and model reactions [23].

The acidity of zeolites can in theory be tuned to optimize the catalytic activity. One factor that determines the acidity is the silica to alumina ratio, as the number of Brønsted acid sites increases with increasing aluminium content. There is however evidence to suggests that as the aluminium content increases, the acidity of the individual sites decreases, although this issue is open to debate [23]. The acidity may also be altered by poisoning some of the Brønsted acid sites by ion-exchange of a cation such as sodium.

Lewis acidity may also be introduced by the methods mentioned above, this can in some cases result in very strong acidic sites. In addition, substitution of aluminium with another trivalent element such as Ga, Fe or In may alter the acidity of the zeolite. Calculations and experiments have agreed on the following ranking in terms of acidity: Al(OH)Si > Ga(OH)Si > Fe(OH)Si > In(OH)Si > B(OH)Si. This substitution may be done by direct synthesis or post-treatment [23].

2.4 Catalyst Characterization

Catalyst characterization employs a wide variety of techniques. Catalysts are usually complicated materials, and is often consisting of an active material deposited on the surface of a porous support. Promoters may also be added. It is important to consider the materials and structure of the catalysts, as well as what information one desires when choosing characterization techniques. In the sections below, the characterization techniques used to extract information about the catalysts

relevant to DME synthesis is presented.

2.4.1 Nitrogen Adsorption

The surface area of porous materials can be estimated by an adsorption isotherm. An inert gas such as nitrogen or argon, is physisorbed on the surface of the porous material and the amount of gas needed to form a complete monolayer is determined. When the porous material is a catalyst, adsorption can take place either on the support of the catalyst, or on the active material of the catalyst. An example of an adsorption isotherm used to determine the surface area is the Brunauer, Emmet and Teller isotherm (BET isotherm) [17].

The BET isotherm is expressed below in equation 2.7, taken from [17].

$$\frac{p}{v_a(p_0 - p)} = \frac{1}{v_0 \cdot \chi} + \frac{(\chi - 1)}{v_0 \cdot \chi}\frac{p}{p_0} \tag{2.7}$$

Where p is the pressure, p_0 is the equilibrium pressure of the condensed gas, χ is the ratio of desorption rate constants for the second and first layer respectively, v_0 is the volume of the gas adsorbed in the first layer, and v_a is the total volume of the gas adsorbed.

In order to calculate the surface area, the volume of the gas adsorbed in the monolayer must be determined. Plotting $\frac{p}{v_a(p_0-p)}$ versus $\frac{p}{p_0}$ yields a straight line with slope $\frac{(\chi-1)}{v_0 \cdot \chi}$ and y-axis intercept $\frac{1}{v_0 \cdot \chi}$.

The volume of the gas adsorbed in the monolayer can then be used to find the surface area if the area occupied by the molecules in the adsorbing gas is known, as shown in equation 2.8 below.

$$S_{BET} = \frac{p \cdot v_0 \cdot A_0}{k_B \cdot T \cdot m} \quad \left[\frac{m^2}{g}\right] \tag{2.8}$$

Where S_{BET} is the surface area per mass of the catalyst or support, k_B is the Boltzmann constant, A_0 is the area occupied by the molecules in the adsorbing gas, T is the temperature and m is the mass of the catalyst or support.

The BET isotherm is valid under the following assumptions:

- Dynamic equilibrium between adsorbate and adsorptive
- In the first layer, molecules absorb on equivalent adsorption sites
- Molecules in the first layer constitute the adsorption sites for molecules in the second layer and so on
- Interactions between adsorbates are assumed to be nonexistent

- The adsorption-desorption conditions are the same for all layer except for the first layer
- The adsorption energy for the molecules in all layers except the first is equal to the condensation energy
- The multilayer grows to infinite thickness at the saturation pressure

2.4.2 X-ray Diffraction

X-ray diffraction is a characterization technique used to determine a sample's crystallinity, which crystalline phases are present and how many phases there are, and it can be used to estimate particle sizes [28].

Diffraction occurs when a wave encounters a series of regularly spaced obstacles that are able to scatter the wave and which are separated by a distance comparable to the wavelength [29]. X-rays have wavelengths comparable to the interatomic distance [28, 29]. When a beam of X-rays impinges on a solid material, like a catalyst, a portion of this beam will be scattered by the electrons associated with the atoms or ions that lies in the pathway of the beam [29]. This scattering of the beam allows for interference, which can be constructive (reinforcing) or destructive. Bragg's law, presented below in equation 2.9, gives the conditions for constructive interference:

$$n\lambda = 2dsin\theta \tag{2.9}$$

Where λ is the wavelength, n is the diffraction order, d is the interatomic distance, and θ is the incident angle of the X-ray.

If Bragg's law is not satisfied, then the interference will be destructive and yield a low intensity diffracted beam [29]. The diffracted beams are recorded, and diffraction patterns are generated based on this information [28]. The diffraction patterns are characteristic for crystal planes of different crystal structures, and also for species, as the geometry of unit cells in crystal structures depend on atomic radius [28, 29].

2.4.3 Copper Dispersion

The dispersion of the active material on the catalyst support is often a parameter of great interest. It is usually desirable to have as much of the active material as possible on the surface, where it is most accessible to the reactants. The activity of a catalyst is often reported as the turnover frequency (TOF) or equivalent, which reports the activity based on the number of moles reacted per active site, i.e. surface atoms of the active material, and time. The dispersion is defined as

the ratio of surface atoms to the total number of atoms in the material, as shown in equation 2.10 [30, 31].

$$D = \frac{n_s}{n_t} \tag{2.10}$$

Where n_s is the number of atoms on the surface, and n_t is the total number of atoms.

The dispersion of the active material on a catalyst can be determined by different methods. When the active material is copper, nitrous oxide titration is the most common technique. Nitrous oxide reacts selectively with copper according to equation 2.11 [32, 33, 34].

$$N_2O + 2Cu \rightleftharpoons Cu^{1+} - O - Cu^{1+} + N_2 \tag{2.11}$$

As nitrous oxide will oxidize all copper atoms present in the material, and not just the copper atoms on the surface, it is necessary to find a way to distinguish between surface and bulk oxidation. Sato et al. proposed an experimental method for distinguishing surface oxidation from bulk oxidation [32]. By measuring the dispersion for different exposure lengths and at different temperatures, they found that after the initial fast oxidation of the surface copper atoms, the bulk oxidation proceeds as a nearly linear function of the square root of exposure length.

In the experimental work by Sato et al., the dispersion was determined on the basis of two reductions; the material was reduced, and the uptake of hydrogen was measured volumetrically, then nitrous oxide was introduced to the system for a prescribed period of time, after which a second reduction was performed and the uptake of hydrogen was measured again [32]. For the present work, the dispersion was determined in a thermogravimetric instrument, as described in section 3.3.3. The advantage of performing the experiment in the TGA instrument is that only one reduction was needed, as the mass change associated with N_2O exposure was monitored continuously. For the same reason, there was no need to perform multiple experiments with different exposure lengths to measure the apparent dispersion as Sato et al. did.

The dispersion is calculated based on the change in sample mass during reduction and during N_2O exposure. The mass change during reduction is due to copper atoms being reduced. In the calculation it is assumed that all copper atoms were present as Cu^{2+} prior to the reduction, as shown below:

$$Cu^{2+}O^{2-} \rightarrow Cu^0 \tag{2.12}$$

To calculate the number of moles of copper in the sample, the mass loss is therefore converted to moles of oxygen atoms as shown below:

$$n_{Cu_t} = \frac{\Delta m}{A_O} \tag{2.13}$$

Where n_{Cu_t} is the total number of moles of copper atoms in the sample, while Δm is the mass change and A_O is the molar mass of an oxygen atom.

The amount of copper on the catalyst surface is calculated based on a plot of mass change as a function of the square root of the exposure time. By using linear regression and extrapolating to time zero, the mass change due to oxidation of surface copper is found. This mass change is converted to moles of oxygen in the same manner as shown above. For each mole of oxygen atoms, there are two moles of copper atoms as two copper atoms are bound to one oxygen atom.

2.4.4 Temperature-Programmed Desorption

Temperature-programmed desorption (TPD) is often used to characterize the acidic or basic properties of surfaces or decomposition phenomena of adsorbed species at given temperatures [28]. TPD experiments can be run in a thermogravimetric analysis (TGA) instrument. The TGA instrument monitors the mass of a sample while a temperature program is run. TPD experiments consist of three phases; pretreatment, adsorption and desorption [28].

During the desorption phase, the temperature is increased to allow for desorption at progressively stronger acidic sites. At stronger acidic sites, the probe molecule is bound more strongly, thereby requiring more energy for desorption to occur. TPD experiments indicate the number of acidic sites in the zeolite, as well as the strength of the acidic sites. However, care must be made when interpreting the data. It is necessary to distinguish between physisorbed and chemisorbed probe molecules, as well as Brønsted and Lewis acid sites [23].

The heat of adsorption can be determined from TPD experiments provided that appropriate kinetic models are applied [23, 28]. This was however considered beyond the scope of this project, instead, TPD data from different catalysts were compared to find possible trends.

Different probe molecules may be used for TPD experiments. Ammonia is probably the most commonly applied probe for TPD experiments, due to its small kinetic diameter and it being a relatively strong base. The small kinetic diameter of ammonia makes it suitable to probe acidic sites located within narrow pores [23, 35, 36].

Isopropylamine is another suitable probe, due to its ability to distinguish between Brønsted and Lewis acid sites. The desorption of isopropylamine from Brønsted acid sites is characterized by the desorption product being propene and ammonia. Desorption of excess isopropylamine, either from Lewis acid sites or physisorbed species, desorbs unreacted [26, 37, 38].

Even though TPD is the one of the most commonly applied methods for acidity characterization of solid catalysts, it is somewhat limited [23, 25, 26]. The adsorption energy is not easily determined, and the distribution of acidic sites of different strength is not precise. The adsorption energy is difficult to determine because of the complex kinetics of the desorption; readsorption may occur and the probe may diffuse into the zeolite micropores [36]. It is common for ammonia TPD experiments to yield two peaks, indicating that there are at least two groups of sites with different ranges of acid strengths [23]. Moreover, adsorption energies obtained from ammonia TPD experiments are dependent on the conditions used, e.g. an experiment conducted under vacuum might yield different adsorption energies than an experiment conducting with inert gas flow [26].

2.4.5 Adsorption Microcalorimetry

Adsorption microcalorimetry can also be used to characterize acidity and basicity in heterogeneous catalysis [23, 25, 26, 39]. The advantage of this method is that it allows for direct measurement of the heat evolved during the adsorption process [25, 26, 39, 40]. By coupling adsorption microcalorimetry with a volumetric setup, the heat of adsorption can be related to the coverage on the catalyst. This provides a powerful tool for characterization of acidic sites on solid catalysts.

A Tian-Calvet microcalorimeter was used for measurements. This is a heat-flow calorimeter that measures the heat flows occurring between, the sample and the thermostated jacket, and between a reference cell and the same jacket [28, 39]. The thermostated jacket is kept at a constant temperature while the adsorption of probe molecules onto the catalyst sample generate a heat flow through the thermal detector that is recorded as a function of time.

The volumetric setup allows for determination of the volume adsorbed onto the catalyst sample. Successive doses of the probe molecule are introduced to the catalyst sample within the calorimetric cell. Between each dose, thermal equilibrium is reached. Pressure and heat evolution is recorded continuously [25, 28, 39].

By waiting for thermal equilibrium between each dose, the basic probe will adsorb onto the strongest acidic sites first, and then onto sites of weaker acid strength. By minimizing the dose, a good correlation between the adsorbed amount and the adsorption energy of the sites can be found. A high adsorption energy corresponds to strong acidic sites, while a low adsorption energy corresponds to weaker acidic sites [25, 28, 39].

Microcalorimetry, like TPD studies can not completely characterize the acidity of solid acids. From microcalorimetric studies, the acid strength and the distribution of acidic sites of given strength can be determined. However, the nature of the acidic site, e.g. Brønsted or Lewis acid sites, can not be determined. It is therefore recommended to characterize the solid acid with another technique, such as infrared (IR) spectroscopy, in addition [26, 40].

Auroux [25] has written a comprehensive review on microcalorimetry and zeolites. The effect of the probe molecule, adsorption temperature, pretreatment, Si/Al ratio, and more, is considered. Regarding adsorption temperature, it was concluded that at room temperature, it was not possible to distinguish between weak and strong acidic sites, and at temperatures above 300 °C, the decomposition of ammonium ions became predominant. An adsorption temperature between 150 and 300 °C was therefore recommended for ammonia adsorption experiments [25, 41, 42].

When H-ZSM-5 is calcined at high temperatures, dehydroxylation and dealumination may occur [23, 25]. At pretreatment temperatures above 402 °C, dehydroxylation has been observed. This leads to a decrease in the number of Brønsted acid sites, while the number of strong Lewis acid sites increases. To avoid dehydroxylation and dealumination, it is therefore recommended to do the pretreatment at temperatures lower than 400 °C [25].

The distribution of acid site strength obtained from microcalorimetric studies usually gives high initial heats of adsorption, above 150 $^{kJ}/_{mol}$, followed by a plateau around 150 $^{kJ}/_{mol}$. After the plateau at 150 $^{kJ}/_{mol}$, a sharp decrease is usually observed [23, 25, 42, 43]. The heats of adsorption are quite consistent between different studies, but the adsorbed amounts may differ slightly.

Chapter 3

Materials and Methods

3.1 Risk Evaluation

Prior to any experimental work, risk assessments were performed. The main risks are associated with working with combustible and/or toxic gases under pressure, CO in particular. To reduce the risk, leak testing was performed prior to all experiments. Leak testing was performed with inert gas first, if possible, then with small amounts of hydrogen, using handheld detectors cross sensitive to hydrogen, to detect leaks. Central gas alarms are also installed in the laboratories that are sensitive to CO and hydrogen.

For the use of ammonia gas in the calorimetric experiments, leak test were performed with small amounts of hydrogen, using handheld detectors cross sensitive to hydrogen, to detect leaks prior to introducing ammonia. The amounts of ammonia used in experiments were small, and leaks are easily detectable by the characteristic smell.

The full risk assessment is attached in appendix A

3.2 Catalyst Synthesis

3.2.1 Preparation of Methanol Catalyst

The copper/zinc catalyst was prepared by coprecipitation according to an experimental procedure supplied by Universal Oil Products (UOP). The catalyst was synthesized as a part of the specialization project conducted during the fall of 2013.

Salts of copper, zinc and alumina were dissolved in deionized water. Two other solutions were made; one containing sodium carbonate, and one containing sodium acetate, both dissolved in deionized water. The sodium acetate solution was added to a beaker and heated in an oil bath with continuous stirring. The other two solutions were added simultaneously to the sodium acetate by pumps, while maintaining stirring. The temperature and the pH of the solution in the oil bath were kept constant by regulating the flow of metal solution and sodium carbonate solution.

At the end of the addition of the solutions, the stirring and heating was kept for another 30 minutes. The solution was then transferred to a 4 L beaker, and deionized water was added. When the precipitate had settled, the top layer was separated from the precipitate by using a large Buchner funnel with vacuum. More deionized water was added and the procedure was repeated. The washing procedure was repeated until about 5 L of deionized water was added to the solution.

The precipitate was then dried in a forced air oven at 100 °C for about 20 hours. After drying, the catalyst was allowed to cool before it was crushed using a mortar and pestle. The catalyst was then sieved to ensure a grain size of less than 0.6 mm. The sample was finally calcined in air flow with the following temperature program: from ambient temperature to 400 °C in 2 hours, holding at 400 °C for 2 hours and then decreasing the temperature to ambient temperature in about 4 hours.

A sample of the calcined catalyst was analyzed by high resolution Inductively Coupled Plasma Mass Spectrometry (ICP-MS) to determine the sodium level in the catalyst. The ICP-MS analysis identifies metals present in a material quantitatively.

3.2.2 Preparation of ZSM-5

The ZSM-5 zeolite was acquired commercially in the ammonium form, NH_4^+. The zeolite was calcined in air flow at 500 °C. During calcination, the ammonium ions decompose and the hydrogen form of the zeolite is obtained; H-ZSM-5.

Portions of H-ZSM-5 were subjected to ion exchange of varying extent. $NaNO_3$ salt was weighed according to the desired ion exchange extent and mixed with H-ZSM-5 and water. The molar concentration of $NaNO_3$ in water was kept constant for all ion exchange experiments. The mixture of sodium nitrate and zeolite was heated under continuous stirring in an oil bath. The temperature in the oil bath was kept constant at 80 °C. After about 15 hours, the mixture was filtered and washed extensively with deionized water. The zeolite was then dried in a forced air oven over night and subsequently calcined and sieved.

The ion-exchanged zeolites were named as Na(X),H-ZSM-5 Y, where X refers to the attempted extent of ion-exchange while Y refers to the molar ratio of $SiO_2 : Al_2O_3$.

These experiments were performed as a collaboration between F. Dadgar and myself. Samples of the ion-exchanged zeolites were analyzed by high resolution ICP-MS to determine the extent of the ion exchange.

3.3 Catalyst Characterization

3.3.1 Nitrogen Adsorption

Catalyst samples were analyzed in a Micromeritics TriStar 3000 instrument to determine BET surface area. Between 50 and 100 μg was used in the experiments. The samples were degassed at 200 °C over night prior to the measurements. These experiments were performed as a part of the specialization project.

3.3.2 X-ray Diffraction

Powder X-ray diffraction (XRD) patterns were obtained by using a Bruker D8 Advance DaVinci Diffractometer. The phases were identified by the DIFFRAC^{plus} EVA software installed in the laboratory. All the samples were analyzed in the range of 2θ between 20°and 80°. These experiments were performed as a part of the specialization project.

3.3.3 Nitrous Oxide Titration

The dispersion of copper on the homemade methanol catalyst was measured by nitrous oxide (N_2O) titration in a thermogravimetric analysis (TGA) instrument. The method was similar to the ones presented by Meland [33] and Phan et al. [34], which were adapted from the method presented by Sato et al. [32]. Several trials were needed in order to find a suitable temperature program for the nitrous oxide titration due to poor temperature control of the TGA instrument at temperatures below 100 °C. The homemade catalyst (batch 2) was tested twice to check the reproducibility.

The method consists of a pretreatment section for degassing, followed by a reduction section before the catalyst sample was exposed to nitrous oxide. The mass of the catalyst was monitored throughout the experiment. The temperature program applied is given in table 3.1. The reduction and the nitrous oxide titration were run as separate, consecutive programs.

Table 3.1: *Temperature program used for N_2O titration experiment in thermogravimetric analysis instrument.*

Step	T_{start}	T_{end}	Detail	Gas
1	30 °C	200 °C	5 $^{\circ C}/_{min}$	Ar
2	200 °C	200 °C	1 hour	Ar
3	200 °C	50 °C	2 $^{\circ C}/_{min}$	Ar
4	50 °C	50 °C	30 min	Ar
5	50 °C	250 °C	1 $^{\circ C}/_{min}$	7 vol% H_2 in Ar
6	250 °C	250 °C	1 hour	7 vol% H_2 in Ar
1	30 °C	50 °C	1 $^{\circ C}/_{min}$	Ar
2	50 °C	50 °C	2 hours	Ar
3	50 °C	50 °C	30 min	10 vol% N_2O in Ar

3.3.4 Temperature-Programmed Desorption

The acidic catalysts were investigated by temperature-programmed desorption in the thermogravimetric analysis (TGA) instrument. Two different basic probes were used; ammonia and isopropylamine. These experiments were performed as a collaboration between my co-supervisor F. Dadgar and myself.

NH_3 TPD

Ammonia TPD was used to characterize all of the acidic catalysts, including the ion-exchanged zeolites. The probe gas used was a gas mixture containing about 1 % ammonia in argon. Pretreatment, adsorption and desorption was performed in the TGA instrument. The temperature program applied is given below in table 3.2.

Table 3.2: *Temperature program used for ammonia temperature-programmed desorption experiment in thermogravimetric analysis instrument.*

Step	T_{start}	T_{end}	Detail	Gas
1	30 °C	600 °C	10 $^{\circ C}/_{min}$	Ar
2	600 °C	600 °C	60 min	Ar
3	600 °C	100 °C	10 $^{\circ C}/_{min}$	Ar
4	100 °C	100 °C	60 min	Ar
5	100 °C	100 °C	30 min	1 vol% NH_3 in Ar
6	100 °C	100 °C	90 min	Ar
7	100 °C	800 °C	5 $^{\circ C}/_{min}$	Ar

Some of the acidic catalysts investigated were subjected to a different temperature program. The difference between the two temperature programs was the pretreatment temperature. For the second temperature program, the pretreatment tem-

perature was lowered to 250 °C. Pretreatment temperature may affect the acidity of zeolites, as mentioned in section 2.4.5.

H-ZSM-5 80, H-ZSM-5 30, Na(30),H-ZSM-5 80 and Na(30),H-ZSM-5 30 were subjected to the temperature program presented in table 3.2. Na(40),H-ZSM-5 80, Na(60),H-ZSM-5 80, Na(80),H-ZSM-5 80 and γ alumina were subjected to the temperature program with lower pretreatment temperature. H-ZSM-5 80 was tested again with the new temperature program to see if the lower pretreatment temperature would affect the results.

Isopropylamine TPD

For the isopropylamine TPD experiments, pretreatment and adsorption were performed ex situ to protect the instrument. As isopropylamine TPD experiments had not been performed in this laboratory before, the experimental procedure was developed based on literature.

The procedure included a pretreatment step, which was performed using the degassing unit typically used prior to BET measurements. The catalyst sample was heated to 200 °C under vacuum for a prescribed period of time. The catalyst sample was then exposed to isopropylamine, by placing the sample container and a small vial of isopropylamine (liquid form) inside a closed container. The sample was exposed to isopropylamine for a prescribed time, before it was placed inside the TGA instrument.

The applied temperature program consisted of a temperature ramp from room temperature to 100 °, at a heating rate of 5 °C per minute. The temperature ramp was followed by an isothermal stage at 100 °C, and finally a temperature ramp from 100 °C to 430 °C. Argon gas was flowed for the entire temperature ramp, and the exhaust gas from the TGA instrument was analyzed with MS.

Table 3.3 lists the catalysts that were investigated by TPD and the probe gas used. The ion-exchanged zeolites are abbreviated as for instance Na(30),H-ZSM-5 30, meaning that the 30 % replacement of hydrogen atoms with sodium atoms was targeted.

Table 3.3: *Acidic catalysts investigated by NH_3 TPD and/or isopropylamine TPD*

Catalyst	**Probe gas**
H-ZSM-5 30	NH_3, Isopropylamine
H-ZSM-5 80	NH_3, Isopropylamine
Na(30),H-ZSM-5 30	NH_3
Na(30),H-ZSM-5 80	NH_3, Isopropylamine
Na(40),H-ZSM-5 80	NH_3
Na(60),H-ZSM-5 80	NH_3
Na(80),H-ZSM-5 80	NH_3
γ alumina	NH_3

3.3.5 Adsorption Calorimetry

Adsorption microcalorimetry was performed using a Tian-Calvet heat-flow microcalorimeter connected to a homemade volumetric apparatus. The setup was build by E. Patanou, and a detailed description of the setup can be found in her PhD thesis [39]. A process flow diagram (PFD) of the setup is included in figure 3.1, and was taken from [39].

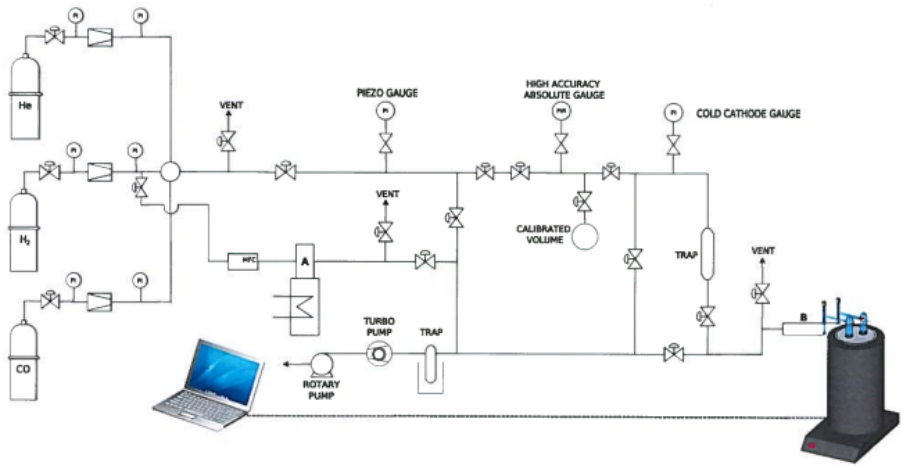

Figure 3.1: *Process flow diagram of the calorimetry setup, taken from [39].*

Adsorption microcalorimetry had not been applied for ammonia in this laboratory before. The setup was therefore modified slightly for this project; a separate stainless steel gas line for feeding ammonia was added, and the existing vent from the vacuum pump was replaced with a stainless steel gas line (a rubber vacuum tube was used previously). Every part of the setup was checked for ammonia compatibility prior to start-up.

The experimental procedure was developed in this project based on literature and experimental experience with CO and H_2 microcalorimetry [39]. The following sections provide short descriptions of the various parts of the setup.

The Microcalorimeter

The microcalorimeter used is a Setaram C80 heat flux Tian-Calvet calorimeter. The operating temperature range for this calorimeter is from 0 °C to 300 °C. The

sensor within the calorimeter is very sensitive, capable of detecting heat flows as low as 0.1 μW [39].

The calorimeter is connected to a computer, and software supplied with the instrument was used to monitor temperature changes and changes in heat flow. The software also contains an analysis section that allows for integration of the heat flow peaks associated with each dose of probe gas.

The Volumetric Setup

The amount of probe gas that is adsorbed on the sample for each dose is determined volumetrically. Accurate volumetric measurements are therefore important. Two parameters are crucial in this respect; the leak rate (rate of vacuum decay), and the accuracy of the volume calibration. The volumetric apparatus consist of a vacuum system, pressure gauges and the dosing section. The apparatus is made of Pyrex glass and is sealed by O-ring stopcock valves and Pyrex-to-metal seal adaptors.

Vacuum is achieved by two pumps; one rotary pump (Pfeiffer DUO 5M) and a turbo pump (Pfeiffer HiPace 80). The rotary pump is started first, and when the pressure in the system is reduced sufficiently ($< 10^{-2}$ mbar), the turbo pump is started. The system is capable of reaching high vacuum conditions ($< 10^{-7}$ mbar) [39].

The vacuum system facilitates to evacuate and keep the lines of the volumetric apparatus clean before and after measurements. The vacuum system can also be connected to the pretreatment section to facilitate evacuation of the sample prior to calorimetric measurements.

Four pressure gauges are connected to the volumetric setup. The pressure gauges have different ranges, as they are used to show the pressure of different sections of the volumetric setup. The first pressure gauge is placed at the ultra-high vacuum side of the turbo pump. This pressure gauge is mainly used to monitor the pressure in the system prior to the start-up of the turbo pump. The range of this pressure gauge is from atmospheric pressure to 10^{-4} mbar. A pressure gauge, MKS Piezo, is placed near the inlet of the dosing section. This pressure gauge is used as an initial measure of the probe gas dose. For accurate measurements of the dose of probe gas, a high capacitance manometer (MKS Baratron) is used. This pressure gauge is calibrated to be very accurate in the range between 1 and 10 torr (1.33 - 13.3 mbar). This pressure gauge is connected to a computer and Labview software facilitates logging of pressure data. The final pressure gauge, the cold cathode gauge, monitors the pressure of the volumetric setup under ultra-high vacuum conditions.

The Dosing Section

The dosing section consists of Pyrex tubing and is connected to the gas feed line and to the vacuum system. The internal volume of the dosing section was measured prior to the experiments. A volumetric flask of known volume is connected to the dosing section. An overview of the dosing section is shown below in figure 3.2.

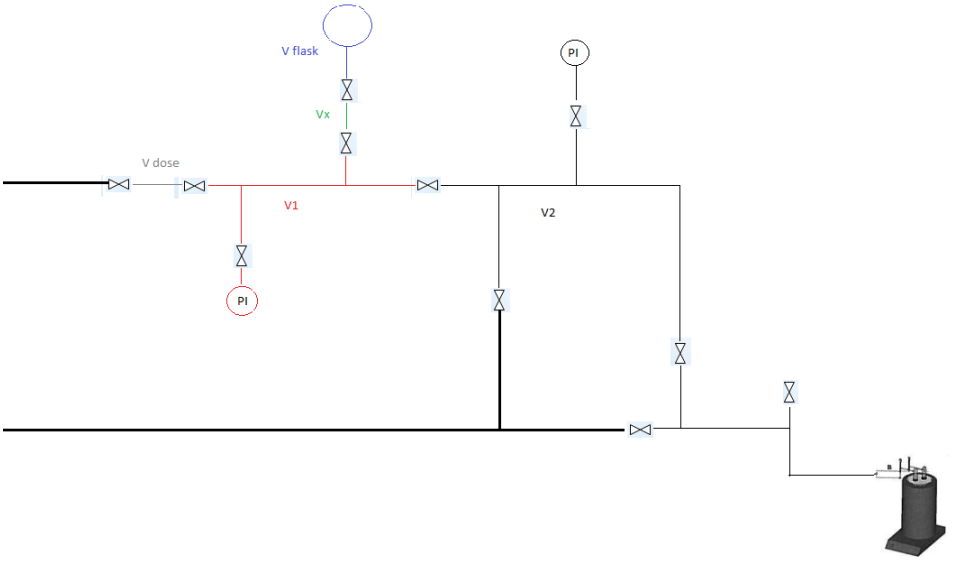

Figure 3.2: *Schematic overview of the relevant part of the dosing section. The calibrated volumes are shown in different colors, e.g. the volume called V_1 is shown in red.*

The volume of the volumetric flask, V_{flask} in figure 3.2, was determined by E. Patanou in 2011. The volume was determined by weighing the volumetric flask filled with distilled water at a known temperature. By measuring the density of the distilled water at the same temperature, the volume of the water could be calculated. The procedure was repeated several times and an average value was taken.

To find the volume V_1 in figure 3.2, several measurements were made. First, the volume V_0 was measured, this volume is the sum of V_{flask}, V_1 and V_x. The volume V_0 was measured by introducing ammonia into the dosing section and then isolating the volume V_0 by closing the appropriate valves. The pressure was then recorded as p_i. The volumetric flask was then isolated by closing the valve on top of the flask, and evacuating the rest of the system. When the pressure was sufficiently low, the volume V_0 was again isolated, and the ammonia gas trapped inside the volumetric flask was expanded into the isolated volume. The pressure was recorded as p_f. This procedure was repeated several times. The volume of V_0 was then calculated

by using the ideal gas law as shown below:

$$V_0 = \frac{p_i}{p_f} \cdot V_{flask} \tag{3.1}$$

The next step was to measure the volume V_x. This was done in a similar manner as for V_0; Ammonia was introduced into V_0 and the pressure was recorded (p_i). The volume V_x and V_{flask} was then isolated and the rest of the system was evacuated. At a sufficiently low pressure, the V_0 was again isolated and the gas was expanded into volume and the pressure was recorded (p_f). This procedure was repeated several times. The volume of V_x was then calculated as:

$$V_x = \frac{p_f}{p_i} \cdot (V_0 - V_{flask}) \tag{3.2}$$

The volume V_1 can now be calculated:

$$V_1 = V_0 - V_{flask} - V_x \tag{3.3}$$

The remaining volumes, V_2 and V_{dose} was measured using the same principle. Ammonia gas was introduced to the dosing section, and the volume V_1 was isolated and the initial pressure recorded. The gas was then expanded into the unknown volume, and the final pressure was recorded. This was repeated several times for both remaining volumes. The recorded pressures and calculated volumes are included in appendix E.

Microcalorimetric Cells

Two cells are used for adsorption microcalorimetry, one empty reference cell, and one cell with sample. The cells are identical and homemade, and consist partly of Pyrex glass and partly of quartz. An illustration of the cell is shown in figure 3.3, taken from [39].

Both the inlet and outlet of the cell are fitted with stopcock vacuum valves. Inside the cell is a sinter that the sample is placed upon. The cell is designed to allow for plug-flow like behavior of the gas during pretreatment. Gas flows inside the inner glass tube and comes out into the main part of the cell below the sinter. The gas then flows upwards through the catalyst sample.

Pretreatment

The catalyst sample usually requires pretreatment prior to the adsorption calorimetry experiment. For zeolites, pretreatment consists of heating under inert gas flow or vacuum or both, to remove adsorbed species. The pretreatment section

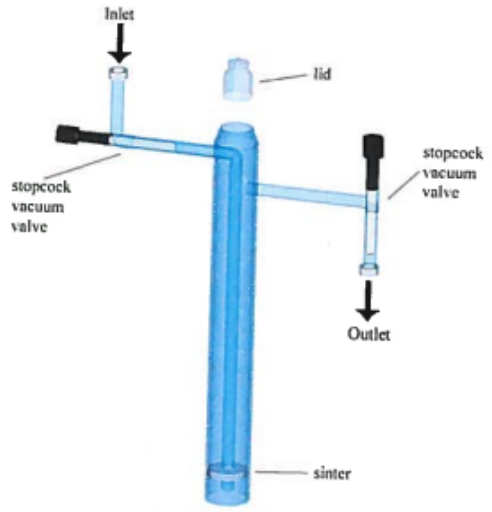

Figure 3.3: *Sketch of the microcalorimetric cell used for adsorption microcalorimetry experiments, taken from [39]*

in this setup includes a furnace connected to the gas feed lines and the vacuum system. The furnace temperature is controlled by an Eurotherm controller.

The microcalorimetric cells are placed within the furnace during pretreatment. Gas flow to the cell is controlled by a mass flow controller (MFC). When gas is flowed during the pretreatment, the gas coming out from the cell is connected to the ventilation. If no gas is used during pretreatment, the cell is connected to the vacuum system to facilitate evacuation of the cell. During the last stage of pretreatment, the cell is evacuated to remove the pretreatment gas (if used) and to clean the catalyst surface prior to the adsorption calorimetry measurement.

When the cell has been evacuated sufficiently, the inlet and outlet valves on the cell are closed and the cell is transported to the calorimeter.

Experimental Procedure

A sample of catalyst was weighed and placed inside the microcalorimetric cell. The cell was placed inside the furnace and a temperature program was run. The catalyst sample was heated to 390 °C under helium flow at 50 $^{ml}/_{min}$. The temperature was kept at 390 °C, and helium flow was kept for 2 hour, after which the cell was evacuated (at the same temperature). Inert gas flow was used for the first part of the pretreatment in order to avoid sending desorbed water to the vacuum system. The sample was evacuated at 390 °C overnight.

The sample was then cooled before it was transported to the calorimeter. When a stable baseline reading from the calorimeter was established and a satisfactory vacuum was achieved ($< 10^{-5}$ torr), dosing of probe gas began. Between each dose, thermal and pressure equilibrium was reached, the baseline of calorimeter was re-established and the pressure no longer changing, indicating that the adsorption process had reached equilibrium. Successive doses were sent to the cell until the surface was saturated. The pressure and heat signal was recorded continuously.

Several adsorption microcalorimetry experiments were carried out for the H-ZSM-5 (30) zeolite as establishing a practical and reliable experimental procedure proved to be difficult.

Evacuation and readsorption were attempted to determine the amount of irreversibly adsorbed ammonia. After the initial adsorption was performed, the calorimetric cell was closed while the rest of the system was evacuated overnight. The next morning, the calorimetric cell was evacuated until the recorded baseline was stable. Doses of probe gas were then sent until the catalyst sample was saturated.

Analysis

The adsorbed amount was determined volumetrically based on the measured volumes, V_1, V_{dose} and V_2, and the pressure data recorded. For each dose sent to the calorimetric cells, two pressures were recorded; p_1, measured for V_1 and V_{dose} and p_2, measured as the gas expanded into V_2. The amount of gas adsorbed, $\Delta n_{a,i}$, was calculated assuming the ideal gas law as shown below in equation 3.4 [39]:

$$\sum_{i=1}^{n} \Delta n_{a,i} = \sum_{i=1}^{n} \Delta n_{dose,i} - \Delta n_{gas,i} + \Delta n_{lost,i} \tag{3.4}$$

Δn_i corresponds to molar amounts of gas, either the dose amount, gas phase amount or amount lost due to isolation of the dosing volume from the volume of the cells between doses. These amounts were calculated based on the ideal gas law, as shown below in equation 3.5 [39]:

$$\Delta n_{dose,i} = \frac{p_{1,i} \cdot (V_1 + V_{dose})}{R \cdot T_{room,i}} \tag{3.5a}$$

$$\Delta n_{gas,i} = \frac{p_{2,i} \cdot (V_1 + V_{dose} + V_2)}{R \cdot T_{cell,i}} \tag{3.5b}$$

$$\Delta n_{lost,i} = \frac{p_{2,i-1} \cdot V_2}{R \cdot T_{room,i}} \tag{3.5c}$$

As seen from equation 3.5, the temperature of the calorimetric cell is used to calculate the amount of ammonia in the gas phase after the adsorption has taken place.

The pressure used for this calculation is recorded as the pressure of the combined volume of V_1, V_{dose} and V_2. As the temperature of the cell is substantially higher than the temperature of the rest of the dosing section, the amount of ammonia left in the gas phase after adsorption is underestimated. For the purpose of these experiments however, this error is assumed to be insignificant.

$\Delta n_{lost,i}$ is calculated to account for the amount of ammonia left within the system from one dose to the next. The volume of the dosing section connected to the cell is isolated from the rest of the dosing section between every dose to determine the amount of ammonia in each dose. The ammonia left within the system from the previous dose is therefore added when the adsorbed amount of ammonia is calculated for the next dose.

To calculate the heat of adsorption, $\Delta H_{a,i}$, the amount of heat evolved as dose i adsorbed, ΔQ_i, is divided by the adsorbed amount, $\Delta n_{a,i}$ as shown in equation 3.6.

$$\Delta H_{a,i} = \frac{\Delta Q_i}{\Delta n_{a,i}} \tag{3.6}$$

From these data, several plots may be derived. The most important one for acidity characterization is the plot of the heat of adsorption as a function of the adsorbed amount. Another important plot is the volumetric isotherm; adsorbed amount of gas plotted as a function of pressure for a cycle of adsorption (I), followed by desorption by evacuating the cell and then adsorption again (II). The irreversibly adsorbed volume, which characterizes the strong sites of the catalyst, is then calculated as the difference between the adsorbed volumes in (I) and (II) [43].

3.4 Catalyst Testing

3.4.1 Experimental Set-up

The setup used for the activity measurement was designed for converting synthesis gas into methanol. The setup is mainly 1/4 inch stainless steel pipes with Swagelok fittings. Gas is fed to the setup via two high pressure pipelines: one pipeline for H_2 and one pipeline for N_2 and premixed synthesis gas. The pipelines are equipped with reduction valves, manual valves, filters and manometers. The gas lines also have valves that allows for connection to the ventilation system.

Figure 3.4 shows a process flow diagram (PFD) of the setup. This PFD was created in Microsoft Visio by F. Dadgar in 2011. The setup has been modified since this PFD was made, but these are minor adjustments. Synthesis gas and nitrogen is now fed via the same pipeline to the setup and the pipeline used for GC analysis of the dry product gas is moved closer to the reactor outlet.

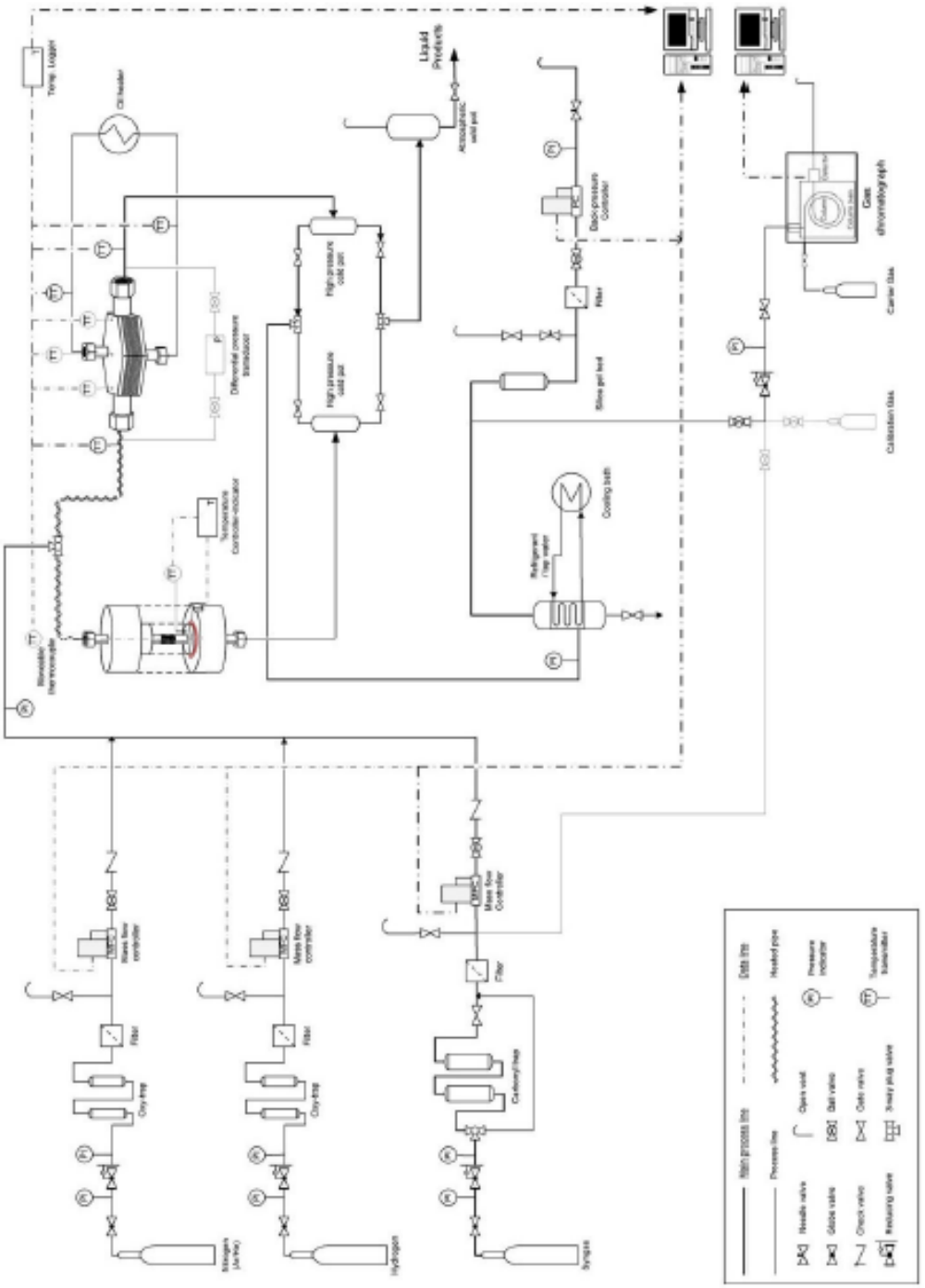

Figure 3.4: *Process flow diagram of the experimental setup designed to convert synthesis gas into methanol. The flow diagram was made using Microsoft Visio by F. Dadgar.*

As seen in figure 3.4, the synthesis gas flows over a lead oxide trap designed to remove carbonyls from the gas. It is possible to bypass this trap, for example when nitrogen is flown through this pipeline. A sidestream going to the GC shortly after this carbonyl trap allows for feed gas analysis.

The pipeline going into the reactor is heated by electric heating bands and insulated to avoid large temperature gradients over the inlet section of the reactor. A thermocouple is placed on the pipeline, near the reactor inlet to monitor the temperature in the feed gas.

The gas flow to the reactor is controlled by Bronkhorst digital mass flow controllers (MFC), which were calibrated for the gases and pressures used in the experiment by A. Montebelli in the fall of 2013 [44]. The calibration curves are shown in appendix F. The reactor pressure is controlled by a Bronkhorst digital back pressure controller. Additionally, a manometer displays the pressure visually.

The temperature of the reactor is monitored by a movable thermocouple inside the reactor. A computer by the setup allows for acquisition of data such as temperature and GC analyses, and for monitoring and controlling the temperature, pressure and flow rate in the setup.

The lead oxide trap was always bypassed for the methanol synthesis experiments. This was done because the lead oxide trap removes CO_2 from the gas stream until the trap is saturated and because It is assumed that the carbonyl problem is negligible today because of the aluminium lining used in the gas bottles.

3.4.2 Reactor

A laboratory scale tubular fixed-bed reactor was used to perform the activity measurements. The reactor is made of stainless steel with $^1/_2$ inch diameter (inner diameter: 9.14 mm and length: 434 mm). The reactor was fitted with Swagelok VCR-fittings [15]. A thermowell is centered inside the reactor and contains a movable thermocouple. A stainless steel cylinder capped with a steel mesh was placed inside the reactor to prevent catalyst or inert materials to escape the reactor. Quartz wool was inserted into the reactor before and after the catalyst, to keep the catalyst bed in place.

The reactor is placed inside an aluminium block and heated by a Kanthal furnace using an Eurotherm temperature controller. The catalyst bed temperature was measured by moving the thermocouple along the reactor axis. The temperature of the catalyst bed was adjusted by adjusting the furnace temperature.

3.4.3 Analysis

The product stream exiting the reactor consists of a mixture of unreacted syngas components, water and methanol vapor and possible byproducts. To avoid con-

densation of water and methanol in the pipes, the product stream is cooled in a pressure vessel, so that the condensed water and methanol is trapped in the vessel. This vessel is connected to an atmospheric tank, where the liquid products can be collected for analysis.

A portion of the dry product gas is sent to the analysis section, while the rest of the gas is depressurized and vented.

The setup is connected via piping to a gas chromatograph (Agilent 6890N) facilitating online analysis of product gas or feed gas. When feed gas analyses are performed, the feed gas bypasses the reactor and is sent directly to the gas chromatograph (GC). The GC is equipped with both a thermal conductivity detector (TCD) and a flame ionization detector (FID). The TCD can detect all gases in the product stream (H_2, N_2, CO_2, CH_4 and CO), while the FID is used to detect hydrocarbons in the liquid product. To analyze the liquid product, the liquid is injected manually to the GC by a syringe.

The GC instrument was calibrated by A. Montebelli in the fall of 2013 [44].

The conversion of different components was calculated as shown below. Nitrogen is used as an internal standard, since nitrogen is inert (neither formed nor consumed).

$$X_{CO} = \frac{F_{CO,in} - F_{CO,out}}{F_{CO,in}} \tag{3.7}$$

where F_i denotes the molar flow of component i. F_i is related to the molar fraction of component i (y_i) as shown below:

$$F_{CO,in} = y_{CO,in} \cdot F_{tot,in} \tag{3.8}$$

$$F_{CO,out} = y_{CO,out} \cdot F_{tot,out} \tag{3.9}$$

Substituting these two equation into equation 3.7 gives:

$$X_{CO} = \frac{y_{CO,in} \cdot F_{tot,in} - y_{CO,out} \cdot F_{tot,out}}{y_{CO,in} \cdot F_{tot,in}} \tag{3.10}$$

The GC analyzes the feed stream and product stream, and gives the concentration of each component. The concentration of a component is related to the area of the peak and the retention factor for that component as shown below:

$$y_i = A_i \cdot k_i \tag{3.11}$$

To minimize errors related to using the retention factors to determine the concentrations of the components, the fact that nitrogen is inert (internal standard) is used to relate the total molar outflow to the total molar feed as shown below:

$$F_{N_2,in} = F_{N_2,out} \tag{3.12}$$

$$y_{N_2,in} \cdot F_{tot,in} = y_{N_2,out} \cdot F_{tot,out} \tag{3.13}$$

$$F_{tot,out} = \frac{y_{N_2,in}}{y_{N_2,out}} \cdot F_{tot,in} \tag{3.14}$$

The expression for the total molar outflow is then substituted into equation 3.10:

$$X_{CO} = \frac{y_{CO,in} \cdot F_{tot,in} - y_{CO,out} \cdot F_{tot,in} \frac{y_{N_2,in}}{y_{N_2,out}}}{y_{CO,in} \cdot F_{tot,in}} \tag{3.15}$$

The total molar flow then cancels, and by rearrangement we get:

$$X_{CO} = \frac{\frac{y_{CO,in}}{y_{N_2,in}} - \frac{y_{CO,out}}{y_{N_2,out}}}{\frac{y_{CO,in}}{y_{N_2,in}}} \tag{3.16}$$

The molar concentrations (y_i) can now be substituted for the area and retention factor of each component (equation 3.11). The retention factors are the same in the feed and product, so they cancel each other out.

$$X_{CO} = \frac{\frac{A_{CO,in}}{A_{N_2,in}} - \frac{A_{CO,out}}{A_{N_2,out}}}{\frac{A_{CO,in}}{A_{N_2,in}}} \tag{3.17}$$

The conversion of CO_2 is calculated in the same way as in equation 3.17. The total carbon conversion is calculated as shown below:

$$X_{CO+CO_2} = f_{CO} \cdot X_{CO} + f_{CO_2} \cdot X_{CO_2} \tag{3.18}$$

Where f_i is a scaling factor, calculated as shown below for CO:

$$f_{CO} = \frac{F_{CO}}{F_{CO} + F_{CO_2}} \tag{3.19}$$

The scaling factor for CO_2 is calculated in the same way. The number of moles of CO and CO_2 is calculated from the GC result by using the corresponding retention factors:

$$f_{CO} = \frac{A_{CO} \cdot k_{CO}}{A_{CO} \cdot k_{CO} + A_{CO_2} \cdot k_{CO_2}} \tag{3.20}$$

When steady state was reached in the reactor, the pressure vessel was emptied. The time was recorded, and after a certain period of time, the procedure was repeated. This time, the liquid collected was analyzed to find the methanol content as well as identifying byproducts. The liquid product was weighed, and the amount of methanol in the product was estimated using a density meter (Anton Paar: DMA 4500). The rate of methanol formation was then taken as the estimated mass of methanol produced divided by the time elapsed between the first and second time the vessel was emptied.

GC analysis (offline analysis) of the product was used qualitatively to check for byproducts. The GC analysis of the liquid product was performed qualitatively to check if byproducts were formed.

To verify the conversion calculations, a mass balance on carbon can be performed. The amount of carbon coming into the system should be equal to the amount of carbon coming out; meaning that the amount of carbon detected by the GC in the feed gas analysis should be equal to the amount of carbon detected by the GC in the product gas and in the liquid product, i.e. carbon in feed gas = carbon in product gas + carbon in liquid product.

The amount of carbon coming out in the liquid product was taken as the rate of methanol formation. The amount of carbon in the product gas and feed gas is the sum of the amount of CO, CH_4 and CO_2.

$$F_{CO,in} + F_{CO_2,in} = F_{CH_3OH,out} + F_{CO_2,out} + F_{CH_4,out} + F_{CO,out} \tag{3.21}$$

For experiments like these, there is usually always an error in the carbon balance. This could be due to leakages, simplifications done when treating the data from the GC etc. The error in the carbon balance is therefore calculated:

$$E = 100\% \cdot \left(1 - \frac{F_{CO,in} + F_{CO_2,in}}{F_{CH_3OH,out} + F_{CO_2,out} + F_{CH_4,out} + F_{CO,out}}\right) \tag{3.22}$$

An error up to 5 % is usually acceptable for these types of experiments.

3.4.4 Catalyst Reduction

The catalyst was reduced in the reactor prior to the activity measurement. The reduction procedure was based on a procedure found in [15]. The total flow rate was 350 Nml/min, with 3 vol% H_2 and the rest N_2, at ambient pressure. The temperature program is given below in table 3.4. The temperature is increased in a careful manner to avoid sintering.

Table 3.4: *Reduction procedure for Cu/ZnO/* Al_2O_3 *catalyst. 350 nml/min flow rate, with 3 vol% hydrogen in nitrogen and ambient pressure.*

Step	**Start Temperature [K]**	**End Temperature [K]**	**Time [hour]**
1	Ambient	433	02:20
2	433	473	02:30
3	473	473	02:00
4	473	493	02:30
5	493	493	02:00
6	493	528	02:30
7	528	528	03:00

3.4.5 Methanol Synthesis

The activity test was begun after the catalyst reduction was completed. Premixed synthesis gas was used for all experiments with a composition of 65 % H_2, 25 % CO, 5 % CO_2 and 5 % N_2. The contact time was chosen to be 300 $^{ms \cdot g_{cat}}/_{ml}$ and the pressure was 50 bar for all experiments. The temperature was adjusted to obtain a WABT of 255 °C. The Weighted Average Bed Temperature (WABT) is defined as:

$$WABT = \sum_{i=1}^{n} w_i \cdot T_i \tag{3.23}$$

Where w_i is the mass of the catalyst in the i^{th} fraction of the catalyst bed and T_i is the measured temperature for the i^{th} fraction of the catalyst bed. The WABT was measured by moving the thermocouple along the reactor axis. The length and position of the catalyst bed relative to the thermowell was measured using a ruler.

Methanol synthesis experiments were performed to compare the activity of the homemade catalyst to the activity of the commercial catalyst. The activity of diluted commercial catalyst was also tested. The catalyst was then diluted with silicon carbide at the ratio of 5:1. The homemade catalyst was tested as a part of the specialization project conducted in the fall of 2013.

The kinetics of the methanol synthesis was investigated by varying the temperature and the contact time for the diluted commercial catalyst.

Chapter 4

Results

4.1 Catalyst Synthesis

4.1.1 Methanol Catalyst

Two batches of the $Cu/Zn/Al_2O_3$ catalyst were synthesized, as described in section 3.2.1. Both batches were analyzed by high resolution Inductively Coupled Plasma Mass Spectrometry (ICP-MS) by an external laboratory. ICP-MS identifies metals present in a material quantitatively.

The original report from the high resolution ICP-MS analysis is included in appendix B. Table 4.1 gives the metal concentration of copper, zinc, aluminium and sodium in the two batches of $Cu/Zn/Al_2O_3$ catalyst. Metal concentrations listed in the synthesis procedure are included as reference.

Table 4.1: *Calculated metal concentrations for homemade methanol catalysts based on high resolution ICP-MS analyses. Metals present in trace amounts were neglected.*

Batch	**Cu**	**Zn**	**Al**	**Na**
#	wt%	wt%	wt%	wt%
1	23.0	33.3	8.60	5.31
2	22.4	33.6	8.36	4.57
reference	24.3	36.2	10.2	$1.7 \cdot 10^{-5}$

As seen in table 4.1, the amount of copper, zinc and aluminium is similar to the amounts listed in the reference. The amount of sodium however, is considerably higher in the synthesized catalysts compared to the reference value listed in the synthesis procedure. The amount of sodium identified by the ICP-MS analysis was 5.31 wt% and 4.57 wt% for the first and second batch respectively. According to the

synthesis procedure, the amount of sodium in the catalyst should be less than 100 ppm. Hayer [1] and Bakhtiary-Davijany [15] both report sodium concentrations in the ppm levels for catalysts synthesized by the same procedure.

4.1.2 ZSM-5 Catalyst

Several batches of ion-exchanged ZSM-5 zeolites were prepared, as described in section 3.2.2. Different extents of ion-exchange were attempted by varying the amount of sodium added. Ion-exchange extent of 30 %, 40 %, 60 % and 80 % was attempted for the ZSM-5 zeolite with molar $SiO_2 : Al_2O_3$ ratio of 80. 30 % of the protons were attempted to be exchanged with sodium for the ZSM-5 zeolite with molar $SiO_2 : Al_2O_3$ ratio of 30.

To determine the extent of ion-exchange, high resolution ICP-MS analyses were obtained from an external supplier, for the zeolites with intended 30 % ion exchange. To determine the validity of the analysis, the hydrogen form of the zeolites were analyzed as well. The analyses were performed twice.

The original report from the high resolution ICP-MS analysis is included in appendix B. Table 4.2 gives the metal concentration of silicon, aluminium and sodium.

Table 4.2: *Calculated metal concentrations for various zeolites as determined by ICP-MS analyses. Metals present in trace amounts were neglected.*

Sample	**Na** wt%	**Si** wt%	**Al** wt%
H-ZSM-5 80 1	0.004	32.5	0.97
H-ZSM-5 80 2	0.002	72.2	3.25
H-ZSM-5 30 1	0.006	20.6	0.82
H-ZSM-5 30 2	0.003	45.5	2.75
Na,H-ZSM-5 80 1	0.10	32.8	0.36
Na,H-ZSM-5 80 2	0.11	41.9	0.94
Na,H-ZSM-5 30 1	0.38	34.1	1.13
Na,H-ZSM-5 30 2	0.31	41.6	2.45

As seen in table 4.2, the concentration of the metals differs considerably between the first and second analysis for the same sample.

Based on the results given in table 4.2, the molar ratio of silica to alumina was calculated, to determine the validity of the results. The extent of ion-exchange was also calculated as molar percentage of sodium to aluminium. The calculated molar ratios and extent of ion-exchange are given in table 4.3.

As seen in table 4.3, the calculated molar ratio of silica to alumina is not consistent between the analyses (e.g. H-ZSM-5 80 1 and H-ZSM-5 80 2), nor between zeolites with the same molar silica to alumina ratio (e.g. H-ZSM-5 80 1 and Na,H-ZSM-5

Table 4.3: *Calculated molar ratio of silica to alumina, and molar percentage of sodium to aluminium in various zeolites as determined by ICP-MS analyses.*

Sample	$\mathbf{SiO_2/Al_2O_3}$ mol/mol	$\mathbf{Na/Al}$ mol%
H-ZSM-5 80 1	64.3	0.14
H-ZSM-5 80 2	72.2	0.21
H-ZSM-5 30 1	20.6	0.26
H-ZSM-5 30 2	45.5	0.38
Na,H-ZSM-5 80 1	32.8	32.4
Na,H-ZSM-5 80 2	41.9	13.0
Na,H-ZSM-5 30 1	34.1	39.7
Na,H-ZSM-5 30 2	41.6	14.9

80 1). Furthermore, the calculated molar ratio of silica to alumina is not consistent with the expected values. H-ZSM-5 is found to have a calculated molar silica to alumina ratio of 64 and 72 for the first and second analysis respectively. According to the supplier, this ratio should be 80 [45].

The extent of ion-exchange (mol%) is also not consistent. The extent of ion-exchange is between 13 and 15 mol% for the first analysis, and between 32 and 40 mol% for the second analysis. The extent of ion-exchange attempted was 30 % for both samples.

As the overall quality of the results of the ICP-MS analysis seems to be too low for quantification, the extent of ion-exchange cannot be determined. Qualitatively, it is useful for confirming the presence of sodium and that the amount of silicon is higher than aluminium.

4.2 Catalyst Characterization

4.2.1 Nitrogen Adsorption

The Micromeritics TriStar 3000 instrument was used to determine the surface area of relevant catalysts. Table 4.4 below gives the surface area, as determined by the BET method, for the various catalysts investigated.

Table 4.4: *Surface area of catalysts relevant for DME synthesis as determined by the BET method.*

Catalysts	$\mathbf{S_{BET}}$ m^2/g
$Cu/ZnO/Al_2O_3$ batch 1	42.8 ±0.2
$Cu/ZnO/Al_2O_3$ batch 2	63.3 ±0.2
$Cu/ZnO/Al_2O_3$ reference [1, 15]	80
γ alumina	194 ±0.8
HZSM-5 80	377 ±15
HZSM-5 80 reference [45]	425

As seen in the table 4.4, the BET surface area was determined to be about 43 and 63 m^2/g for the first and second batch of homemade methanol catalyst respectively. Both batches have lower surface area than the reference; Bakhtiary-Davijany and Hayer both report surface areas of about 80 $^{m^2}/_g$ [1, 15].

The surface area of H-ZSM-5 80 was determined to be 377 ±15 $^{m^2}/_g$. This is substantially lower than the value reported by the supplier. The applicability of the BET isotherm for zeolites will be considered in the discussion. The surface area of the other methanol dehydration catalyst, γ alumina, is about half that of the zeolite.

4.2.2 X-ray Diffraction

The Bruker D8 Advance DaVinci X-ray Diffractometer was used to analyze samples of the catalysts relevant to DME synthesis. The diffraction patterns for the homemade methanol catalyst (batch 1), γ alumina and H-ZSM-5 80 are shown in figure 4.1. The diffraction patterns were modified (removal of background, smoothing of peaks) using $DIFFRAC^{plus}$ EVA software. The crystalline phases of the samples are matched to reference patterns (vertical lines).

As seen in figure 4.1a, the phases in the homemade methanol catalyst are matched to CuO, $Cu_{0.02}Zn_{0.98}O$ and $Zn_6Al_2O_9$. Due to overlapping peaks, the particle size of CuO was not determined, as this was considered to be beyond the scope of this project. Since the diffractograms of the two batches of homemade methanol catalysts were more or less identical, only the diffractogram of the first batch is shown.

The diffractogram of the zeolite, figure 4.1c indicates a high degree of crystallinity as the peaks are sharp and well defined. Comparing the diffractograms of γ alumina and the zeolite, the peaks are less sharp and defined for γ alumina, indicating a lower degree of crystallinity, as expected. The peaks for both the zeolite and γ alumina are reasonably well matched with the reference patterns.

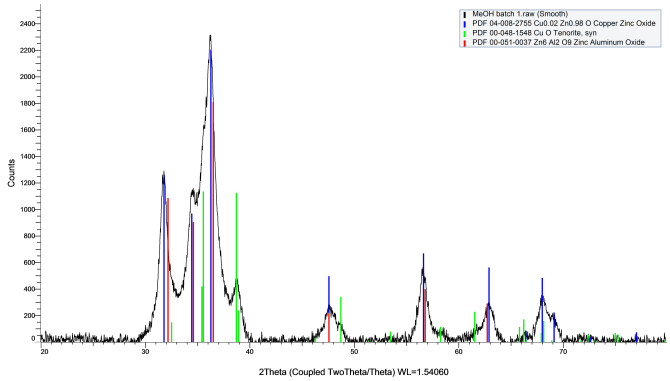

(a) $Cu/ZnO/Al_2O_3$

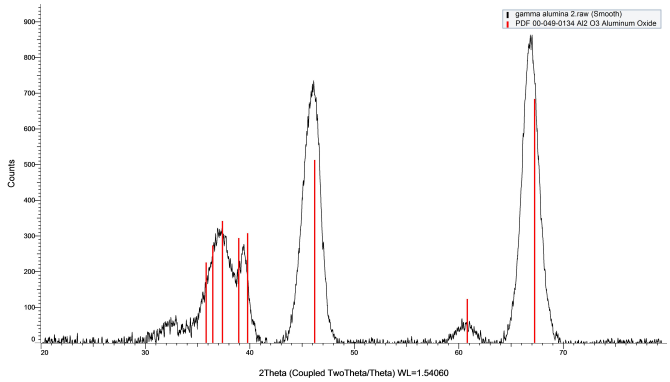

(b) γ *alumina*

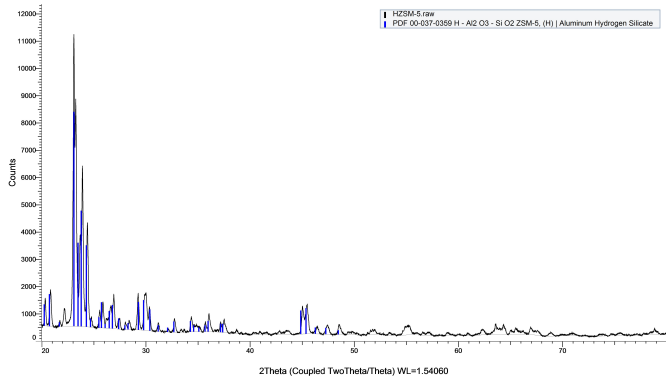

(c) *H-ZSM-5*

Figure 4.1: *X-ray Diffraction patterns for catalysts relevant to DME synthesis. The vertical lines represents reference peaks, matched to the diffraction pattern using* $DIFFRAC^{plus}$ *EVA software*

4.2.3 Nitrous Oxide Titration

The homemade methanol catalyst (batch 2) was investigated by nitrous oxide titration to determine the copper dispersion. Appendix C shows the calculations as well as the raw data for the catalyst reduction.

The homemade methanol catalyst was tested twice. Figure 4.2 shows the raw data for the N_2O titration.

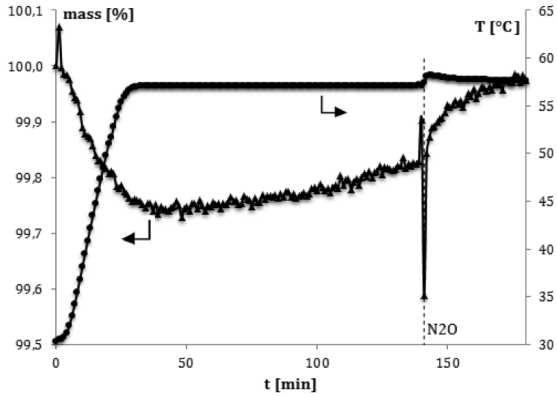

(a) *Homemade methanol catalyst, 1. trial*

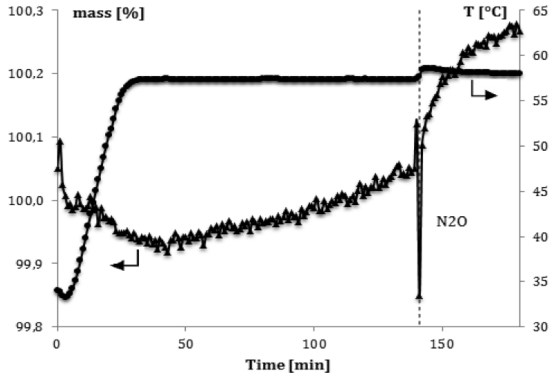

(b) *Homemade methanol catalyst, 2. trial*

Figure 4.2: *Mass change and temperature as a function of time. The dashed vertical lines represents N_2O introduction.*

As seen in figure 4.2a and 4.2b, the temperature increased slightly upon N_2O introduction. This caused some disturbance in the sample mass, which complicated the calculation of the dispersion.

Figure 4.3 shows the mass change as a function of the square root of the exposure time. Linear regression was performed using Excel and the y-intercept of this line

was used to calculate the dispersion as shown in Appendix C.

The mass change was calculated based on the mass just prior to the introduction of N_2O. This mass was taken as 100 %, and the following recorded masses were normalized on this basis.

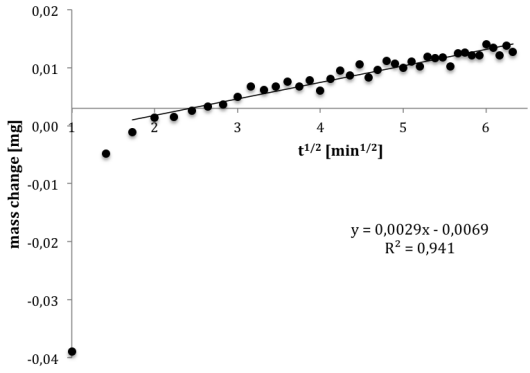

(a) *Homemade methanol catalyst, 1. trial*

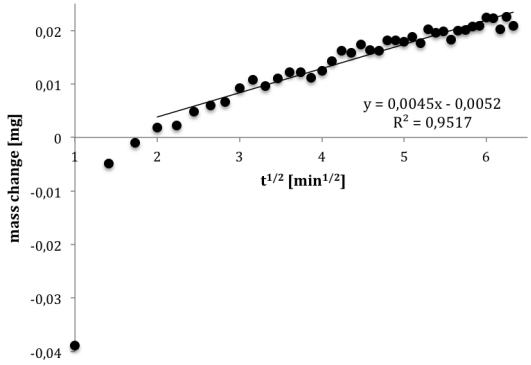

(b) *Homemade methanol catalyst, 2. trial*

Figure 4.3: *Mass change as a function of the square root of exposure length. Linear regression was performed using Excel.*

As seen in figure 4.3a and 4.3b, the linear fit is fairly good. The first few points were omitted when performing the linear regression. This affected the y-intercept of the line, and therefore the calculated dispersion.

Table 4.5 shows the calculated dispersion for the homemade catalyst, based on mass change during reduction and based on copper loading, as determined by the ICP-MS analysis.

Table 4.5: *Calculated dispersion for homemade methanol catalyst based on mass change during reduction and based on copper loading (*)*

Catalysts	**Dispersion** %	**Dispersion*** %
Homemade, trial 1	1.6	1.7
Homemade, trial 2	0.9	1.2

As seen in table 4.5, the calculated dispersion is higher for the first trial than for the second trial, independent of calculation method. The dispersion calculated for the second trial is significantly higher when the copper loading is used in the calculation. The calculated dispersion is more consistent for the different calculation methods for the first trial. In any case, a low dispersion is found for the homemade methanol catalyst.

4.2.4 Temperature Programmed Desorption

Ammonia TPD

The acidic methanol dehydration catalysts were characterized by ammonia temperature-programmed desorption in a thermogravimetric analysis (TGA) instrument, as described in section 3.3.4. Two different temperature programs were used, but this was assumed not to affect the results. H-ZSM-5 80 was analyzed with both temperature programs and the results were very similar, as shown in appendix D.

Figure 4.4 shows the variation in catalyst mass as a function of temperature for H-ZSM-5 30, H-ZSM-5 80 and γ alumina.

As seen in figure 4.4a, the mass loss is greatest for H-ZSM-5 30, indicating that this catalyst has the highest concentration of acid sites. The shape of the curve is nearly identical for the two zeolites.

The mass loss for γ alumina is in between that of the two zeolites. Unlike the two zeolites, the curve of γ alumina shows a continued decrease at temperatures above 500 °C, indicating the presence of stronger acid sites.

From figure 4.4b, where the differential mass change is plotted as a function of temperature, It is again observed that the shape of the curves for the two zeolites is nearly identical. Two minima are observed for the zeolites, indicating the presence of two major groups of acid sites. The first minimum is located at around 200 °C, while the second is located at around 380 °C.

γ alumina also displays two minima, indicating the presence of at least two major groups of acid sites. The first minimum is located at low temperature, about 180 °C, while the second minimum is located at about 320 °C. Both minima are located at slightly lower temperature compared to the minima of the zeolites. This

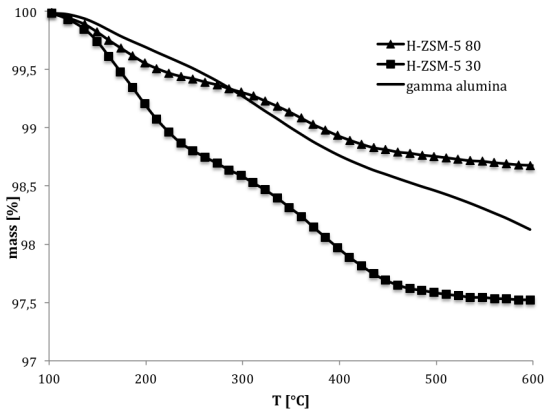

(a) *Mass change*

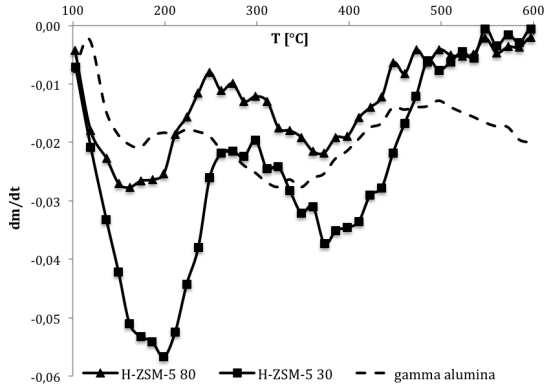

(b) *Differential mass change*

Figure 4.4: *Variation in sample mass during ammonia TPD for H-ZSM-5 30, H-ZSM-5 80 and γ alumina*

indicates that the zeolites have stronger acid sites. However, γ alumina also displays a continued decrease at 600 °C. This decrease is most likely due to the presence of a third group of acid sites, with higher acid strength.

Figure 4.5 shows the variation in catalyst mass as a function of temperature for H-ZSM-5 30 and Na(30),H-ZSM-5 30.

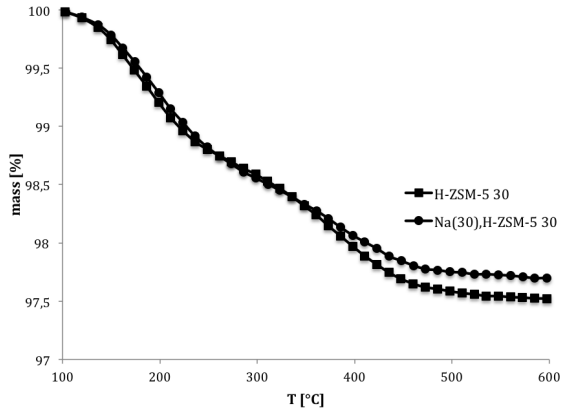

(a) *Mass change*

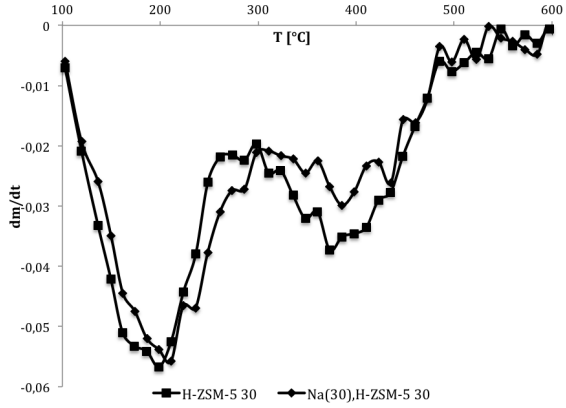

(b) *Differential mass change*

Figure 4.5: *Variation in sample mass during ammonia TPD for H-ZSM-5 30, Na(30),H-ZSM-5 30*

As seen in figure 4.5a, the mass loss of the two zeolites are more or less indistinguishable at low temperature. At higher temperature, around 380 °C, a difference is mass loss can be observed; the mass loss for H-ZSM-5 is greater than the mass loss for the ion-exchanged zeolite. This indicates a higher concentration of acid sites in the fully protonated zeolite. Moreover, the difference in mass loss is mostly evident at high temperature, indicating that sodium has predominantly replaced protons associated with strong Brønsted acid sites.

Figure 4.5b shows the differential mass change as a function of temperature. The trend is the same for both zeolites with two minima, one located at around 200 °C, and one located at around 380 °C. The difference between the two zeolites is most pronounced at high temperature, indicating again that the ion-exchange has

mainly taken place at strong acid sites.

Figure 4.6 shows the variation in catalyst mass as a function of temperature for the fully protonated and the ion-exchanged ZSM-5 zeolites with molar silica to alumina ratio of 80.

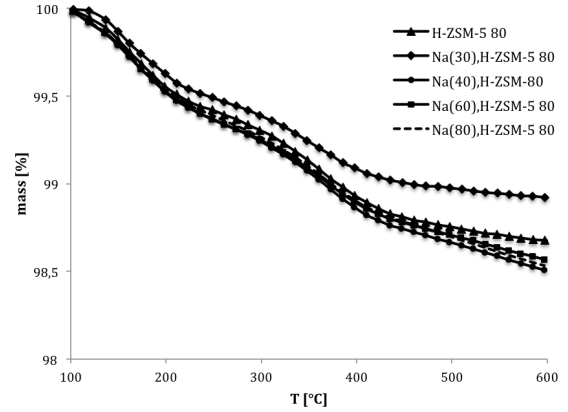

(a) *Mass change*

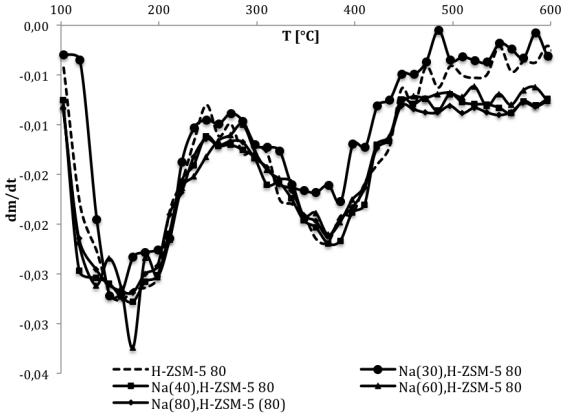

(b) *Differential mass change*

Figure 4.6: *Variation in sample mass during ammonia TPD for H-ZSM-5 80, Na(30),H-ZSM-5 80, Na(40),H-ZSM-5 80, Na(60),H-ZSM-5 80 and Na(80),H-ZSM-5 80*

As seen in figure 4.6a, the zeolite where 30 % of the protons were attempted exchanged with sodium shows the lowest mass loss. The zeolites where 40, 60 and 80 % of the protons were attempted exchanged with sodium show more or less identical mass loss. Surprisingly, the mass loss associated with these zeolites is nearly identical to the mass loss of the fully protonated zeolite. When more and more of the protons are exchanged with sodium, it is expected to see a decrease in

the acid site concentration, which should manifest by showing less and less mass loss during ammonia TPD. As the extent of ion-exchange has not been confirmed, it is likely that the extent of ion-exchange for these zeolites is lower than intended. Another possible explanation for the strange behavior is the fact that the zeolites where 40, 60 and 80 % of the protons were attempted exchanged with sodium were analyzed by a different temperature program.

The difference in mass loss between H-ZSM-5 80 and Na(30),H-ZSM-5 80 is more pronounced at high temperature, indicating that sodium has predominantly replaced protons associated with strong acid sites.

In figure 4.6b, more or less identical behavior is observed for all the zeolites. Two minima can be observed for all catalysts, indicating the presence of two major groups of acid sites.

The total mass loss during the temperature ramp was calculated for all catalysts. The catalyst mass just prior to the temperature ramp was used as the initial mass, and the catalyst mass at the end of the temperature ramp was used as the final mass. The mass loss occurring between 100 and 300 °C and between 300 and 600 °C was also calculated. This is shown in table 4.6.

Table 4.6: *Calculated total mass loss and mass loss at low temperature (Δm_{weak}) and at high temperature (Δm_{strong}), for the investigated acidic catalysts during NH_3 TPD experiments.*

Catalyst	$\mathbf{\Delta m_{tot}}$ wt%	$\mathbf{\Delta m_{weak}}$ wt%	$\mathbf{\Delta m_{strong}}$ wt%
H-ZSM-5 30	2.48	1.41	1.07
H-ZSM-5 80	1.64	0.68	0.94
H-ZSM-5 80 (2)	1.63	0.74	0.89
γ alumina	1.87	0.72	1.15
Na(30),H-ZSM-5 30	2.30	1.44	0.86
Na(30),H-ZSM-5 80	1.27	0.61	0.66
Na(40),H-ZSM-5 80	1.49	0.75	0.74
Na(60),H-ZSM-5 80	1.43	0.75	0.69
Na(80),H-ZSM-5 80	1.47	0.7 1	0.74

As seen in table 4.6, the total mass loss is greatest for H-ZSM-5 30. The total mass loss for Na(30),H-ZSM-5 30 is about 7 % lower than the mass loss for the fully protonated zeolite. This indicates that the extent of ion-exchange is likely lower than the intended 30 %. The mass loss at low temperature is about the same, while the mass loss at high temperature is significantly higher for the fully protonated zeolite. This indicates that sodium has mainly replaced hydrogen at strong acid sites. Both zeolites have higher mass loss at low temperature than at high temperature.

Note that the total mass loss for the two experiments on H-ZSM-5 80 is very similar. The zeolite pretreated at low temperature has a higher mass loss at low

temperature and a lower mass loss at high temperature compared to the zeolite pretreated at high temperature.

The total mass loss for γ alumina is somewhat higher than for H-ZSM-5 80, but lower than the total mass loss for H-ZSM-5 30, as observed in figure 4.4a. The mass loss at high temperature is significantly higher than at low temperature for this catalyst, indicating that the concentration of strong acid sites is greater than the concentration of weak acid sites. γ alumina has the highest mass loss at high temperature, indicating that γ alumna has the highest concentration of strong acid sites.

The calculated total mass loss for the ion-exchanged ZSM-5 zeolites with molar silica to alumina ratio are quite similar to the total mass loss for the fully protonated zeolite. The lowest total mass loss is observed for the zeolite with intended 30% ion-exchange. The total mass loss for this zeolite is about 23 % lower than for the fully protonated zeolite. The mass loss at low temperature is very similar, but the mass loss at high temperature is significantly lower for the ion-exchanged zeolite. This indicates that sodium has mainly replaced hydrogen at strong acid sites.

The total mass loss observed for the zeolites with 40 %, 60 % and 80 %, are very similar to each other, and actually higher than for the zeolite with 30 % ion-exchange. This indicates that the extent of ion-exchange is lower than intended for these zeolites. Another possibility is that the temperature program used has affected the results. The three ion-exchanged zeolites with 40, 60 and 80 % ion-exchanged were all analyzed with the second temperature program with lower pretreatment temperature. The mass loss at low temperature and high temperature is very similar for these zeolites. Compared to the fully protonated zeolite, the mass loss at low temperature is very similar, and the mass loss at high temperature somewhat lower.

Isopropylamine TPD

The acidic catalysts were also investigated by temperature-programmed desorption with isopropylamine as the probe gas, as described in section 3.3.4. The TPD experiments were performed in a thermogravimetric analysis (TGA) instrument coupled with mass spectrometry (MS). Different experimental protocols were tried, as the procedure for isopropylamine TPD in TGA instruments is not established and straightforward. The different experimental protocols were as follows:

- Protocol 1: no pretreatment, exposure to isopropylamine vapor overnight
- Protocol 2: degassed at 200 °C overnight and subsequently exposed to isopropylamine vapor for 5 hours
- Protocol 3: degassed at 200 °C for 24 hours and subsequently exposed to liquid isopropylamine and subsequently dried at 100 °C in a forced air oven

- Protocol 4: degassed at 200 °C for 24 hours and subsequently exposed to isopropylamine vapor for 20 hours

Figure 4.7 shows mass change as a function of temperature for H-ZSM-5 with a molar $SiO_2 : Al_2O_3$ ratio of 30, subjected to different experimental protocols.

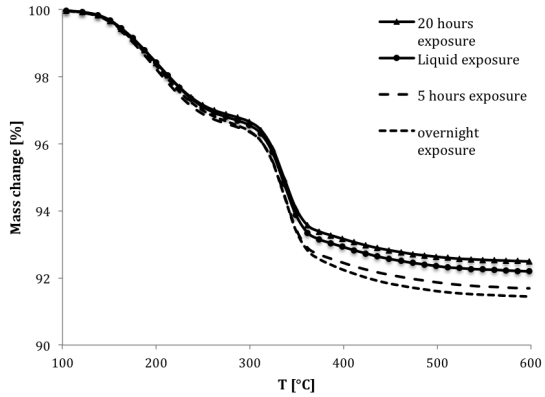

(a) *Mass change*

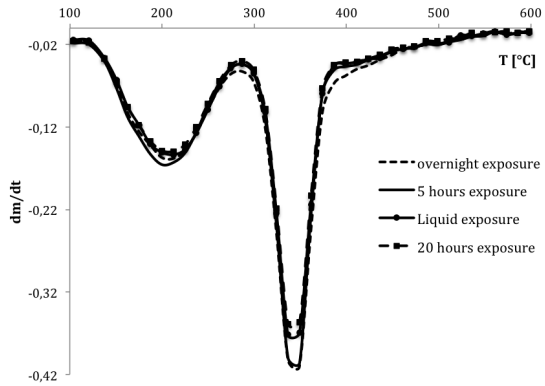

(b) *Differential mass change*

Figure 4.7: *Variation in sample mass during isopropylamine TPD for H-ZSM-5 30. The samples were subjected to pretreatment at varying length and subsequently exposed to isopropylamine, also at varying length*

As seen in figure 4.7a, the samples display more or less identical behavior at low temperature. At high temperature, above 350 °C, some differences can be observed; the samples labeled overnight exposure and 5 hours exposure display slightly higher mass loss compared to the other two samples.

Figure 4.7b shows the differential mass change as a function of temperature for H-ZSM-5 30 subjected to different experimental protocols. Two well defined minima

can be observed for all experimental protocols. The difference between the experimental protocols is again most pronounced at high temperature The first minimum is observed at around 200 °C, while the second minimum is located at around 350 °C. The second minimum is most likely due to desorption from Brønsted acid sites, as this is known to occur between 300 and 380 °C [26, 38].

Table 4.7 summarizes the different experimental protocols and gives the total mass loss during the temperature ramp.

Table 4.7: *Experimental protocols for isopropylamine TPD experiments on H-ZSM-5 with molar ratio of SiO_2 : Al_2O_3 of 30. The total mass loss obtained with the different experimental protocols is included.*

Protocol	**Pretreatment**	**Exposure**	**Mass loss**
1	None	vapor, overnight	8.56 %
2	200 °C, overnight	vapor, 5 hours	8.31 %
3	200 °C, 24 hours	liquid, dried overnight at 100 °C	7.81 %
4	200 °C, 24 hours	vapor, 20 hours	7.51 %

As seen in table 4.7, the total mass loss for the H-ZSM-5 30 catalyst varied some with the experimental procedure. The highest mass loss is observed with no pretreatment and exposure to isopropylamine vapor overnight, while the lowest mass loss is observed with pretreatment for 24 hours and exposure to isopropylamine vapor for 20 hours. Observing higher mass loss without pretreatment is natural, as adsorbed impurities are not desorbed prior to isopropylamine exposure. However, the mass was not monitored during pretreatment or adsorption, so it is difficult to draw a conclusion about the suitability of the different experimental protocols.

Figure 4.8 shows the variation in sample mass as a function of temperature for Na(30),H-ZSM-5 80, H-ZSM-5 80 and H-ZSM-5 30. All samples were analyzed using experimental protocol 1.

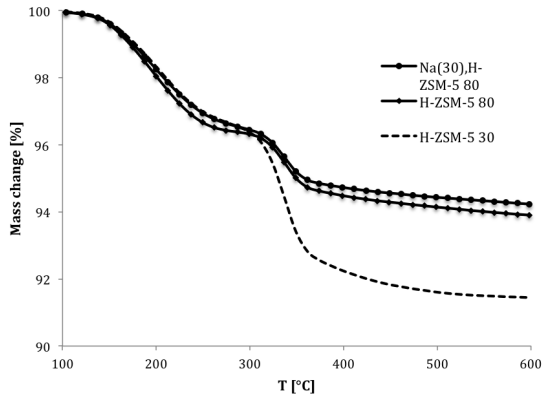

(a) *Mass change*

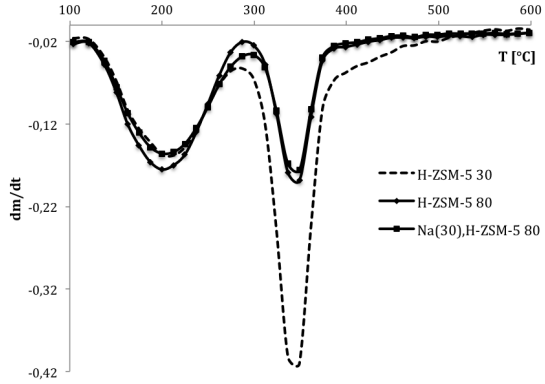

(b) *Differential mass change*

Figure 4.8: *Variation in sample mass during isopropylamine TPD for H-ZSM-5 30, H-ZSM-5 80 and Na(30),H-ZSM-5 80.*

As seen in figure 4.8a the mass change is very similar at low temperature. At higher temperature, above 300 °C, H-ZSM-5 30 displays significantly higher mass loss than the two ZSM-5 zeolites with molar silica to alumina ratio of 80. This indicates that the concentration of acid sites is significantly higher for H-ZSM-5 30 compared to H-ZSM-5 80 and Na(30),H-ZSM-5 80.

The difference between the two zeolites with the same molar silica to alumina ratio is small at all temperatures, but some difference can be observed at higher temperatures. This indicates that sodium has predominantly replaced protons associated with strong Brønsted acid sites.

Two well defined minimums can be observed for all zeolites in figure 4.8b, indicating that there are two major groups of acid sites in the catalysts. The minima are located at the same temperature for all samples.

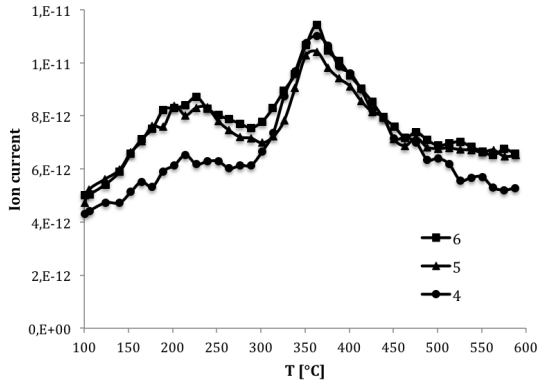

(a) *Ammonia (m/z = 17)*

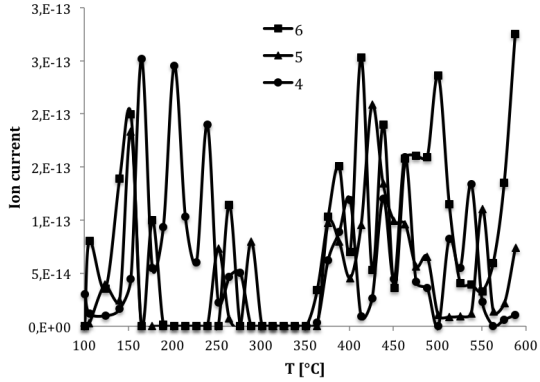

(b) *Propene (m/z = 41)*

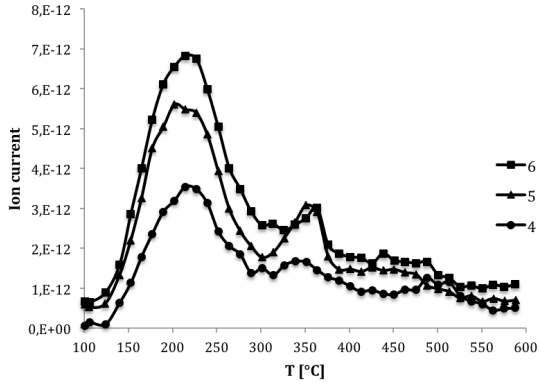

(c) *Isopropylamine (m/z = 44)*

Figure 4.9: *MS analysis of exhaust from thermogravimetric analysis instrument for isopropylamine TPD experiments on H-ZSM-5 30 (4), H-ZSM-5 80 (5) and Na(30),H-ZSM-5 80 (6).*

Figure 4.9 shows the results of the MS analysis for the H-ZSM-5 30, Na(30),H-ZSM-5 (80) and H-ZSM-5 80. The base peak (most abundant ion) is shown for ammonia, isopropylamine and propene, as the desorption product from Brønsted acid sites is known to be propene and ammonia, while the desorption product from Lewis acid sites is known to be isopropylamine [26, 38].

As seen in figure 4.9a, ammonia has two peaks, one at around 200 °C and one at 380 °C for all samples. The peak at low temperature is higher for the zeolites with molar silica to alumina ratio of 80, than for the zeolite with molar ratio of 30. The second peak is nearly identical among the zeolites, and higher than the first peak. The temperature range for the ammonia peaks corresponds well with the temperature range in which the minima were observed in figure 4.8b. This indicates that the mass loss associated with both minima have contributions of desorption from Brønsted acid sites for all zeolite, albeit this contribution is small for the zeolite with molar silica to alumina ratio of 30.

As seen in figure 4.9c, isopropylamine also has two peaks, in about the same temperature range as ammonia. This suggests that the mass loss associated with both minima have contributions of desorption from either Lewis acid sites or desorption of physisorbed probe. The peak at low temperature is highest for the ion-exchanged zeolite, and lowest for the zeolite with molar silica to alumina ratio of 30. The peak at high temperature is lower for all samples. H-ZSM-5 80 and Na(30),H-ZSM-5 80 have nearly identical isopropylamine peaks at high temperature, and the peaks are significantly higher than for H-ZSM-5 30.

As the MS results for propene, figure 4.9b are very noisy, the analysis is not very precise. Note also that the intensity of the signal is lower than for ammonia and isopropylamine. Nevertheless, two peaks may be observed, at more or less the same temperatures as for ammonia and isopropylamine. This again indicates that the two minimums observed have contributions of desorption from Brønsted acid sites.

The MS analysis is however somewhat simplified, as only the base peaks are shown for each compound.

4.2.5 Adsorption Microcalorimetry

Volume calibrations were carried out as described in section 3.3.5 and are included in appendix E. There was some difficulty with the calibration of the volume V_2 (see section 3.3.5). This affected the calculations, rendering the results somewhat uncertain. To try to account for this uncertainty, the adsorbed amount for each dose is calculated with two different average values for V_2.

Several adsorption calorimetry experiments were performed with the H-ZSM-5 zeolite with a molar ratio of $SiO_2 : Al_2O_3$ of 30. As characterization of acidic catalysts using ammonia as probe gas had not been carried out in this setup before, the experimental procedure was developed by trial and error. The main difficulty

was in adjusting the amount of catalyst used and the amount of probe gas sent in each dose.

Figure 4.10 shows the results of the second experiment, where the differential heat of adsorption is plotted as a function of the adsorbed amount of ammonia per unit cell (u.c.) of catalyst. The number of unit cells in the catalyst sample was calculated by using the molecular mass of a unit cell as shown in appendix E.

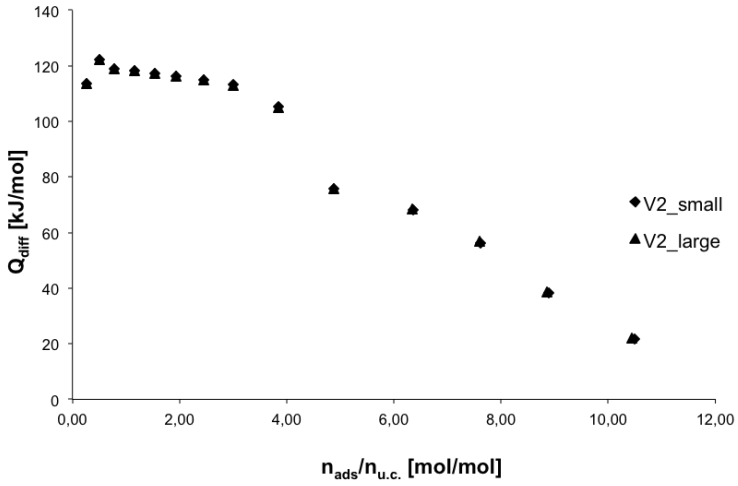

Figure 4.10: *Differential heat of adsorption as a function of adsorbed amount of ammonia per u.c. of H-ZSM-5 30, 2. trial. Two sets of data are shown for different average values of* V_2.

As seen in figure 4.10, the differential heat of adsorption is quite stable around 120 kJ/mol initially. As the catalyst sample becomes more and more saturated with ammonia, the differential heat of adsorption decreases. As one unit cell consists of 6 aluminium atoms, 1:1 coverage is obtained at $n_{ads}/n_{u.c.} = 6$. Note that nearly identical results are obtained for the two different average values of V_2.

The initial differential heat of adsorption is lower than expected. Auroux [25, 43] reports the initial heat of adsorption to be between 150 and 160 kJ/mol for H-ZSM-5 with similar molar silica to alumina ratios and at identical conditions. The suspected reason for obtaining lower initial heat of adsorption is too large dosing amounts relative to the catalyst mass.

Figure 4.11 shows the differential heat of adsorption as a function of the amount of ammonia adsorbed per unit cell of catalyst for the third trial. The catalyst mass and the initial dosing amounts were decreased compared to the second trial.

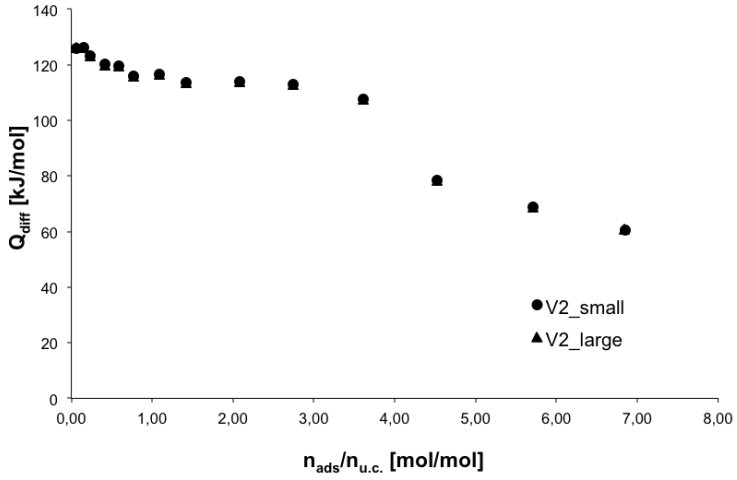

Figure 4.11: *Differential heat of adsorption as a function of adsorbed amount of ammonia per u.c. of H-ZSM-5 30, 3. trial. Two sets of data are shown for different average values of* V_2.

As seen in figure 4.11, the initial heat of adsorption is about 125 kJ/mol. This is somewhat higher than for the second trial, but it is still lower than expected. The suspected reason for obtaining lower initial heat of adsorption is still too large dosing amounts relative to the catalyst mass. The results obtained with the two different average values of V_2 are nearly identical.

Another attempt to probe the strongest acidic sites were performed, this time with lower initial dosing amounts, and larger amount of catalyst compared to the other trials. Figure 4.12 shows the differential heat of adsorption as a function of the amount of ammonia adsorbed per u.c. of catalyst for this trial.

As seen in figure 4.12, the initial heats of adsorption is very low, less than 100 kJ/mol. The doses associated with these heats were very small, resulting in poorly defined peaks, as seen in the thermograph included in appendix E. The baseline integration of these peaks is therefore uncertain, and the points should thus be ignored as measurement errors. It is also evident from figure 4.12 that the uncertainty associated with the volume calibration is significant for this experiment. The set of data where the adsorbed amount has been calculated with the smaller value of V_2 gives significantly higher heats of adsorption than the when the larger value of V_2 is used.

With the smaller value of V_2, the initial heat of adsorption (ignoring the first three points), falls into the range reported by Auroux [25, 43]. However, the uncertainty associated with these results remains high.

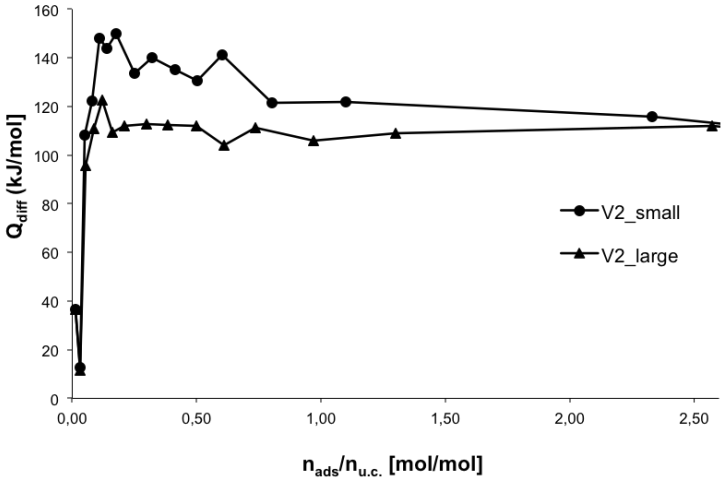

Figure 4.12: *Differential heat of adsorption as a function of adsorbed amount of ammonia per u.c. of H-ZSM-5 30, 2. trial. Two sets of data are shown for different average values of* V_2.

Adsorption Isotherms

The amount of irreversibly adsorbed ammonia was determined by subjecting the catalyst to a cycle of adsorption (I), followed by desorption by evacuation of the calorimetric cell and finally readsorption (II). Figure 4.13 shows the recorded isotherms for the first and second adsorption cycle, with adsorbed amount of ammonia as a function of pressure.

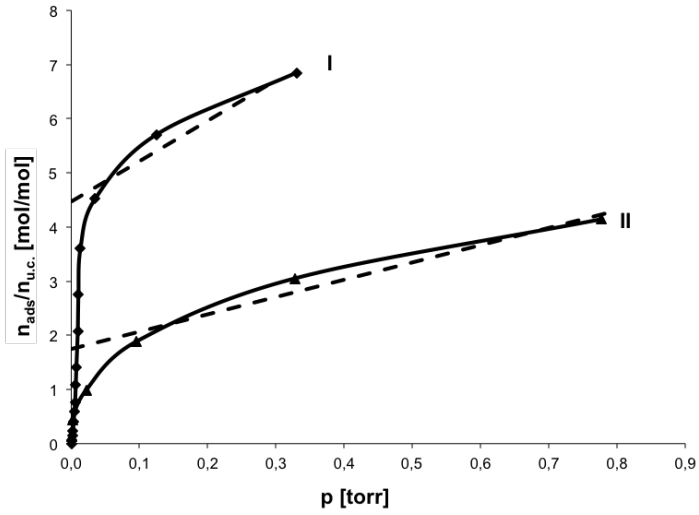

Figure 4.13: *Adsorbed amount of ammonia per u.c. of catalyst as a function of pressure for a cycle of adsorption (I) - desorption - readsorption (II). Linear regression was performed using Excel for the last three data points for each series (dashed lines).*

As seen in figure 4.13, the adsorbed amount of ammonia per unit cell of catalyst is higher for the first round of adsorption (I) compared to the second round (II). This means that some of the ammonia is reversibly and therefore weakly adsorbed. The amount of irreversibly adsorbed ammonia was calculated by subtracting the second isotherm from the first. Linear regression was performed for the last three data points for each adsorption series. This is shown as dashed lines in figure 4.13.

To calculate the irreversibly adsorbed amount of ammonia, the y-intercept of the second isotherm was subtracted from the y-intercept of the first isotherm. The amount of irreversibly adsorbed ammonia was calculated to be 2.7 moles of ammonia adsorbed per mole of unit cell. This value is reasonable agreement with literature. Auroux [43] reports the irreversibly adsorbed volume of ammonia to be 2.2 molecules per unit cell for H-ZSM-5 with molar silica to alumina ratio of 27 at the identical conditions.

4.3 Methanol Synthesis

Methanol synthesis experiments have been performed to compare the activity of the homemade catalyst to the activity of the commercial catalyst. The activity of diluted commercial catalyst was also investigated. The catalyst was diluted with silicon carbide at the ratio of 5:1. The activity was measured at 50 bar, WABT =

255 °C and a contact time of 300 $^{ms \cdot g_{cat}}/_{ml}$. Premixed synthesis gas was used for all experiments with a composition of 65 % H_2, 25 % CO, 5 % CO_2 and 5 % N_2.

The mass flow controllers were calibrated prior to the experiments by A. Montebelli [44]. The calibration curves are included in appendix F.

Figure 4.14 compares the CO conversion of the homemade catalyst with the initial CO conversion for the commercial catalyst (undiluted and diluted case). The first CO conversion shown is the first measurement after the temperature, pressure and flow was established.

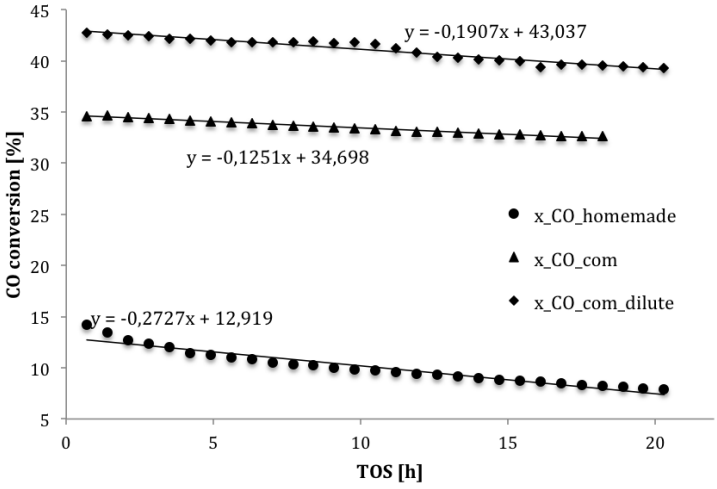

Figure 4.14: *CO conversion, at identical conditions; 50 bar, WABT = 255 °C and a contact time of 300* $^{ms \cdot g_{cat}}/_{ml}$*, as a function of time on stream (TOS) for three methanol synthesis experiments in a fixed bed reactor.*

As seen in figure 4.14, the activity of the commercial catalyst is significantly higher than the activity of the homemade catalyst. The activity of the diluted commercial catalyst is somewhat higher than for the undiluted commercial catalyst. The activity is decreasing nearly linearly for all three cases.

Based on the slope of the regression lines, it seems that the deactivation rate is higher for the homemade catalyst than for the two cases with commercial catalyst. The diluted commercial catalyst seems to be deactivating more quickly than the undiluted commercial catalyst.

The CO conversion was calculated from the results of the online GC analysis and the result of the feed analysis, as shown in section 3.4.3. The carbon balance was calculated for the first experiment. The error in the carbon balance never exceeded 2.2 %. The feed analysis and carbon balance calculation are shown in appendix G.

A sample of the liquid product from the first experiment was analyzed qualitatively

with gas chromatography. The analysis revealed that the main component was methanol (water is not detected by GC). This analysis is included in appendix H.

4.4 Activity of Diluted Commercial Catalyst in Methanol Synthesis

The activity of the diluted commercial catalyst was measured for a long period of time at different temperatures and contact times. The conditions applied are shown in table 4.8. The time interval refers to the real time of the experiment, i.e. time 0 is the start of the experiment.

Table 4.8: *Temperature and flow conditions applied for methanol synthesis with diluted commercial catalyst, at 50 bar pressure in a fixed bed reactor.*

Time interval h	**WABT** °C	**Contact time** $ms \cdot g_{cat}/ml$
8-73	255	300
73-102	239	300
102-125	220	300
125-149	255	300
149-173	240	300
173-195	220	300
195-205	255	300
205-225	265	300
225-249	275	300
249-274	255	300
274-297	255	150
297-313	240	150
313-325	276	150
325-341	255	150
341-345	255	300

As seen in table 4.8, the standard conditions, WABT = 255 °C and contact time = 300 $ms \cdot g_{cat}/ml$, were applied every so often in order to assess the deactivation of the catalyst.

4.4.1 Deactivation

The CO conversion was observed to decrease continuously over time, due to deactivation. Figure 4.15 shows the CO conversion at the standard condition as a function of TOS. The gaps represent activity measurements at other temperatures.

As seen from figure 4.15, it is not straightforward to assess the deactivation of the catalyst in this way. The linear fit is not very good, as the deactivation rate is

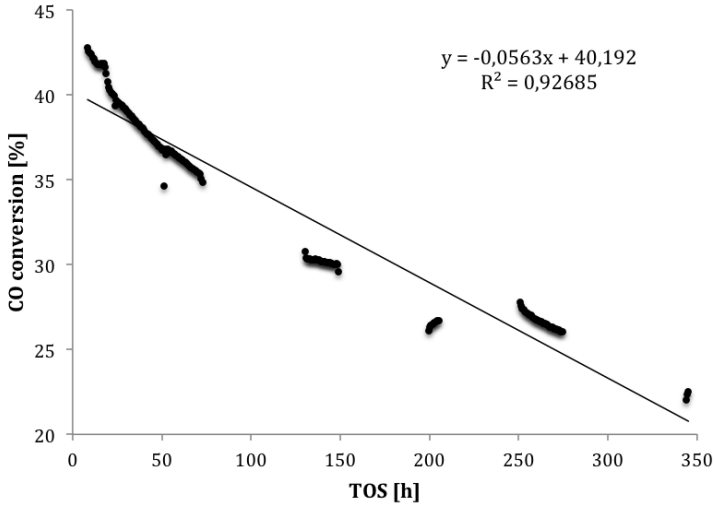

Figure 4.15: *CO conversion, at standard conditions; WABT = 255 °C and a contact time of 300* $^{ms \cdot g_{cat}}/_{ml}$*, as a function of time on stream (TOS) for methanol synthesis with diluted commercial catalyst. The gaps represent activity measurements at other conditions.*

likely changing throughout the experiment. Furthermore, it is difficult to assess if the effect observed is due to deactivation or due to the establishment of steady state conditions in the reactor.

In appendix I, the CO conversion is plotted as a function of time for all the cases where the standard conditions were applied, separately. From these plots, it is easier to fit a straight line, and it can be observed that the rate of deactivation is changing throughout the experiment.

Evidence of deactivation can also be seen from temperature profiles of the catalyst bed measured at different times during the experiment. The temperature in the catalyst bed was measured by moving the thermocouple along the reactor axis. This was done each time the temperature was changed. Figure 4.16, shows the measured temperature profiles at different times.

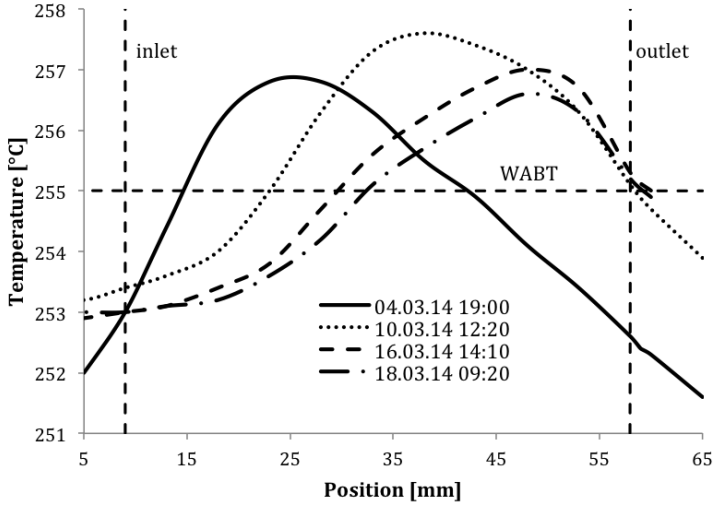

Figure 4.16: *Temperature measured as a function of position within the fixed bed reactor, the dashed vertical lines represent the start and end of the catalyst bed.*

As seen in figure 4.16, the peak bed temperature was close to the reactor inlet in the beginning. As time progressed, the peak bed temperature moved closer and closer to the reactor outlet. The peak bed temperature suggests where the activity of the catalyst is highest, as the reaction is exothermic.

The fact that the peak bed temperature moves toward the reactor outlet suggests that the area where the activity is highest is moving away from the reactor inlet. This indicates that the catalyst particles closest to the reactor inlet deactivates first.

The position of the catalyst bed, as well as the positioning of the thermocouple, were measured using a ruler and is hence not very accurate. Even though there are some uncertainties associated with these measurements, the trend observed appears consistent.

4.4.2 Effect of Temperature

To assess the effect of temperature on the CO conversion, the temperature was varied. The pressure and contact time was kept constant at 50 bar and 300 $[^{ms \cdot g_{cat}}/_{ml}]$. Figure 4.17 shows the CO conversion as a function of temperature, along with the equilibrium CO conversion at the conditions applied. The equilibrium CO conversion data was taken from [15].

The measured CO conversion was adjusted to account for deactivation using the regression line shown in figure 4.15, as shown in appendix I.

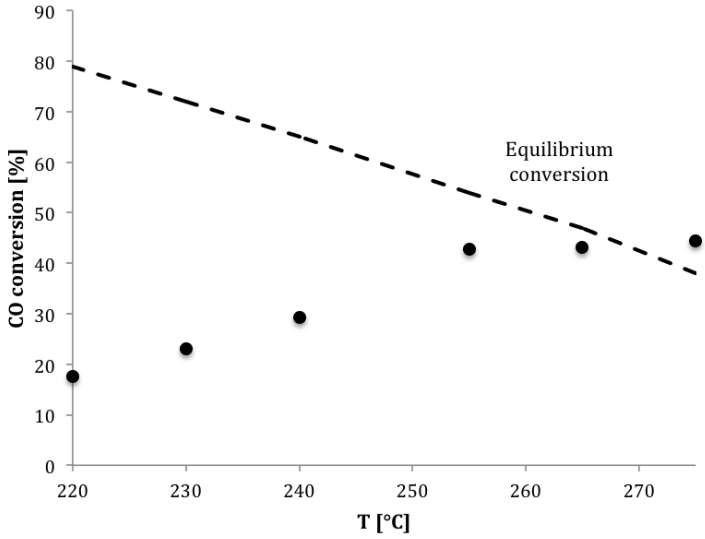

Figure 4.17: *The initial CO conversion plotted as a function of temperature. The initial CO conversion was adjusted to account for deactivation. The dashed line shows the equilibrium CO conversion, taken from [15].*

As seen in figure 4.17, the CO conversion is increasing with increasing temperature. As the temperature increases, the measured CO conversion levels off and moves closer and closer to the equilibrium conversion. At 275 °C, the CO conversion is higher than the equilibrium conversion. This is most likely due to the inaccuracy by which the deactivation was accounted for.

4.4.3 Reaction Rate at Differential Conditions

To assess the effect of temperature on the reaction rate, the CO conversion was measured at a lower contact time. The contact time was adjusted to obtain differential conditions in the reactor. To account for deactivation, the CO conversion was measured at WABT = 255 °C before and after temperature changes.

Figure 4.18 shows the CO conversion as a function of time on stream (TOS) for WABT = 255 °C and a contact time of 150 $[^{ms \cdot g_{cat}}/_{ml}]$.

As seen in figure 4.18, the CO conversion is decreasing nearly linearly.

The CO conversion was measured at different temperatures under this flow, and the reaction rate was calculated based on the initial CO conversion at the given temperature. Appendix J shows how the reaction rate was calculated.

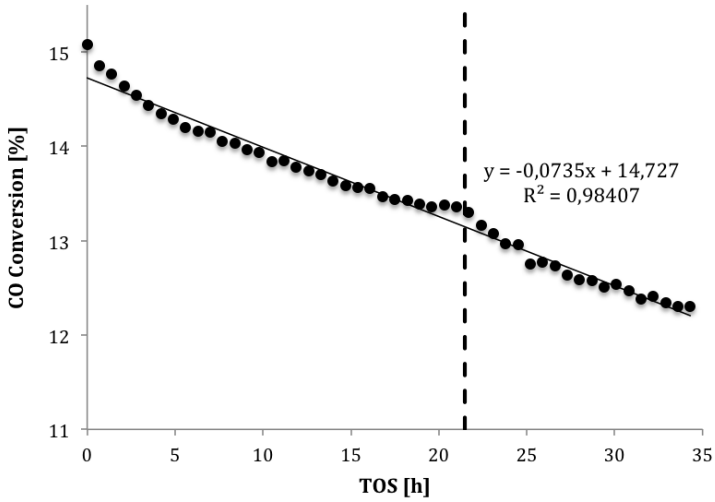

Figure 4.18: *CO conversion as a function of time on stream (TOS) for methanol synthesis in fixed bed reactor with diluted commercial catalyst. The CO conversion is shown for standard conditions; WABT = 255 °C and a contact time of 150* $^{ms \cdot g_{cat}}/_{ml}$*. The dashed vertical line represents the time where the temperature was changed (not shown).*

Table 4.9 gives the calculated CO conversion and reaction rates at different temperatures. The CO conversion and the reaction rates were adjusted to account for deactivation as explained in appendix I and appendix J.

Table 4.9: *Measured CO conversion and calculated CO reaction rate at different temperatures under differential conditions*

WABT °C	$\mathbf{X_{CO}}$ %	$\mathbf{-r_{CO}}$ $^{mmol}/_{s \cdot g_{cat}}$
240	10.1	0.23
255	15.1	0.34
276	23.2	0.52

The reaction rates given in table 4.9 were used to find the apparent activation energy according to the Arrhenius equation. The natural logarithm of the reaction rates was plotted as a function of the inverse temperature. Linear regression was used to fit a line to these points, and the slope of this line was used to calculate the activation energy. Figure 4.19 shows the natural logarithm of the reaction rate as a function of the inverse temperature.

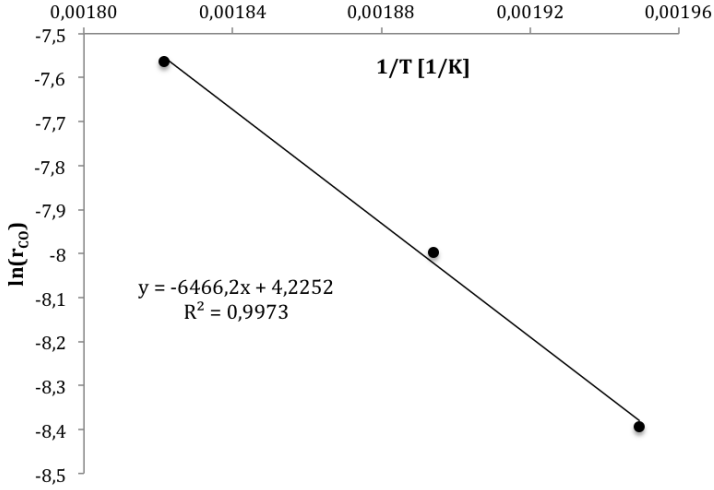

Figure 4.19: *Natural logarithm of calculated reaction rates as a function of 1/T. The reaction rate was measured at 50 bar and a contact time of 150* $[^{ms \cdot g_{cat}}/_{ml}]$*. Linear regression was performed using Excel.*

As seen in figure 4.19, the linear fit is quite good. The slope of the regression line was used to calculate the apparent activation energy as shown below:

$$ln(r) = ln(k) + \frac{-E_A}{R \cdot T} \tag{4.1}$$

$$E_A = -a \cdot R \tag{4.2}$$

Where a is the slope of the line and R is the universal gas constant. The apparent activation energy was calculated to be 53.7 kJ/mol.

Chapter 5

Discussion

5.1 Methanol Catalysts

5.1.1 Characterization

The synthesized methanol catalysts were analyzed by high resolution ICP-MS. The amount of sodium was found to be about 5.3 and 4.6 wt% in the first and second batch respectively. This is well above the maximum value of 100 ppm reported in the synthesis procedure. Catalysts synthesized previously following the same procedure have shown sodium concentrations in the ppm levels [1, 15].

High concentration of sodium in the catalysts is undesirable, as sodium is considered a catalyst poison that affects the activity of the catalyst. Even though the catalyst precursors were washed with deionized water according to the synthesis procedure, it seems likely that the washing was insufficient. As the removal of sodium was insufficient, it is likely that also the removal of nitrate residues was insufficient. As mentioned in section 2.1.1, the presence of nitrate residues during calcination promotes metal agglomeration [20]. Metal agglomeration is undesired as it reduces the dispersion. This may affect the activity of the catalyst as a linear correlation between surface copper surface area and activity has been shown [18].

The presence of nitrate residues during calcination cannot be confirmed as ICP-MS analyses only identifies metals presents. Furthermore, the catalysts were calcined prior to the analyses, which would have removed any nitrate residues. However, judging by the low dispersion and activity, as well as the poor stability of the catalyst, it seems quite likely that the removal of nitrates prior to calcination was insufficient.

The homemade methanol catalyst was further characterized by nitrogen adsorption, N_2O titration and x-ray diffraction. The BET surface area was found to be about 43 and 63 m^2/g for the first and second batch of homemade catalyst respectively.

In comparison, catalysts synthesized by the same procedure previously had surface areas of about 80 m^2/g [1, 15].

The low surface area of both catalysts may be explained by the high concentration of sodium. Furthermore, insufficient removal of nitrates prior to calcination may have caused metal agglomeration as mentioned. Metal agglomeration may have caused large particles to form, which may have blocked some of the pores, resulting in a lower surface area.

The reason for obtaining a higher surface area for the second batch compared to the first batch could be due to more experience, resulting in better control of temperature and pH. Another factor to consider is that the sodium concentration was somewhat lower for the second batch.

The dispersion of the second batch of homemade catalyst was determined by N_2O titration. The dispersion was found to be 1.6 and 0.9 % in the first and second analysis respectively. To validate the results, the copper dispersion was also calculated based on the copper loading determined by the ICP-MS analysis. The total amount of copper was then found to be overestimated in both analyses, but more so in the second analysis. The dispersion was found to be 1.7 and 1.2 % for the first and second analysis respectively, when using the copper loading from ICP-MS analyses in calculations. The difference in dispersion between the first and second analysis is still significant, albeit lower than before.

The reason for obtaining a higher dispersion in the first analysis is uncertain, but measurement errors are a likely cause. The experimental procedure was developed based on literature [32, 33, 34]. There were however some instrumental issues, resulting in the need for many trials in order to find a suitable temperature program. The thermogravimetric analysis (TGA) instrument exhibited poor temperature control at low temperature. After a dialogue with the instrument supplier, it was decided to turn off the 'Sample Temperature Control' (STC) for the steps at low temperature, meaning that the temperature was regulated based solely on furnace temperature. This resulted in a more stable temperature, but it also led to not being able to control the temperature of the sample. The temperature of the samples was higher than the set point in both analyses, and the temperature was slightly higher in the second analysis compared to the first. Additionally, the temperature increased slightly upon introduction of N_2O, as seen in figure 4.2.

The difficulties with the experimental protocol discussed above, may partially explain the unreliability of the calculated dispersions. According to Sato et al. [32] however, the dispersion is not affected by temperature or exposure length with the method they developed.

Other measurement errors includes the determination of the sample mass. The fact that the mass of the sample was normalized based on the mass just prior to N_2O introduction may not be entirely correct. However, as the calculations were performed in the same way for both samples, the error should be the same in both analyses. Additionally, the disturbance in sample mass upon introduction of N_2O

made it difficult to fit a straight line to the data points. To improve the linear fit, some of the initial points were ignored. This affected the y-intercept of the regression line, which in turn affected the calculated dispersion.

A dispersion between 1-2 % is quite low compared to similar catalysts. Phan et al. [34] used N_2O titration to determine the dispersion of $CuO/ZnO/Al_2O_3$ powders prepared by different methods. The dispersion was determined to between 12 and 32 %, depending on the preparation method used. Meland [33] reported a dispersion of about 15 % for a similar $CuO/ZnO/Al_2O_3$ catalyst, using N_2O titration. The reason for the low dispersion obtained may be explained by the high concentration of sodium in the catalyst. Sodium adsorbed on surface copper atoms may have reduced the amount of copper available for N_2O titration. Additionally, the presence of nitrate residues during calcination may have caused metal particle growth. Large particle size affects the dispersion negatively, as larger and fewer particles have lower surface are than many small particles.

Powder x-ray diffraction was used to analyze the homemade methanol catalyst. The diffraction patterns were very similar for the two batches, and the phases were matched to CuO, $Cu_{0.02}Zn_{0.98}O$ and $Zn_6Al_2O_9$. The peaks were overlapping, so it was considered to be beyond the scope of this work to determine the particle size of copper from this analysis. The dispersion found from N_2O titration could therefore not be verified. However, the dispersion seems reasonable based on the low activity observed, as discussed in the next section.

5.1.2 Activity

Methanol synthesis experiments were carried out in an experimental setup designed to convert synthesis gas into methanol. The experimental conditions were chosen to be: 50 bar, WABT = 255 °C and a contact time of 300 $^{ms \cdot g_{cat}}/_{ml}$. Premixed synthesis gas was used for all experiments with a composition of 65 % H_2, 25 % CO, 5 % CO_2 and 5 % N_2. The activity of the homemade catalyst (batch 2) was compared to the activity of the commercial catalyst.

The CO conversion was found to be significantly lower for the homemade methanol catalyst than for the commercial catalyst. The initial CO conversion was about 14 % for the homemade catalyst, compared to about 35 % for the commercial catalyst. It is expected to observe higher activity for a commercial catalyst, as this catalyst has been extensively optimized. However, the difference in activity seems unreasonably high. The high concentration of sodium is assumed to be directly and indirectly responsible for the low activity.

High concentration of sodium is assumed to affect the activity, as sodium is known to be a catalyst poison. Furthermore, the high sodium concentration implies a high probability of nitrate residues being present during calcination. As discussed, this may be the reason for the low dispersion obtained. The low dispersion of the homemade methanol catalyst may also be a factor in the low observed activity, as

a linear correlation between copper surface area and methanol synthesis activity has been shown [18].

When the commercial catalyst was diluted with silicon carbide, even higher activity was achieved. Although this is in accordance with findings by Bakhtiary-Davijany [15], the difference in initial activity seems high. The initial CO conversion for the commercial catalyst diluted 5:1 with SiC was about 43 %. Observing higher activity with diluted catalyst may be due to better temperature control, eliminating local hot spots. As the assumed deactivation mechanism is sintering, temperature control is crucial. Another factor to consider is the temperature of the catalyst bed. Temperature gradients were observed over the diluted catalyst bed, as seen in figure 4.16. The temperature gradients over the undiluted bed was likely even more severe than for the diluted catalyst bed. As the rate of reaction is increasing with temperature, this may partially explain the difference in activity. Other factors which may explain the difference in initial activity is related to the experimental uncertainties which will be discussed below.

Linear regression was performed for the initial CO conversion plotted as a function of TOS, to assess the deactivation. The CO conversion was seen to decrease nearly linearly for all three cases. This is as expected, as copper based methanol catalysts are known to loose about 1/3 of the activity during the first 1000 hours of operation due to sintering of the copper particles [15].

The decrease in activity was steeper for the homemade catalyst than for the two cases of commercial catalyst. This may indicate that the homemade catalyst is deactivating more rapidly than the commercial catalyst. Higher deactivation rate may be attributed to the high sodium content of the homemade catalyst. Another factor to consider is the likelihood of particle agglomeration during calcination. Recent findings suggest that interparticle distance is a crucial parameter for sintering [19]. Particles placed closer together are more prone to sintering, than particles with longer interparticle distance. Clustering of metal particles during sintering would therefore likely increase sintering.

The decrease in activity was also steeper for the diluted commercial catalyst compared to the undiluted commercial catalyst. The reason for this is unknown, as it is unlikely that diluting the catalyst would result in a higher deactivation rate. A lower deactivation rate for the diluted catalyst would be more natural, as the dilution should result in better temperature control.

However, assessing deactivation is not a straightforward matter, and the observed decrease in activity could be due to a number of other factors. First of all, the initial activity is taken as the first measurement point of with the correct temperature, flow and pressure. The time required to reach the desired conditions was not the same in all cases. Longer adjustment period would likely result in lower initial activity, and could also result in a lower observed deactivation rate, as the deactivation rate is assumed to be highest in the beginning.

Secondly, the temperature of the catalyst bed was adjusted by adjusting the tem-

perature of the furnace. The correct furnace temperature was found by trial and error. A higher initial temperature would likely affect the deactivation rate, as the assumed deactivation mechanism is sintering. Higher initial temperature causing more rapid deactivation may also result in a lower initial activity, as the initial activity was taken as the first measurement after the correct conditions, temperature, pressure and flow, were established. Furthermore, the observed decrease in CO conversion may be due to the establishment of steady state conditions in the reactor. It is not easy to separate the effect of deactivation from the effect of instability prior to reaching steady state conditions.

Based on GC analysis of the liquid product, a mass balance with respect to carbon was calculated for the experiment with the homemade catalyst. The liquid product was found to be 99 % methanol. The error in the carbon balance was calculated to be maximum 2.2 % Errors up to 5 % in the carbon balance is normally accepted for this type of experiments. As the selectivity of the commercial catalyst is assumed to be the same or better than the homemade catalyst, these calculations were not performed for the experiments with commercial catalyst.

5.1.3 Kinetics

The methanol synthesis experiment with diluted commercial catalyst will be discussed in the following sections.

Deactivation

The temperature in the catalyst bed was measured several times during the experiment. The peak bed temperature was observed to move from a position close to the reactor inlet to a position closer to the reactor outlet as time progressed, as seen in figure 4.16. As the methanol synthesis is exothermal, the peak bed temperature suggests where the activity is highest. Observing higher activity near the reactor inlet is natural, as this portion of the catalyst particles comes into contact with the synthesis gas first.

The fact that the peak temperature was moving away from the reactor inlet suggests that the catalyst particles closest to the inlet is deactivating first. This also supports the assumption of sintering as the deactivation mechanism, as the portion of catalyst exposed to the highest temperature initially, deactivates first.

Evidence of deactivation was also observed when the standard conditions were applied. As seen in figure 4.15, the CO conversion was continually decreasing throughout the experiment. The rate of decrease is activity was seen to change throughout the experiment, as seen in appendix I. The rate of decrease was highest in the beginning, and then leveled out somewhat. After measuring the activity at high temperature (265 and 275 °C), the rate of decrease was observed to increase somewhat. This further supports sintering as the deactivation mechanism.

The assessment of deactivation is a difficult topic, as discussed above. Nevertheless, the measured activity was adjusted to account for the observed deactivation. For simplicity, the regression line shown in figure 4.15 was used to adjust the activity. This is not strictly correct, as the deactivation rate was seen to change during the experiment. However, a more detailed analysis of the deactivation was considered beyond the scope of this project.

Kinetics

The activity was measured at different temperatures and contact times. As seen in figure 4.17, the CO conversion increased with increasing temperature. The increase in activity was observed to be nearly linear at low temperature. As the temperature was increased beyond 255 °C, the activity was observed to level off and move closer and closer to the equilibrium conversion. The CO conversion shown was measured at a contact time of 300 $^{ms \cdot g_{cat}}/_{ml}$, and the activity was adjusted to account for deactivation as discussed above.

The trend observed in figure 4.17 is similar to results obtained by Bakhtiary-Davijany [15]. At low temperature, the activity is far from the equilibrium conversion, and the increase in activity as a function of temperature is due to the rate of reaction increasing as a function of temperature. As the activity comes closer and closer to the equilibrium conversion, the rate of reaction becomes more and more limited by the equilibrium conversion, and the activity is seen to level off.

The CO conversion approached the equilibrium conversion at high temperature. At 275 °C, the calculated CO conversion is actually higher than the equilibrium conversion. This is likely due to errors associated with the adjustment of the CO conversion to account for deactivation. As mentioned previously, the method used to adjust the activity represents a simplification and the result may not be correct.

The activity was also measured at lower contact time, 150 $^{ms \cdot g_{cat}}/_{ml}$. The measured CO conversion was then lower at all temperatures, and approaching differential conditions. The rate CO consumption was determined, and an Arrhenius plot was made, where the natural logarithm of the reaction rate was plotted as a function of the inverse temperature. From this plot, the apparent activation energy was determined to be 54 kJ/mol. This is somewhat lower than activation energies reported in literature; Phan et al. [34] reports an activation energy of about 74 kJ/mol, while Bakhtiary-Davijany reports an activation energy of 67 kJ/mol.

The reason for obtaining a lower apparent activation energy may be due to several factors. Firstly, the method used for adjusting the reaction rate to account for deactivation is not very accurate as discussed previously. Secondly, although a good linear fit was obtained, only three data points were used to determine the line. The method by which the reaction rate was determined is another factor to consider. As the activity was low, the rate of reaction was determined based on the concentration in the feed and the concentration in the product. As gradients may exists in fixed bed reactors, this is not strictly correct.

5.2 Acidic Dehydration Catalysts

Samples of the ZSM-5 catalyst were analyzed by high resolution ICP-MS to determine the extent of ion-exchange. Both H-ZSM-5 catalysts and ion-exchanged catalysts were analyzed. The results of the analyses were however not reliable, as significantly different results were obtained in the first and second analysis of the same catalyst. Furthermore, the calculated molar silica to alumina ratios were not consistent between the analyses, nor between the ion-exchanged zeolite and the fully protonated zeolite.

Additionally, the calculated molar ratio of the two H-ZSM-5 catalysts differed significantly from the molar ratio given by the supplier. The H-ZSM-5 zeolites were acquired commercially in ammonium form and had only been calcined to obtain the hydrogen form. It is unlikely that the silica to alumina ratio was affected by the calcination. The results of the ICP-MS analyses were therefore disregarded and the intended extent of ion-exchange was used to distinguish between the catalysts.

The surface area of the protonated ZSM-5 catalyst with molar silica to alumina ratio of 80 was determined by nitrogen adsorption. The BET surface area was determined to be between 362 and 392 m^2/g. According to the supplier, the surface area should be about 425 m^2/g [45]. The reason for obtaining a lower surface area is most likely due to the fact that the BET isotherm is not strictly applicable to microporous materials like zeolites. The BET isotherm is only valid under the assumption of multilayer adsorption, as mentioned in section 2.4.1. Multilayer adsorption is limited in micropores, and may therefore result in an underestimation of the surface area [17].

5.2.1 Acidity Characterization

Ammonia Temperature-Programmed Desorption

The dehydration catalysts were characterized by ammonia temperature-programmed desorption. Advanced analysis to find adsorption energies were not performed as this was considered to be beyond the scope of this project. The results of the analyses were used to qualitatively compare the different catalysts to each other.

As seen in figure 4.4a and table 4.6, the total mass loss was decreasing in the order:

H-ZSM-5 30 > γ alumina > H-ZSM-5 80

As the mass loss is assumed to be mostly due to ammonia desorbing from acid sites, the acid site concentration is assumed to follow the same trend. Some of the mass loss, especially at low temperature, may be due to desorption of physisorbed ammonia. This is not assumed to affect the acid site concentration trend, as physisorbed ammonia is assumed to be present in all catalysts. The amount of physisorbed ammonia may be dependent on the surface area.

The results of the ion-exchanged zeolites will be discussed separately below.

Observing higher acid site concentration for H-ZSM-5 30 compared to H-ZSM-5 80 is in accordance with theory, as the amount of acid sites in zeolites are correlated with the aluminium content. Each protonated oxygen bridge between silicon and aluminium corresponds to a Brønsted acid site [23]. However, the acid site concentration may deviate some from the aluminium content, as some aluminium atoms may have been dislodged from regular framework positions. It is also plausible that some of the framework aluminium atoms are associated with cations other than hydrogen.

The acidity of γ alumina is less predictable compared to the zeolites. The concentration of acid sites for γ alumina found by ammonia TPD cannot be confirmed, since no other characterization regarding the number of surface acid sites has been performed. However, as the concentration of aluminium is quite high, it seems likely that the acid site concentration is high as well.

As seen in figure 4.4a, the shape of the differential mass change curve as a function of temperature for the two zeolites is very similar. The curve for γ alumina has a continued decrease at high temperature, unlike the two zeolites. This indicates that γ alumina has stronger acid sites compared to the zeolites, as the desorption temperature is an indication of the bonding strength between the probe and the catalyst [23].

All the ZSM-5 zeolites showed a similar trend with two well defined minima when the differential mass change was plotted as a function of temperature, indicating that there are two major groups of acid sites. This is consistent with literature [23, 26]. The minima were located between 100 and 200 °C and between 300 and 400 °C for all zeolites.

γ alumina on the other hand, had two well defined minima, in addition to a continued decrease at high temperature. The continued decrease at high temperature indicates the possible presence of a third minimum, but this can not be determined as the experiment was stopped prematurely. The first minimum was located at low temperature, while the second minimum was located at about 320 °C, which is somewhat lower than for the zeolites. This indicates that the strong acid sites found in the zeolites are somewhat stronger than the acid sites associated with the second minimum for γ alumina. However, the possible presence of a third minimum located at higher temperature, indicates that γ alumina has a third group of acid sites that are significantly stronger than for the zeolites.

The total mass loss occurring at high temperature, between 300 and 600 °C, was calculated for all acidic catalysts. The following trend was found:

γ alumina > H-ZSM-5 30 > H-ZSM-5 80

The mass loss occurring at high temperature is most likely due to adsorption of ammonia from strong acid sites, as any ammonia adsorbed in excess is assumed to have desorbed at lower temperature. The concentration of strong acid sites is

therefore likely following the same trend. As γ alumina has predominantly Lewis acid sites, it is not surprising that this catalyst has the highest concentration of strong acid sites. All zeolites were observed to follow the same trend when the differential mass change was plotted as a function of temperature. It is therefore as expected that the concentration of strong acid sites follows the same trend as for the total concentration of acid sites.

Comparing H-ZSM-5 30 with Na(30),H-ZSM-5 30, it was observed that the mass loss at low temperature was very similar. At higher temperature however, the ion-exchanged zeolite showed lower mass loss, as seen in figure 4.5a and table 4.6. This indicates that the concentration of weak acid sites is very similar, and that the concentration of strong acid sites is lower for the ion-exchanged zeolite. This again indicates that sodium has predominately replaced protons associated with strong acid sites. This is in agreement with the findings of Garcia-Trenco and Martinez [6].

The total mass of Na(30),H-ZSM-5 30 was about 7 % lower than for H-ZSM-5 30. This suggests that the extent of ion-exchange is lower than the intended 30 %. This can not be confirmed however, due to the unreliability of the ICP-MS analyses.

The results of H-ZSM-5 80 compared with the ion-exchanged ZSM-5 with the same molar silica to alumina ratio, were quite unexpected. The total mass loss for the zeolite with 30 % intended ion-exchange was lower than the zeolites with intended 40, 60 and 80 % ion exchange. Furthermore, the mass loss for the zeolites with intended 40, 60 and 80 % ion exchange was nearly identical. When more and more of the protons are exchanged with sodium, it is expected to see a decrease in the acid site concentration, which should manifest by lower mass loss during the temperature-programmed desorption. As the extent of ion-exchange has not been confirmed, it is difficult to say what the reason for this behavior is. But it is likely that the intended extent of ion-exchange was not reached. Another possibility is that the temperature program used has affected the results. The three ion-exchanged zeolites with 40, 60 and 80 % ion-exchanged were all analyzed with the second temperature program with lower pretreatment temperature. This will be discussed further below.

The total mass loss for the ZSM-5 catalysts with intended 40, 60 and 80 % ion-exchange was also seen to be quite similar compared to the fully protonated zeolite. This makes is more plausible that something went wrong when preparing the ion-exchanged zeolites, and that the intended extent of ion-exchange was not reached.

The zeolite with intended 30 % ion-exchange was seen to have similar concentration of weak acid sites, and significantly lower concentration of strong acid sites compared to H-ZSM-5 80. The zeolites with intended 40, 60 and 80 % ion-exchange had similar concentration of weak acid sites compared to H-ZSM-5 80. The concentration of strong acid sites was somewhat lower than for H-ZSM-5 80, but the difference was less significant for these zeolites compared to the zeolite with intended 30 % ion-exchange. This suggests that sodium predominantly replaced protons associated with strong Brønsted acid sites.

As mentioned, two different temperature programs were used for the ammonia TPD experiments. Most of the catalysts were subjected to a temperature program with a pretreatment temperature of 600 °C. γ alumina, and the zeolites with intended 40, 60 and 80 % ion exchange were subjected to a temperature program with a pretreatment temperature of 250 °C. As mentioned in section 2.4.5 the pretreatment temperature may affect zeolite acidity. At pretreatment temperatures above 402 °C, evidence of dehydroxylation has been observed [25]. Dehydroxylation decreases the number of Brønsted acid sites while creating strong Lewis acid sites as explained in section 2.3.

However, H-ZSM-5 80 were analyzed with both temperature programs, and results of the two analyses were quite similar. At high temperature, the mass loss of associated with a pretreatment temperature of 600 °C was somewhat higher than with lower pretreatment temperature. This indicates that pretreatment at high temperature may have resulted in a higher concentration of strong acid sites. Nevertheless, the difference between the two analyses was small.

The acid sites concentration of the ZSM-5 catalysts with 40, 60 and 80 % ion-exchange was found to be greater than expected as mentioned above. These zeolites were pretreated at lower temperature compared to the other ZSM-5 80 catalysts. As mentioned previously, pretreatment at temperature higher than 402 °C may lead to dehydroxylation of Brønsted acid sites. Dehydroxylation leads to lower acid site concentration while creating stronger acid sites. The lower pretreatment temperature may therefore have led to the unexpectedly high concentration of acid sites in the ZSM-5 catalysts with 40, 60 and 80 % ion-exchange. However, this does not explain why these zeolites have nearly identical mass loss.

Isopropylamine Temperature-Programmed Desorption

Isopropylamine TPD experiments were also performed. Since isopropylamine TPD experiments had not been performed in this laboratory before, the experimental protocol was developed based on literature. The experimental procedure should be considered as a first trial only. As adsorption of isopropylamine was not permitted in the thermogravimetric analysis (TGA) instrument, pretreatment and adsorption was performed ex situ, meaning that the sample mass could not be monitored for these steps. Different methods for pretreatment and adsorption were tried for the H-ZSM-5 30 zeolite.

All protocols, except protocol 1 (which did not include a pretreatment step), involved degassing at 200 °C at varying length. Placing the catalyst inside a sealed container together with an open beaker containing isopropylamine constituted the adsorption step for protocol 1, 2 and 3. Protocol 4 involved dripping isopropylamine directly onto the catalyst and subsequent drying inside a forced air oven.

The results obtained with the various protocols were very similar at low temperature. At high temperature, some differences could be observed. Protocol 1 and 2

showed similar results, with higher mass loss at high temperature compared to protocol 3 and 4. The fact that higher mass loss was observed with less pretreatment may be explained by the desorption of impurities or water during the temperature ramp. However, as the difference was mostly observed at temperatures higher than the pretreatment temperature, desorption of physisorbed species seems less likely.

All protocols showed two well defined minima when the differential mass change was plotted as a function of temperature, indicating that there are two major groups of acid sites. The first minimum was observed at around 200 °C, while the second minimum was located at around 350 °C. The second minimum is most likely due to desorption from Brønsted acid sites, as this is known to occur between 300 and 380 °C [26, 38].

Based on the results of these analyses, it was difficult to conclude on which experimental protocol was most suitable. Both pretreatment and adsorption protocols were varied simultaneously, and the mass of the catalyst could not be monitored during either steps. Additionally, all samples were exposed to the atmosphere when transferring the sample from one sample holder to the next. As the observed difference was small in any case, protocol 1 was chosen due to its simplicity for the analysis of H-ZSM-5 80 and Na(30),H-ZSM-5 80.

Comparing the results of H-ZSM-5 30, H-ZSM-5 80 and Na(30),H-ZSM-5 80, the mass loss at low temperature is very similar for all catalysts. At high temperature, there is a substantial difference between H-ZSM-5 30 and the two others. A small difference between H-ZSM-5 80 and Na(30),H-ZSM-5 80 was also observed at high temperature. These results are qualitatively very similar to the results obtained with ammonia TPD.

The exhaust gas from the isopropylamine TPDs was investigated by mass spectrometry (MS). The desorption of isopropylamine from Brønsted acid is characterized by the desorption product being propene and ammonia. Desorption from Lewis sites or isopropylamine adsorbed in excess, desorbs unreacted [26, 37, 38].

The results revealed two peaks for ammonia and isopropylamine for all catalysts, located in the same temperature intervals as the minima observed in figure 4.8b. Propene was detected at a lower level than the other two, and the signal was very noisy. The fact that both ammonia and isopropylamine was detected in both temperature intervals suggests that both groups of acid sites have contributions of Lewis and Brønsted acid sites.

The ammonia peak for H-ZSM-5 30 at low temperature was significantly smaller than the ammonia peak at high temperature. The opposite was observed for the isopropylamine. This indicates that the minimum at low temperature is mostly due to desorption of physisorbed isopropylamine or weak Lewis acid sites, and that the minimum at high temperature is mostly due to desorption from Brønsted acid sites.

The ammonia peak for H-ZSM-5 80 and Na(30),H-ZSM-5 80 at low temperature was smaller than the ammonia peak at high temperature, but the difference was

less pronounced than for H-ZSM-5 30. This indicates that the minima at low temperature have a higher contribution of Brønsted acid sites for these catalysts compared to H-ZSM-5 30.

The isopropylamine peak at low temperature is significantly higher at low temperature than at high temperature for H-ZSM-5 80 and Na(30),H-ZSM-5 80. Compared to H-ZSM-5 30, the isopropylamine peak at high temperature is higher for these zeolites. This indicates that the minima at high temperature has a higher contribution of desorption from Lewis acid sites in the H-ZSM-5 80 catalysts compared to H-ZSM-5 30.

However, the analysis of the MS data is somewhat simplified. The molecules were identified only on the peak associated with the most abundant ions, and only the ion current for this ion is shown. Additionally, the results of propene and ammonia should be viewed together, as desorption from Brønsted acid sites is characterized by the presence of both molecules. As only the base peaks are included for each desorption product, the peaks may have contributions from other species. Especially at low temperature, there is a possibility that the peak with m/z = 17 has contributions from water as well as from ammonia. Furthermore, the MS instrument was not calibrated, so a precise quantitative analysis is not possible.

Adsorption Calorimetry

Adsorption calorimetry experiments using ammonia as probe gas were attempted. As ammonia had not been used as probe gas in this laboratory before, the experimental procedure was developed based on literature studies, and experimental experience with H_2 and CO. The goal was to determine the heat of adsorption for the different acid sites present in the acidic catalysts. However, there was not enough time to develop a sufficiently good experimental protocol, due to several experimental difficulties.

As the adsorbed amount was determined volumetrically, volume measurements were performed prior to the experiments. Unfortunately, there was a problem when measuring the volume V_2 (see section 3.3.5). The measured volume varied significantly between measurements, and an average value could not be determined with sufficient accuracy. It was not enough time to figure out what the problem was, as both the gas used for the measurements and the temperature of the calorimeter was changed compared to previous experiments.

However, the measured volume seemed to be affected by the evacuation time used between measurements, as the volume measured at the start of the day, when the setup had been evacuating overnight, was significantly higher than measurements made after evacuation for about 30 minutes. It was therefore decided to calculate two average values, one lower value, corresponding to short evacuation times, and one high value corresponding to long evacuation times.

The second and third trials gave initial heats of adsorption of around 120-130

kJ/mol. The difference between using the high and low average values for V_2 was insignificant. The differential heat of adsorption was also observed to be more or less constant up to a coverage corresponding to about 0.5 ammonia atoms per aluminium atoms. Various initial heat of adsorption is reported in literature, but most reports values above 150 $^{kJ}/_{mol}$ [23, 25, 42, 43]. The initial heats observed in the experiments are significantly lower than reported values. The reason is assumed to be too large doses of probe gas initially. When a large amount of ammonia is sent, ammonia is adsorbed on many acid sites, and the recorded heat flow is then an average value for the different acid sites.

The fact that the differential heat of adsorption is found to be more or less constant for a wide range of coverage further supports the hypothesis that the doses were too large. Auroux [43] reports differential heat of adsorption of about 150 kJ/mol up to a coverage of about 1 ammonia atom per unit cell of catalyst. At higher coverages, the differential heat of adsorption dropped quickly to about 85 kJ/mol. The adsorption temperature and the pretreatment temperature used in the experiments of Auroux were the same as the ones used in this project.

A final trial was made with more catalyst than previously, and smaller initial doses. For this trial however, the doses were likely too small in the beginning, as the peaks in the thermograph associated with these doses were poorly defined, making the determination of the differential heat difficult. The doses were increased some after the initial very small ones, and more well defined peaks were observed. Ignoring the first few doses, the initial heat of adsorption was found to be 150 or 120 kJ/mol. The two values correspond to using either the high or low average volume of the calorimetric cells.

As the difference between using the two different average volumes for V_2 cannot be ignored, new volume measurements should be performed. Also, the method for measuring the volumes should be revised. The method used for the volume measurements was the same as what had been done previously. However, the volume V_2, should be split in two; so that the volume of the cells would be measured separately.

Chapter 6

Conclusions

Catalyst characterization by high resolution ICP-MS revealed that both batches of the $Cu/ZnO/Al_2O_3$ synthesized had sodium concentrations of about 5 wt%. The maximum concentration of sodium is 100 ppm according to the synthesis procedure provided by UOP. High concentration of sodium is unfortunate since sodium is a catalyst poison, which may affect the activity of the catalyst. The high concentration of sodium is assumed to imply presence of nitrate residues during calcination. Nitrate residues promote metal particle agglomeration during calcination, which likely affects the activity and the stability of the catalyst [20, 19].

The BET surface area, determined by nitrogen adsorption, was 43 and 63 $^{m^2}/_g$ for the first and second batch respectively. Catalysts synthesized by the same procedure have had surface areas of about 80 $^{m^2}/_g$ [1, 15]. X-ray diffraction results identified copper oxide, copper zinc oxide and aluminium zinc oxide for both batches of calcined catalyst. Due to overlapping peaks, the particle size of copper oxide was not determined. The dispersion of the second batch of catalyst was determined to be between 0.9 and 1.7 % by nitrous oxide titration. In comparison, similar catalysts, investigated with the same method, had dispersions between 15 and 32 %. The validity of the experimental procedure is somewhat uncertain. The high concentration of sodium may have directly or indirectly led to the low dispersion observed.

Activity measurements of the second batch of copper/zinc oxide catalyst revealed low activity. The initial CO conversion measured was about 14 %, compared to 35 and 43 % for the commercial catalyst, undiluted and diluted 5:1 with SiC respectively, under identical conditions. The conversion was observed to decrease nearly linearly in all cases. The activity of the homemade catalysts was however seen to decrease more rapidly than for the commercial catalyst.

The drop in activity could be explained by deactivation due to sintering, transient conditions in the reactor or measurement errors. It is normal for copper based catalysts to loose some activity during the first hours of operation due to sintering

[15]. The error in carbon balance was calculated to be maximum 2.2 % for the experiment with homemade catalyst. The high sodium content of this catalyst may also be a factor in the observed decrease in activity.

The CO conversion for the diluted commercial catalyst was seen to increase with increasing temperature. The conversion was approaching the equilibrium conversion at high temperatures. This is in accordance with findings by Bakhtiary-Davijany [15]. Based on activity measurements at differential conditions, the activation energy was determined to be about 54 kJ/mol. This is somewhat lower than values reported by Phan et al. [34] and Bakhtiary-Davijany [15]. The reason for this is assumed to be due to inaccuracies in adjusting the activity to account for deactivation, as well as the fact that only three data points were used.

The activity of the diluted commercial catalyst was seen to decrease continuously over a time period of 2 weeks, which indicates that the catalyst was deactivating continuously. The deactivation rate was also seen to change throughout the experiment. Temperature profiles measured at different points in time further supported the claim of deactivation by sintering.

BET surface area was determined for methanol dehydration catalysts, i.e. γ alumina and HZSM-5. The surface area of the zeolite was determined to be 377 ± 15 m^2/g, while the surface area of γ alumina was 194 m^2/g. X-ray diffraction results correctly identified the materials.

Batches of ion-exchanged zeolites were prepared. ICP-MS analyses were obtained to determine the extent of ion-exchange. These analyses were however disregarded, as the results seemed unreliable.

Acidity characterization by temperature-programmed desorption (TPD) with ammonia and isopropylamine was performed. The results indicated that the concentration of acid sites is in the order: H-ZSM-5 (30) > γ alumina > H-ZSM-5 80. This is as expected for the zeolites. The results obtained for TPD experiments with ion-exchanged zeolites were somewhat unexpected, as the acid site concentration was not found to be correlated with the intended extent of ion-exchange. However, these results were associated with some uncertainty, as the extent of ion-exchange was not determined.

The results also indicated that γ alumina has the highest concentration of strong acid sites, although this experiment was likely stopped prematurely. All zeolites were found to have two major groups of acid sites, in accordance with findings in literature [23, 26]. It was also found that sodium had predominantly replaced hydrogen at strong acid sites.

The TPD experiments with isopropylamine showed similar trends as the TPD experiments with ammonia. Two major groups of acid sites were found for the zeolites investigated, in accordance with literature [38]. MS results indicate that both groups of acid sites had contributions of both Brønsted and Lewis acid sites. The experimental protocol was developed in this project, and needs further refinement. Moreover, the MS analysis was somewhat simplified.

Adsorption calorimetry with ammonia was attempted for H-ZSM-5 30. Establishing the experimental protocol turned out to be challenging, but qualitatively reasonable results were achieved.

Chapter 7

Suggestions for Future Work

In this section, some ideas for future work are presented.

The behavior of the $Cu/ZnO/Al_2O_3$ catalyst in methanol synthesis was investigated. Even though the stability of this catalyst is a known issue, the deactivation mechanism is still not well understood. It is of interest to study the stability of this catalyst during direct DME synthesis. Recent findings suggest that the synthesis method of this catalyst may be optimized to increase the stability, by controlling the interparticle distance between copper particles.

The dispersion of a homemade $Cu/ZnO/Al_2O_3$ catalyst was attempted to be determined by N_2O titration. The results were somewhat uncertain. A better experimental procedure is therefore needed. Concerning the deactivation of the catalyst, it would be interesting to determine the dispersion of fresh and used catalyst, to see if there is any evidence of sintering.

Studying the stability of acidic dehydration catalysts is also of importance. The acidity of the catalyst, both with respect to acid site concentration and acid site strength, is assumed to affect the dehydration activity. The acidity of zeolites can easily be modified in different ways. Ion-exchange was attempted in this project. Other methods include various heat treatments, substitution of aluminium with another trivalent cation and steaming.

To find correlations between acidity and activity, characterization of the acidic catalysts is crucial. Temperature-programmed desorption and adsorption calorimetry were attempted in this project. The experimental procedures for adsorption calorimetry and isopropylamine TPD needs more work however. Additionally, other characterization methods should be investigated to validate the results. Infrared spectrometry is a very useful tool in this respect, as IR spectrometry can identify the nature as well as the strength of the acid sites.

Bibliography

[1] F. Hayer. *Direct Synthesis of Dimethyl Ether in Microstructured Reactors*. PhD thesis, NTNU, 2011.

[2] T. Ogawa, N. Inoue, T. Shikada, and Y. Ohno. Direct dimethyl ether synthesis. *Journal of Natural Gas Chemistry*, 12:219–227, 2003.

[3] A. Garcia-Trenco, S. Valencia, and A. Martinez. The impact of zeolite pore structure on the catalytic behavior of CuZnAl/zeolite hybrid catalysts for the direct DME synthesis. *Applied Catalysis A: General*, 468:102–111, 2013.

[4] L. Wang, Y. Qi, D. Fang, S. Meng, and Z. Liu. Research on the acidity of the double-function catalyst for DME synthesis from syngas. *Catalysis Letters*, 106, 2006.

[5] Y. Wang, Y. Zhao, F. Xiao, and D. Li. Combustion and emission characteristics of a diesel engine with DME as port premixing fuel under different injection timing. *Energy Conversion and Management*, 77:52–60, 2013.

[6] A. Garcia-Trenco and A. Martinez. Direct synthesis of DME from syngas on hybrid CuZnAl/ZSM-5 catalysts: New insights into the role of zeolite acidity. *Applied Catalysis A: General*, 411-412:170–179, 2012.

[7] A. Scragg. *Biofuels; Production, Application and Development*. Cambridge University Press, UK, 2009.

[8] P. Basu. *Biomass Gasification and Pyrolysis: Practical Design and Theory*. Elsevier, Amsterdam, 2010.

[9] Q. Ge, Y. Huang, F. Qiu, and S. Li. Bifunctional catalysts for conversion of synthesis gas to dimethyl ether. *Applied Catalysis A: General*, 167:23–30, 1998.

[10] F. S. Ramos, A. M. Duarte de Farias, L. E. P. Borges, J. L. Monteiro, M. A. Fraga, E. F. Sousa-Aquiar, and L. G. Appel. Role of dehydration catalyst acid properties on one-step DME synthesis over physical mixtures. *Catalysis Today*, 101:39–44, 2005.

[11] G. R Moradi, S. Nosrati, and F. Yaripor. Effect of the hybrid catalysts pre-

paration method upon direct synthesis of dimethyl ether from synthesis gas. *Catalysis Communications*, 8:598–606, 2007.

[12] I. Kikkawa, Y. & Aoki. Dimethyl ether fuel proposed as an alternative to LNG. *Oil & Gas Journal*, 96(14), 1998.

[13] A. Garcia-Trenco and A. Martinez. The influence of zeolite surface-aluminium species on the deactivation of CuZnAl/zeolite hybrid catalysts for the direct DME synthesis. *Catalysis Today*, 227:144–153, 2014.

[14] A. Garcia-Trenco, A. Vidal-Moya, and A. Martinez. Study of the interaction between components in hybrid CuZnAl/HZSM-5 catalysts and its impact in the syngas-to-DME reaction. *Catalysis Today*, 179:43–51, 2012.

[15] H. Bakhtiary-Davijany. *Performance Assessment of a Packed Bed Microstructured Reactor - Heat Exchanger for Methanol Synthesis from Syngas.* PhD thesis, NTNU, 2010.

[16] J. A. Moulijn, M. Makkee, and A. Van Diepen. *Chemical Process Technology.* John Wiley & Sons Ltd, 2001.

[17] I. Chorkendorff & J. W. Niemantsverdriet. *Concepts of Modern Catalysis and Kinetics.* Wiley-VCH Verlag GmbH & Co. KGaA, Weinheim, 2 edition, 2007.

[18] J. Nakamura, I. Nakamura, T. Uchijima, Y. Kanai, T. Watanabe, M. Saito, and T. Fujitani. A surface science investigation of methanol synthesis over a Zn-deposited polycrystalline Cu surface. *Journal of Catalysis*, 160:65–75, 1996.

[19] G. Prieto, J. Zecevic, H. Friedrich, K. P de Jong, and P. E. de Jong. Towards stable catalysts by controlling collective properties of supported metal nanoparticles. *Nature Materials*, 12:34–39, 2013.

[20] G. Prieto, K. P de Jong, and P. E. de Jong. Towards 'greener' catalyst manufacture: Reduction of wastewater from the preparation of Cu/ZnO/Al2O3 methanol synthesis catalysts. *Catalysis Today*, 215:142–151, 2013.

[21] K. M. Vanden Bussche and G. F. Froment. A steady-state kinetic model for methanol synthesis and the water gas shift reaction on a commercial Cu/ZnO/Al2O3 catalyst. *Journal of Catalysis*, 161(1):1–10, 1996.

[22] K. S Yoo, J. H. Kim, M. J. Park, S. J. Kim, O. S. Joo, and K. D. Jung. Influence of solid acid catalyst on DME production directly from synthesis gas over the admixed catalyst of Cu/Zn/Al2O3 and various SAPO catalysts. *Applied Catalysis A: General*, 330:57–62, 2007.

[23] E. G. Derouane, J. C. Védrine, R. R. Pinto, Borges P. M., L. Costa, M. A. N. D. A. Lemos, F. Lemos, and F. R. Ribeiro. The Acidity of Zeolites: Concepts, Measurements and Relation to Catalysis: A Review on Experimental and Theoretical Methods for the Study of Zeolite Acidity. *Catalysis Reviews: Science and Engineering*, 55:454–515, 2013.

[24] T. Poon. Home page of prof. Thomas Poon, 2007. URL `http://ochem.jsd.claremont.edu/tp_research.htm`.

[25] A. Auroux. Acidity and basicity: Determination by adsorption microcalorimetry. *Mol Sieves*, 6:45–152, 2008.

[26] W. E. Farneth and R. J. Gorte. Methods for characterizing zeolite acidity. *Chemical Reviews*, 95:615–635, 1995.

[27] International Zeolite Association. Framework type MFI, 2007. URL `http://izasc.ethz.ch/fmi/xsl/IZA-SC/ftc_fw.xsl?-db=Atlas_main&-lay=fw&-max=25&STC=MFI&-find`.

[28] M. Che and J. C. Védrine, editors. *Characterization of Solid Materials and Heterogeneous Catalysts - From Structure to Surface Reactivity*, volume 2. Wiley-VCH Verlag GmbH & Co. KGaA, Boschstr. 12, 69469 Weinheim, Germany, 2012.

[29] D. G. Callister, W. D. & Rethwisch. *Materials Science and Engineering*. John Wiley & Sons (Asia) Pte Ltd, 111 River Street, Hoboken, NJ, 8 edition, 2011.

[30] G. A. Somorjai. *Introduction to Surface Chemistry and Catalysis*. Wiley, New York, 1994.

[31] M. Bowker. *The Basis and Applications of Heterogeneous Catalysis*. Oxford Chemistry Primers. Oxford University Press., 1998.

[32] S. Sato, R. Takahashi, T. Sodesawa, K. Yuma, and Y. Obata. Distinction between surface and bulk oxidation of Cu through N2O decomposition. *Journal of Catalysis*, 196:195–199, 2000.

[33] H. Meland. *Preparation and Characterization of Cu- and Pt-Based Water-Gas-Shift Catalysts*. PhD thesis, NTNU, 2008.

[34] X. K. Phan, H. Bakhtiary-Davijany, R. Myrstad, P. Pfeifer, and H. J. Venvik. Preparation and performance of Cu-based monoliths for methanol synthesis. *Applied Catalysis A: General*, 405(1-2):1–7, 2011.

[35] G. M. Robb, W. Zhang, and P. G. Smirniotis. Acidity of dealuminated β-zeolites via coupled NH3-stepwise temperature programmed desorption (stpd) and ft-ir spectroscopy. *Microporous and Mesoporous Materials*, 20:307–316, 1998.

[36] M. Niwa and N. Katada. Measurements of acidic property of zeolites by temperature programmed desorption of ammonia. *Catalysis Surveys from Japan*, 1:215–226, 1997.

[37] D. J. Parrillo, A. T. Adamo, G. T. Kokotailo, and R. J. Gorte. Amine adsorption in H-ZSM-5. *Applied Catalysis*, 67:107–118, 1990.

[38] T. J. Gricus Kofke, R. J. Gorte, and W. E. Farneth. Stoichiometric adsorption complexes in H-ZSM-5. *Journal of Catalysis*, 114:34–45, 1988.

[39] E. Patanou. *Adsorption Microcalorimetry Studies on Supported Cobalt Catalysts*. PhD thesis, NTNU, 2012.

[40] A. Auroux, Y. S. Jin, and J. C. Vedrine. Comparative calorimetric studies of the acidity of zeolites by static and temperature-programmed methods of ammonia adsorption and desorption. *Applied Catalysis*, 36:323–330, 1988.

[41] A. Auroux, V. Bolis, P. Wierzchowski, P. C. Gravelle, and J. C. Vedrine. Study of the acidity of ZSM-5 zeolite by microcalorimetry and infrared spectroscopy. *Journal of the Chemical Society, Faraday Transactions 1: Physical Chemistry in Condensed Phases*, 75:2544–2555, 1979.

[42] I. V. Mishin, T. R. Brueva, and G. I Kapustin. Heats of adsorption of ammonia and correlation of activity and acidity in hetereogenous catalysis. *Adsorption*, 11:415–424, 2005.

[43] A. Auroux. Acidity characterization by microcalorimetry and relationship with reactivity. *Topics in Catalysis*, 4:71–89, 1997.

[44] A. Montebelli, C. G. Visconti, G. Groppi, E. Tronconi, S. Kohler, H. J. Venvik, and R. Myrstad. Washcoating and chemical testing of a commercial Cu/ZnO/Al2O3 catalyst for the methanol synthesis over copper open-cell foams. *Applied Catalysis A: General*, 481:96–103, 2014.

[45] Zeolyst. ZSM-5. URL `http://www.zeolyst.com/our-products/standard-zeolite-powders/zsm-5.aspx`.

[46] S. M. Kim, Lee Y. J., J. W. Bae, H. S. Potdar, and K. W. Jun. Synthesis and characterization of a highly active alumina catalyst for methanol dehydration to dimethyl ether. *Applied Catalysis A: General*, 348(1):113–120, 2008.

Appendices

Appendix A

Risk Assessment

NTNU	Hazardous activity identification process	Prepared by	Number	Date
HSE		HSE section	HMSRV2601	22.03.11
		Approved by	Page	Replaces
		The Rector		01.12.06

Unit: *(Institute)* **Kjemisk prosessteknologi** **Date:** 05.05.14

Line manager: **Edd A. Blekkan**

Participants in the identification process (incl. function): Kamilla Risa (student), Farbod Dadgar (Phd student), Hilde Johnsen Venvik (supervisor)

(supervisor, student, co-supervisor, others)

Short description of the main activity/main process: Master project for Kamilla Risa. Direct synthesis of DME.

Is the project work purely theoretical? (YES/NO) NO

*Answer "YES" implies that **supervisor is assured that no activities requiring risk assessment are involved in the work**. If YES, skip rest of the form.*

Signatures: *Responsible supervisor:* Hilde Johnsen Venvik *Student:* Kamilla Risa

ID nr.	Activity/process	Responsible person	Existing documentation	Existing safety measures	Laws, regulations etc.	Comment
1	Changing gas bottles, transport and mounting	Farbod Dadgar, Harry Brun, Kamilla Risa	NTNU HSE Handbook	Safety goggles, gas alarms, transport vehicle	Safety Datasheets	Pressure (200 bar), toxic gases (CO), combustible gases (H2, CH4, CO)
2	Modification of experimental set-up	Farbod Dadgar	NTNU HSE Handbook	Safety goggles, gas alarms, ventilation, emergency stop device	Safety Datasheets, Risk assessment of set-up	Pressure (80 bar), toxic gases, combustible gases (H2, CH4, CO)
3	Leak testing and reactor installing	Farbod Dadgar, Kamilla Risa	NTNU HSE Handbook	Safety goggles, gas alarms, ventilation, emergency stop device	Safety Datasheets, DME set-up manual	Pressure, combustible gases
4	Loading of reactor	Kamilla Risa	NTNU HSE Handbook	Safety goggles, gloves	Safety Datasheets	

5	Reaction experiment	Kamilla Risa, Farbod Dadgar	NTNU HSE Handbook	Safety goggles, gas alarms, ventilation, emergency stop device	Safety Datasheets	Pressure, temperature
6	Catalyst synthesis	Kamilla Risa	NTNU HSE Handbook	Safety goggles, gloves	Safety Datasheets	Salt presursors, solvents
7	Catalyst preparation: calcination	Kamilla Risa, Farbod Dadgar	NTNU HSE Handbook	Safety goggles, gloves, gas alarms, ventilation	Safety Datasheets	Pressure, temperature, fumes
8	Catalyst characterization: TGA	Kamilla Risa	NTNU HSE Handbook	Safety goggles, gloves, gas detectors installed in the lab	Safety Datasheets	Flammable, combustible and toxic gases (H2, CO, N2O). Heat treatment
9	Catalyst characterization: XRD	Kamilla Risa	NTNU HSE Handbook		Safety Datasheet	Radiation
10	Catalyst characterization: Calorimetry	Kamilla Risa	NTNU HSE Handbook	Safety goggles, ventilation	Safety Datasheet	Toxic gas (NH3), heat treatment.
11	Catalyst characterization: BET	Kamilla Risa	NTNU HSE Handbook	Safety goggles, gloves, lab coat	Safety Datasheets	Liquid nitrogen

NTNU HMS /KS	Risk assessment	Prepared by	Nummer	Date
		HSE section	HMSRV2603	04.02.11
		Approved by	Page	Replaces
		The Rector		09.02.10

Unit: *(Institute)* ***Kjemisk prosessteknologi*** **Date:** 05.05.14

Line manager: ***Edd A. Blekkan***

Participants in the identification process (incl. function): *Kamilla Risa (student), Farbod Dadgar (Phd student), Hilde Johnsen Venvik (supervisor)*
(supervisor, student, co-supervisor, others)

Risk assessment of: Master project for Kamilla Risa. Direct synthesis of DME.

Signatures: *Responsible supervisor:* Hilde Johnsen Venvik *Student:* Kamilla Risa

ID nr.	Activity from the identification process form	Potential undesirable incident/strain	Likeli-	Consequence:				Risk value (human)	Comments/status Suggested measures
			(1-5)	Human (A-E)	Enviromen t (A-E)	Economy/ material (A-E)			
1-1	Changing gas bottles, transport and mounting	Leakage of small amount of gas: toxic (CO), combustible (H2, CO, CH4)	3	A	A	A		**A3**	Change of bottles only to be performed under supervision during working hours
1-2	Changing gas bottles, transport and mounting	Leakage of larger amount of gas: toxic (CO), combustible (H2, CO, CH4)	1	C	A	A		**C1**	Change of bottles only to be performed under supervision during working hours
2-1	Modification of experimental set-up	Leakage of small amount of gas: toxic (CO), combustible (H2, CO, CH4)	2	A	A	A		**A2**	Only to be performed under supervision
2-2	Modification of experimental set-up	Leakage of larger amount of gas: toxic (CO), combustible (H2, CO, CH4)	1	B	A	B		**B1**	Only to be performed under supervision

3	Leak testing and reactor installing	Leakage of small amount of gas: toxic (CO), combustible (H2, CO, CH4)	2	A	A	A		**A2**	
4	Loading of reactor	Chemical exposure	4	A	A	A		**A4**	
5	Reaction experiment	Chemical exposure	4	A	A	A		**A4**	
6	Catalyst synthesis	Chemical exposure	4	A	A	A		**A4**	
7	Catalyst preparation: calcination	Chemical exposure	4	A	A	A		**A4**	Ventilation
8-1	Catalyst characterization: TGA	Chemical exposure	4	A	A	A		**A4**	Compulsory training required prior to use of instrument
8-2	Catalyst characterization: TGA	Small leakage of gas: toxic (NH3, N2O), combustible (H2)	3	A	A	A		**A3**	Compulsory training required prior to use of instrument
9	Catalyst characterization: XRD	Radiation	1	A	A	A		**A1**	Compulsory training required prior to use of instrument
10	Catalyst characterization: Calorimetry	Small leakage of toxic gas (NH3)	3	A	A	A		**A3**	Leakage of ammonia gas will be detected by smell before toxic levels are reached. Only small amounts of gas will be used.
11-1	Catalyst charcterization: BET	Chemical exposure	4	A	A	A		**A4**	Compulsory training required prior to use of instrument

11-2	Catalyst characterization: BET	Liquid nitrogen spill	1	B	A	A		**B1**	Compulsory training required prior to use of instrument

Appendix B

High Resolution ICP-MS Analysis

The original data from the ICP-MS analysis is included here. Note that only the results are included. The first batch of homemade methanol catalyst is vessel number 21 (project inr 1) and the second batch is vessel 24 (project inr 4). For the zeolite samples, only relevant metals are included.

- Vessel 37 and 56: H-ZSM-5 80, first and second analysis respectively
- Vessel 38 and 57: Na(30),H-ZSM-5 80, first and second batch respectively
- Vessel 39 and 58: H-ZSM-5 30, first and second analysis respectively
- vessel 40 and 59: Na(30),H-ZSM-5 30, first and second analysis respectively

The concentration of metals is given here as $^{\mu g}/_{g}$. To find the weight percent a metal, the value given was converted to $^{g}/_{g}$ and then multiplied with 100 %. An example calculation for copper in the first batch of methanol catalyst is shown below:

$$229620^{\mu g}/_{g} \cdot 10^{-6} = 0,229620^{g}/_{g} = 0,229620 \cdot 100\% = 22.96wt\% \tag{B.1}$$

Results not calculated back to solid material, blank values

	Digestion overview, filled about by the laboratory																						
	Sample received	UltraClave Date	Serial nr.	Vessel-nr	Smp.weight max 50 mg	Final vol. 216ml (216.6g)	Material	Matrix after digestion	High Solids Info	Remarks	Elements	Al	Cu	Fe	K	Na	P	S	Si	Zn	12 ml PFA vials	Project-Inr
Start formulas											Start formulas											
		14.10.2013	774	26		216,00	blank	0.1M HNO3			9	1	1	1	1	1	1	1	1	56	1
		14.10.2013	774	27		216,00	blank	0.1M HNO3			9	1	1	1	1	1	1	1	1	57	2
		14.10.2013	774	28		216,00	blank	0.1M HNO3			9	1	1	1	1	1	1	1	1	58	3
	Procedure:	1) SiC , 1.5 ml conc. HNO3 + 0.5 ml conc. HF , digested according to shown temerature profile . Tehn diluted to 216 ml																				
		2) sample 1-4 3ml 50% v/v HNO3 , digested according to shown temerature profile . Tehn diluted to 216 ml																				
											Blank values fro co											
Stop formulas											Stop formulas											
number		5	3	3			3	3			3	3	3	3	3	3	3	3				
Average											24											

Results not calculated back to solid material, and not corrected for blank values

	Digestion overview, filled about by the laboratory																						
	Sample received	UltraClave Date	Serial nr.	Vessel-nr	Smp.weight max 50 mg	Final vol. 216ml (216.6g)	Material	Matrix after digestion	High Solids Info	Remarks	Elements	Al	Cu	Fe	K	Na	P	S	Si	Zn	12 ml PFA vials	Project-Inr
Start formulas											Start formulas											
	09.10.2013	14.10.2013	774	21	19,1	216,00	$CuO/ZnO/Al_2O_3$	0.1M HNO3			4	1	1			1			1	51	1
	09.10.2013	14.10.2013	774	22	18,0	216,00	$CuO/ZnO/Al_2O_3$	0.1M HNO3			4	1	1			1			1	52	2
	09.10.2013	14.10.2013	774	23	18,2	216,00	$CuO/ZnO/Al_2O_3$	0.1M HNO3			4	1	1			1			1	53	3
	09.10.2013	14.10.2013	774	24	16,6	216,00	$CuO/ZnO/Al_2O_3$	0.1M HNO3			4	1	1			1			1	54	4
	09.10.2013	14.10.2013	774	25	25,8	219,00	SiC	0.1M HNO + 0.23% HF	Si	not deisolved as excpected	9	1	1	1	1	1	1	1	1	55	5
	Procedure:	1) SiC , 1.5 ml conc. HNO3 + 0.5 ml conc. HF , digested according to shown temerature profile . Tehn diluted to 216 ml																				
		2) sample 1-4 3ml 50% v/v HNO3 , digested according to shown temerature profile . Tehn diluted to 216 ml																				
Stop formulas											Stop formulas											
number		7	5	5			5	5	1	1	5	5	5	1	1	5	1	1	1			
Average											20											

Results calculated back to solid material, and corrected for blank values

	Digestion overview, filled about by the laboratory																						
	Sample received	UltraClave Date	Serial nr.	Vessel-nr	Smp.weight max 50 mg	Final vol. 216ml (216.6g)	Material	Matrix after digestion	High Solids Info	Remarks	Elements	Al	Cu	Fe	K	Na	P	S	Si	Zn	12 ml PFA vials	Project-Inr
Start formulas											Start formulas											
	09.10.2013	14.10.2013	774	21	19,1	216,00	$CuO/ZnO/Al_2O_3$	0.1M HNO3			4	1	1			1			1	51	1
	09.10.2013	14.10.2013	774	22	18,0	216,00	$CuO/ZnO/Al_2O_3$	0.1M HNO3			4	1	1			1			1	52	2
	09.10.2013	14.10.2013	774	23	18,2	216,00	$CuO/ZnO/Al_2O_3$	0.1M HNO3			4	1	1			1			1	53	3
	09.10.2013	14.10.2013	774	24	16,6	216,00	$CuO/ZnO/Al_2O_3$	0.1M HNO3			4	1	1			1			1	54	4
	09.10.2013	14.10.2013	774	25	25,8	219,00	SiC	0.1M HNO + 0.23% HF	Si	not deisolved as excpected	9	1	1	1	1	1	1	1	1	55	5
	Procedure:	1) SiC , 1.5 ml conc. HNO3 + 0.5 ml conc. HF , digested according to shown temerature profile . Tehn diluted to 216 ml																				
		2) sample 1-4 3ml 50% v/v HNO3 , digested according to shown temerature profile . Tehn diluted to 216 ml																				
Stop formulas											Stop formulas											
number		7	5	5			5	5	1	1	5	5	5	1	1	5	1	1	1			
Average											20											

Date of analyses: 16.10.13 sekvens 65

Counting digits = 3

Isotope	Be9(MR)		Na23(MR)		Mg25(MR)		Al27(MR)		Si29(MR)		P31(MR)		S34(MR)		K39(MR)		Ca43(MR)		Ti47(MR)		V51(MR)		Cr53(MR)		Mn55(MR)	
Parameteres	Conc.		Conc.		Conc.		Conc.		Conc.		Conc.		Conc.		Conc.		Conc.		Conc.		Conc.		Conc.		Conc.	
Sample ID	µg/L	RSD, %	µg/L	RSD, %	µg/L	RSD, %	µg/L	RSD, %	µg/L	RSD, %	µg/L	RSD, %	µg/L	RSD, %	µg/L	RSD, %	µg/L	RSD, %	µg/L	RSD, %	µg/L	RSD, %	µg/L	RSD, %	µg/L	RSD, %
Start statistical calculations																										
Dadgar-HNO3-PFA-51-48-56-BLANK	0,002	173,2	0	2,8	0,03	7,5	0,8	49,9	253	2,2	0,0	12,5	5	4,2	0,0	4,3	0	62,4	0,01	0,0	0,00	58,0	-0,03	17,6	0,00	21,7
Dadgar-HNO3-PFA-51-48-57-blank	0,000	0,0	0	2,4	0,24	16,1	1,4	28,0	376	3,2	0,1	5,0	2	2,2	0,2	4,8	4	34,9	0,08	27,2	0,00	87,7	0,06	7,0	0,00	29,4
Dadgar-HNO3-PFA-51-48-58-blank	0,000	0,0	0	1,2	0,20	12,1	1,9	8,9	114	2,8	0,0	7,1	1	2,4	0,1	0,7	1	18,4	0,00	173,2	0,00	15,7	0,03	4,6	0,00	18,9
Stop statistical calculations																										
Average	0,001	57,7	0	2,1	0,16	11,9	1,4	28,9	247	2,7	0,0	8,2	2	2,9	0,1	3,3	2	38,6	0,03	66,8	0,00	53,8	0,02	9,7	0,00	23,3
lues sett =0					**0,16**	**11,9**	**1,4**	**28,9**	**247**	**2,7**			**2**	**2,9**									**0,02**	**9,7**		
Min	0,000	0,0	0	1,2	0,03	7,5	0,8	8,9	114	2,2	0,0	5,0	1	2,2	0,0	0,7	0	18,4	0,00	0,0	0,00	15,7	-0,03	4,6	0,00	18,9
Max	0,002	173,2	0	2,8	0,24	16,1	1,9	49,9	376	3,2	0,1	12,5	5	4,2	0,2	4,8	4	62,4	0,08	173,2	0,00	87,7	0,06	17,6	0,00	29,4
Std	0,001	100,0	0	0,8	0,11	4,3	0,6	20,5	131	0,5	0,0	3,9	2	1,1	0,1	2,2	2	22,2	0,04	93,1	0,00	36,2	0,04	6,9	0,00	5,4
Rsd % <5, 5-10, >10	173,2		199,8		72,1		42,2		53,0		100,6		98,7		77,9		116,6		134,4		69,1		216,4		125,1	
Confidence interval 95%	0,001	141,4	0	1,2	0,16	6,1	0,8	29,0	185	0,7	0,0	5,5	3	1,6	0,2	3,2	3	31,4	0,06	131,7	0,00	51,2	0,06	9,8	0,00	7,7
Confidence interval 95% (%) <5, 5-10, >10	244,9		282,6		102,0		59,6		75,0		142,3		139,6		110,2		164,9		190,1		97,8		306,1		176,9	
Number	3	3	3	3	3	3	3	3	3	3	3	3	3	3	3	3	3	3	3	3	3	3	3	3	3	3

Date of analyses: 16.10.13 sekvens 65

Counting digits = 3

Isotope	Be9(MR)		Na23(MR)		Mg25(MR)		Al27(MR)		Si29(MR)		P31(MR)		S34(MR)		K39(MR)		Ca43(MR)		Ti47(MR)		V51(MR)		Cr53(MR)		Mn55(MR)	
Parameteres	Conc.		Conc.		Conc.		Conc.		Conc.		Conc.		Conc.		Conc.		Conc.		Conc.		Conc.		Conc.		Conc.	
Sample ID	µg/L	RSD, %	µg/L	RSD, %	µg/L	RSD, %	µg/L	RSD, %	µg/L	RSD, %	µg/L	RSD, %	µg/L	RSD, %	µg/L	RSD, %	µg/L	RSD, %	µg/L	RSD, %	µg/L	RSD, %	µg/L	RSD, %	µg/L	RSD, %
Start statistical calculations																										
Dadgar-HNO3-PFA-51-48-51-start-CuO	0,017	17,3	4 690	6,2	0,16	12,4	7 602,6	5,0	18	4,4	0,2	8,4	7	7,3	1,1	5,2	13	18,0	0,33	28,9	0,00	55,6	0,26	16,1	0,31	6,1
Dadgar-HNO3-PFA-51-48-52	0,018	78,7	3 536	1,5	0,28	11,6	6 125,1	0,8	211	2,2	0,2	4,3	3	6,8	0,7	1,7	11	10,6	2,23	3,7	0,01	25,8	0,29	9,3	0,43	5,6
Dadgar-HNO3-PFA-51-48-53	0,022	35,3	3 450	2,9	0,36	1,9	5 997,5	6,3	32	3,9	0,4	3,6	-4	2,9	1,3	1,6	7	23,4	2,45	8,4	0,00	12,5	0,27	15,7	0,39	4,0
Dadgar-HNO3-PFA-51-48-54-slutt-CuO	0,022	35,3	3 515	1,4	0,12	23,7	6 422,4	0,5	12	3,8	0,4	4,6	10	2,4	1,0	3,1	8	15,6	0,96	15,0	0,01	22,3	0,25	13,9	0,26	9,5
Dadgar-PFA-51-48-55-SiC-slutt-HF	0,000	0,0	3	0,2	0,27	6,1	6,3	6,4	688	0,5	0,2	5,5	8	3,6	0,9	2,6	7	16,4	2,39	4,3	2,49	4,8	0,08	15,1	1,94	4,9
Stop statistical calculations																										
Average	0,016	33,3	3 039	2,4	0,24	11,1	5 230,8	3,8	192	3,0	0,3	5,3	5	4,6	1,0	2,8	9	16,8	1,67	12,1	0,50	24,2	0,23	14,0	0,67	6,0
Min	0,000	0,0	3	0,2	0,12	1,9	6,3	0,5	12	0,5	0,2	3,6	-4	2,4	0,7	1,6	7	10,6	0,33	3,7	0,00	4,8	0,08	9,3	0,26	4,0
Max	0,022	78,7	4 690	6,2	0,36	23,7	7 602,6	6,4	688	4,4	0,4	8,4	10	7,3	1,3	5,2	13	23,4	2,45	28,9	2,49	55,6	0,29	16,1	1,94	9,5
Std	0,009	29,3	1 774	2,3	0,10	8,2	2 988,6	2,9	289	1,6	0,1	1,9	5	2,3	0,2	1,5	3	4,6	0,97	10,4	1,11	19,4	0,08	2,8	0,72	2,1
Rsd % <5, 5-10, >10	57,6		58,4		39,9		57,1		150,4		39,2		109,0		22,5		29,3		57,8		220,9		36,7		107,4	
Confidence interval 95%	0,009	29,3	1 774	2,3	0,10	8,2	2 988,6	2,9	289	1,6	0,1	1,9	5	2,3	0,2	1,5	3	4,6	0,97	10,4	1,11	19,4	0,08	2,8	0,72	2,1
Confidence interval 95% (%) <5, 5-10, >10	57,6		58,4		39,9		57,1		150,4		39,2		109,0		22,5		29,3		57,8		220,9		36,7		107,4	
Number	5	5	5	5	5	5	5	5	5	5	5	5	5	5	5	5	5	5	5	5	5	5	5	5	5	5

Date of analyses: 16.10.13 sekvens 65

Counting digits = 3

Isotope	Be9(MR)		Na23(MR)		Mg25(MR)		Al27(MR)		Si29(MR)		P31(MR)		S34(MR)		K39(MR)		Ca43(MR)		Ti47(MR)		V51(MR)		Cr53(MR)		Mn55(MR)	
Parameteres	Conc.		Conc.		Conc.		Conc.		Conc.		Conc.		Conc.		Conc.		Conc.		Conc.		Conc.		Conc.		Conc.	
Sample ID	µg/g	RSD, %	µg/g	RSD, %	µg/g	RSD, %	µg/g	RSD, %	µg/g	RSD, %	µg/g	RSD, %	µg/g	RSD, %	µg/g	RSD, %	µg/g	RSD, %	µg/g	RSD, %	µg/g	RSD, %	µg/g	RSD, %	µg/g	RSD, %
Start statistical calculations																										
Dadgar-HNO3-PFA-51-48-51-start-CuO	0,189	17,3	53 036	6,2	0,08	12,4	85 961	5,0	<1500	4,4	2,1	8,4	51	7,3	12,0	5,2	152	18,0	3,73	28,9	0,06	55,6	2,70	16,1	3,52	6,1
Dadgar-HNO3-PFA-51-48-52	0,220	78,7	42 437	1,5	1,52	11,6	73 484	0,8	<1500	2,2	2,0	4,3	7	6,8	7,8	1,7	132	10,6	26,73	3,7	0,12	25,8	3,27	9,3	5,18	5,6
Dadgar-HNO3-PFA-51-48-53	0,257	35,3	40 947	2,9	2,43	1,9	71 163	6,3	<1500	3,9	4,7	3,6	-71	2,9	15,0	1,6	81	23,4	29,06	8,4	0,05	12,5	3,01	15,7	4,65	4,0
Dadgar-HNO3-PFA-51-48-54-slutt-CuO	0,281	35,3	45 733	1,4	-0,42	23,7	83 551	0,5	<1500	3,8	4,9	4,6	99	2,4	12,8	3,1	108	15,6	12,53	15,0	0,07	22,3	3,02	13,9	3,34	9,5
Dadgar-PFA-51-48-55-SiC-slutt-HF	0,000	0,0	26	0,2	0,95	6,1	42,0	6,4	3 742	0,5	2,0	5,5	50	3,6	8,0	2,6	63	16,4	20,26	4,3	21,11	4,8	0,53	15,1	16,48	4,9
Stop statistical calculations																										
Average	0,189	33,3	36 436	2,4	0,91	11,1	62 840,2	3,8	3 742	3,0	3,1	5,3	27	4,6	11,1	2,8	107	16,8	18,46	12,1	4,28	24,2	2,51	14,0	6,63	6,0
Min	0,000	0,0	26	0,2	-0,42	1,9	42,0	0,5	3 742	0,5	2,0	3,6	-71	2,4	7,8	1,6	63	10,6	3,73	3,7	0,05	4,8	0,53	9,3	3,34	4,0
Max	0,281	78,7	53 036	6,2	2,43	23,7	85 960,9	6,4	3 742	4,4	4,9	8,4	99	7,3	15,0	5,2	152	23,4	29,06	28,9	21,11	55,6	3,27	16,1	16,48	9,5
Std	0,112	29,3	20 881	2,3	1,13	8,2	35 671,0	2,9	#DIV/0!	1,6	1,5	1,9	64	2,3	3,1	1,5	36	4,6	10,44	10,4	9,41	19,4	1,12	2,8	5,56	2,1
Rsd % <5, 5-10, >10	58,9		57,3		124,2		56,8		#DIV/0!		47,9		233,5		28,1		33,7		56,6		219,8		44,8		83,8	
Confidence interval 95%	0,112	29,3	20 881	2,3	1,13	8,2	35 671,0	2,9	#DIV/0!	1,6	1,5	1,9	64	2,3	3,1	1,5	36	4,6	10,44	10,4	9,41	19,4	1,12	2,8	5,56	2,1
Confidence interval 95% (%) <5, 5-10, >10	58,9		57,3		124,2		56,8		#DIV/0!		47,9		233,5		28,1		33,7		56,6		219,8		44,8		83,8	
Number	5	5	5	5	5	5	5	5	1	5	5	5	5	5	5	5	5	5	5	5	5	5	5	5	5	5

Fe57(MR)		Co59(MR)		Ni62(MR)		Cu65(MR)		Zn67(MR)		Ga69(MR)		Rb85(MR)		Sr88(MR)		Y89(MR)		Mo98(MR)		Sn118(MR)		Sb121(MR)		Cs133(MR)		Ba137(MR)		La139(MR)		Ce140(MR)	
Conc. µg/L	RSD, %	Conc. µg/L	RSD, %	Conc. µg/L	RSD, %	Conc. µg/L	RSD, %	Conc. µg/L	RSD, %	Conc. µg/L	RSD, %	Conc. µg/L	RSD, %	Conc. µg/L	RSD, %	Conc. µg/L	RSD, %	Conc. µg/L	RSD, %	Conc. µg/L	RSD, %	Conc. µg/L	RSD, %	Conc. µg/L	RSD, %	Conc. µg/L	RSD, %	Conc. µg/L	RSD, %	Conc. µg/L	RSD, %
0,1	27,6	0,00	173,2	0,0	0,0	0,02	22,3	0,17	39,0	0,002	173,2	0,000	15,1	0,00	33,3	0,001	91,7	0,00	136,1	0,01	8,7	0,00	100,0	0,000	95,2	0,00	0,0	0,000	100,0	0,000	86,6
0,1	24,7	0,00	173,2	0,0	173,2	0,03	14,5	0,76	28,0	0,000	173,2	0,001	48,9	0,01	20,5	0,000	173,2	0,02	252,4	0,00	57,3	0,00	86,6	0,000	173,2	0,00	173,2	0,002	78,9	0,001	53,7
0,2	56,9	0,00	100,0	0,0	106,4	0,00	30,5	0,75	36,4	0,003	27,9	0,001	81,0	0,01	23,1	0,000	87,7	0,00	133,6	0,01	12,7	0,00	35,3	0,000	86,8	0,00	100,0	0,000	94,4	0,001	81,2
0,1	36,4	0,00	148,8	0,0	93,2	0,01	22,4	0,56	34,5	0,002	124,8	0,001	48,3	0,00	25,6	0,000	117,5	0,01	174,1	0,00	26,2	0,00	74,0	0,000	118,4	0,00	91,1	0,001	91,1	0,001	73,8
0,1	24,7	0,00	100,0	0,0	0,0	0,00	14,5	0,17	28,0	0,000	27,9	0,000	15,1	0,00	20,5	0,000	87,7	0,00	133,8	0,00	8,7	0,00	35,3	0,000	86,8	0,00	0,0	0,000	78,9	0,000	53,7
0,2	56,9	0,00	173,2	0,0	173,2	0,03	30,5	0,76	39,0	0,003	173,2	0,001	81,0	0,01	33,3	0,001	173,2	0,02	252,4	0,01	57,3	0,00	100,0	0,000	173,2	0,00	173,2	0,002	100,0	0,001	86,6
0,1	17,8	0,00	42,3	0,0	87,4	0,01	8,0	0,34	5,7	0,001	83,9	0,001	33,0	0,00	6,8	0,000	48,3	0,01	67,8	0,00	27,0	0,00	34,2	0,000	47,6	0,00	86,9	0,001	10,9	0,000	17,6
46,1		86,6		116,1		95,4		61,0		86,7		92,2		53,4		64,2		97,7		91,6		61,9		35,6		86,6		108,9		49,9	
0,1	25,2	0,00	59,8	0,0	123,5	0,02	11,3	0,48	8,1	0,002	118,6	0,001	46,6	0,00	9,6	0,000	68,2	0,01	95,9	0,01	38,2	0,00	48,3	0,000	67,4	0,00	123,0	0,001	15,5	0,001	25,0
65,2		122,5		164,2		135,0		86,2		122,6		130,4		75,5		90,7		138,2		129,6		87,5		50,3		122,5		154,0		70,5	
3	3	3	3	3	3	3	3	3	3	3	3	3	3	3	3	3	3	3	3	3	3	3	3	3	3	3	3	3	3	3	3

Fe57(MR)		Co59(MR)		Ni62(MR)		Cu65(MR)		Zn67(MR)		Ga69(MR)		Rb85(MR)		Sr88(MR)		Y89(MR)		Mo98(MR)		Sn118(MR)		Sb121(MR)		Cs133(MR)		Ba137(MR)		La139(MR)		Ce140(MR)	
Conc. µg/L	RSD, %	Conc. µg/L	RSD, %	Conc. µg/L	RSD, %	Conc. µg/L	RSD, %	Conc. µg/L	RSD, %	Conc. µg/L	RSD, %	Conc. µg/L	RSD, %	Conc. µg/L	RSD, %	Conc. µg/L	RSD, %	Conc. µg/L	RSD, %	Conc. µg/L	RSD, %	Conc. µg/L	RSD, %	Conc. µg/L	RSD, %	Conc. µg/L	RSD, %	Conc. µg/L	RSD, %	Conc. µg/L	RSD, %
2,6	18,2	0,11	15,0	0,2	37,9	20 304,34	4,2	29 423,93	2,6	0,648	10,4	0,001	17,3	0,13	12,8	0,002	31,5	0,03	624,3	0,29	16,6	0,00	100,0	0,000	173,2	0,40	4,7	0,003	16,7	0,001	28,2
2,8	15,6	0,47	1,2	0,3	28,4	18 209,88	1,4	27 067,02	1,4	0,456	2,1	0,000	35,3	0,12	0,5	0,001	35,3	0,05	89,7	0,26	14,3	0,01	42,6	0,001	22,3	0,39	11,1	0,001	51,2	0,013	45,3
2,3	5,2	0,37	5,5	0,2	10,0	16 774,14	4,4	25 756,66	0,9	0,438	1,2	0,001	70,5	0,10	3,1	0,001	48,4	0,06	22,4	0,25	11,2	0,00	86,6	0,001	97,2	0,31	9,1	0,001	43,3	0,019	33,0
2,1	26,1	0,02	16,4	0,2	48,9	17 178,16	1,7	25 820,33	1,5	0,557	5,1	0,003	24,1	0,12	6,9	0,000	87,7	0,03	10128,1	0,32	3,8	0,00	91,7	0,001	94,4	0,39	24,4	0,001	114,6	0,002	45,1
15,4	4,1	0,18	8,7	4,1	8,8	3,88	4,4	7,74	6,9	-0,001	86,6	-0,001	105,1	0,02	11,3	0,021	19,5	0,00	199,2	0,00	18,9	0,00	93,9	0,001	50,0	0,09	16,5	0,032	4,2	0,089	14,3
5,0	13,8	0,23	9,4	1,0	26,8	14 494,08	3,2	21 615,13	2,7	0,420	21,1	0,001	50,5	0,10	6,9	0,005	44,5	0,03	2212,7	0,22	13,0	0,00	83,0	0,001	87,4	0,32	13,2	0,008	46,0	0,025	33,2
2,1	4,1	0,02	1,2	0,2	8,8	3,88	1,4	7,74	0,9	-0,001	1,2	-0,001	17,3	0,02	0,5	0,000	19,5	0,00	22,4	0,00	3,8	0,00	42,6	0,000	22,3	0,09	4,7	0,001	4,2	0,001	14,3
15,4	26,1	0,47	16,4	4,1	48,9	20 304,34	4,4	29 423,93	6,9	0,648	86,6	0,003	105,1	0,13	12,8	0,021	87,7	0,06	10128,1	0,32	18,9	0,01	100,0	0,001	173,2	0,40	24,4	0,032	114,6	0,089	45,3
5,8	9,2	0,19	6,4	1,7	17,5	8 214,85	1,5	12 169,79	2,5	0,250	36,8	0,001	36,8	0,04	5,2	0,009	26,3	0,02	4431,0	0,13	5,9	0,00	23,1	0,000	57,3	0,13	7,6	0,014	42,9	0,037	12,9
114,7		81,2		171,1		56,7		56,3		59,5		187,5		44,2		171,3		66,5		58,2		73,1		41,7		41,9		181,8		145,8	
5,8	9,2	0,19	6,4	1,7	17,5	8 214,85	1,5	12 169,79	2,5	0,250	36,8	0,001	36,8	0,04	5,2	0,009	26,3	0,02	4431,0	0,13	5,9	0,00	23,1	0,000	57,3	0,13	7,6	0,014	42,9	0,037	12,9
114,7		81,2		171,1		56,7		56,3		59,5		187,5		44,2		171,3		66,5		58,2		73,1		41,7		41,9		181,8		145,8	
5	5	5	5	5	5	5	5	5	5	5	5	5	5	5	5	5	5	5	5	5	5	5	5	5	5	5	5	5	5	5	5

Fe57(MR)		Co59(MR)		Ni62(MR)		Cu65(MR)		Zn67(MR)		Ga69(MR)		Rb85(MR)		Sr88(MR)		Y89(MR)		Mo98(MR)		Sn118(MR)		Sb121(MR)		Cs133(MR)		Ba137(MR)		La139(MR)		Ce140(MR)	
Conc. µg/g	RSD, %	Conc. µg/g	RSD, %	Conc. µg/g	RSD, %	Conc. µg/g	RSD, %	Conc. µg/g	RSD, %	Conc. µg/g	RSD, %	Conc. µg/g	RSD, %	Conc. µg/g	RSD, %	Conc. µg/g	RSD, %	Conc. µg/g	RSD, %	Conc. µg/g	RSD, %	Conc. µg/g	RSD, %	Conc. µg/g	RSD, %	Conc. µg/g	RSD, %	Conc. µg/g	RSD, %	Conc. µg/g	RSD, %
29,5	18,2	1,21	15,0	2,6	37,9	229 620	4,2	332 752	2,6	7,323	10,4	0,006	17,3	1,43	12,8	0,022	31,5	0,37	624,3	3,31	16,6	0,01	100,0	0,005	173,2	4,51	4,7	0,032	16,7	0,017	28,2
33,9	15,6	5,66	1,2	3,5	28,4	218 519	1,4	324 804	1,4	5,474	2,1	-0,005	35,3	1,46	0,5	0,014	35,3	0,64	89,7	3,07	14,3	0,07	42,6	0,015	22,3	4,64	11,1	0,014	51,2	0,160	45,3
27,1	5,2	4,38	5,5	2,6	10,0	199 078	4,4	305 683	0,9	5,195	1,2	0,016	70,5	1,22	3,1	0,016	48,4	0,71	22,4	2,95	11,2	0,03	86,6	0,006	97,2	3,65	9,1	0,013	43,3	0,230	33,0
27,8	26,1	0,30	16,4	2,7	48,9	223 523	1,7	335 975	1,5	7,252	5,1	0,036	24,1	1,63	6,9	0,005	87,7	0,36	10128,1	4,12	3,8	0,03	91,7	0,014	94,4	5,13	24,4	0,008	114,6	0,029	45,1
130,6	4,1	1,49	8,7	34,6	8,8	33	4,4	66	6,9	-0,005	86,6	-0,005	105,1	0,19	11,3	0,179	19,5	0,01	199,2	-0,03	18,9	0,01	93,9	0,006	50,0	0,75	16,5	0,273	4,2	0,758	14,3
49,8	13,8	2,61	9,4	9,2	26,8	174 154	3,2	259 856	2,7	5,048	21,1	0,010	50,5	1,18	6,9	0,047	44,5	0,42	2212,7	2,69	13,0	0,03	83,0	0,009	87,4	3,74	13,2	0,068	46,0	0,239	33,2
27,1	4,1	0,30	1,2	2,6	8,8	33	1,4	66	0,9	-0,005	1,2	-0,005	17,3	0,19	0,5	0,005	19,5	0,01	22,4	-0,03	3,8	0,01	42,6	0,005	22,3	0,75	4,7	0,008	4,2	0,017	14,3
130,6	26,1	5,66	16,4	34,6	48,9	229 620	4,4	335 975	6,9	7,323	86,6	0,036	105,1	1,63	12,8	0,179	87,7	0,71	10128,1	4,12	18,9	0,07	100,0	0,015	173,2	5,13	24,4	0,273	114,6	0,758	45,3
45,3	9,2	2,29	6,4	14,2	17,5	98 007	1,5	145 703	2,5	2,990	36,8	0,017	36,8	0,57	5,2	0,074	26,3	0,28	4431,0	1,59	5,9	0,02	23,1	0,005	57,3	1,75	7,6	0,115	42,9	0,304	12,9
91,0		87,8		154,7		56,3		56		59,2		177,4		48,4		156,1		66,3		59,1		78,4		50,0		46,9		169,0		127,3	
45,3	9,2	2,29	6,4	14,2	17,5	98 006,77	1,5	145 703	2,5	2,990	36,8	0,017	36,8	0,57	5,2	0,074	26,3	0,28	4431,0	1,59	5,9	0,02	23,1	0,005	57,3	1,75	7,6	0,115	42,9	0,304	12,9
91,0		87,8		154,7		56,3		56,1		59,2		177,4		48,4		156,1		66,3		59,1		78,4		50,0		46,9		169,0		127,3	
5	5	5	5	5	5	5	5	5	5	5	5	5	5	5	5	5	5	5	5	5	5	5	5	5	5	5	5	5	5	5	5

Pr141(MR)		Sm147(MR)		Lu175(MR)		W182(MR)		Au197(MR)		Tl205(MR)		Pb208(MR)		Th232(MR)		U238(MR)		As75(HR)		Zr90(HR)		Nb93(HR)		Pt195(HR)	
Conc. µg/L	RSD, %	Conc. µg/L	RSD, %	Conc. µg/L	RSD, %	Conc. µg/L	RSD, %	Conc. µg/L	RSD, %	Conc. µg/L	RSD, %	Conc. µg/L	RSD, %	Conc. µg/L	RSD, %	Conc. µg/L	RSD, %	Conc. µg/L	RSD, %	Conc. µg/L	RSD, %	Conc. µg/L	RSD, %	Conc. µg/L	RSD, %
0,000	0,0	0,001	173,2	0,000	0,0	0,001	0,0	0,002	89,2	0,000	173,2	0,01	11,6	0,008	32,0	0,000	173,2	0,00	173,2	0,02	82,6	0,000	0,0	0,00	0,0
0,000	173,2	0,002	173,2	0,001	173,2	0,001	173,2	0,001	106,4	0,000	173,2	0,21	4,7	0,004	90,1	0,000	0,0	0,00	87,7	0,01	57,9	0,002	90,6	0,00	173,2
0,000	0,0	0,001	173,2	0,000	0,0	0,001	173,2	0,000	0,0	0,000	0,0	0,31	4,9	0,002	84,9	0,000	173,2	0,00	87,7	0,00	86,8	0,000	0,0	0,00	173,2
0,000	57,7	0,002	173,2	0,000	57,7	0,001	115,5	0,001	65,2	0,000	115,5	0,18	7,1	0,005	69,0	0,000	115,5	0,00	116,2	0,01	75,8	0,001	30,2	0,00	115,5
0,000	0,0	0,001	173,2	0,000	0,0	0,001	0,0	0,000	0,0	0,000	0,0	0,01	4,7	0,002	32,0	0,000	0,0	0,00	87,7	0,00	57,9	0,000	0,0	0,00	0,0
0,000	173,2	0,002	173,2	0,001	173,2	0,001	173,2	0,002	106,4	0,000	173,2	0,31	11,6	0,008	90,1	0,000	173,2	0,00	173,2	0,02	86,8	0,002	90,6	0,00	173,2
0,000	100,0	0,000	0,0	0,001	100,0	0,000	100,0	0,001	57,1	0,000	100,0	0,16	3,9	0,003	32,1	0,000	100,0	0,00	49,4	0,01	15,6	0,001	52,3	0,00	100,0
173,2		27,2		173,2		8,0		89,9		86,9		88,4		62,6		86,6		86,6		69,4		173,2		86,6	
0,000	141,4	0,001	0,0	0,001	141,4	0,000	141,4	0,001	80,8	0,000	141,4	0,22	5,6	0,004	45,5	0,000	141,4	0,00	69,8	0,01	22,1	0,002	74,0	0,00	141,4
244,9		38,5		244,9		11,3		127,1		122,9		125,0		88,5		122,5		122,5		98,2		244,9		122,5	
3	3	3	3	3	3	3	3	3	3	3	3	3	3	3	3	3	3	3	3	3	3	3	3	3	3

Pr141(MR)		Sm147(MR)		Lu175(MR)		W182(MR)		Au197(MR)		Tl205(MR)		Pb208(MR)		Th232(MR)		U238(MR)		As75(HR)		Zr90(HR)		Nb93(HR)		Pt195(HR)	
Conc. µg/L	RSD, %	Conc. µg/L	RSD, %	Conc. µg/L	RSD, %	Conc. µg/L	RSD, %	Conc. µg/L	RSD, %	Conc. µg/L	RSD, %	Conc. µg/L	RSD, %	Conc. µg/L	RSD, %	Conc. µg/L	RSD, %	Conc. µg/L	RSD, %	Conc. µg/L	RSD, %	Conc. µg/L	RSD, %	Conc. µg/L	RSD, %
0,001	86,6	0,002	91,7	0,001	86,7	0,003	43,3	0,001	110,2	0,145	6,9	0,25	11,0	0,003	44,1	0,000	0,0	0,01	71,3	0,02	68,0	0,004	93,9	0,00	173,2
0,001	137,8	0,004	114,6	0,000	0,0	0,009	52,9	0,004	15,7	0,132	11,5	0,25	6,0	0,003	75,1	0,000	0,0	0,00	0,0	0,03	76,1	0,003	86,6	0,01	173,2
0,001	114,6	0,000	0,0	0,000	0,0	0,006	32,8	0,003	81,7	0,133	10,9	0,27	11,2	0,002	70,5	0,000	173,2	0,00	26,6	0,04	48,0	0,006	20,4	0,00	0,0
0,000	173,2	0,004	173,2	0,000	0,0	0,003	61,9	0,002	121,2	0,117	16,2	0,27	7,7	0,001	52,0	0,000	0,0	0,01	113,5	0,01	28,9	0,002	97,2	0,01	114,6
0,006	4,3	0,004	173,2	0,000	173,2	0,020	27,7	0,005	34,6	0,000	0,0	0,11	10,1	0,012	28,0	0,002	33,2	0,00	86,6	1,01	9,8	0,009	10,8	0,00	0,0
0,002	103,3	0,003	110,5	0,000	52,0	0,008	43,7	0,003	72,7	0,106	9,1	0,23	9,2	0,004	53,9	0,000	41,3	0,00	59,6	0,22	46,2	0,005	61,8	0,00	92,2
0,000	4,3	0,000	0,0	0,000	0,0	0,003	27,7	0,001	15,7	0,000	0,0	0,11	6,0	0,001	28,0	0,000	0,0	0,00	0,0	0,01	9,8	0,002	10,8	0,00	0,0
0,006	173,2	0,004	173,2	0,001	173,2	0,020	61,9	0,005	121,2	0,145	16,2	0,27	11,2	0,012	75,1	0,002	173,2	0,01	113,5	1,01	76,1	0,009	97,2	0,01	173,2
0,002	63,8	0,002	71,5	0,000	77,5	0,007	14,1	0,002	46,2	0,060	6,1	0,07	2,3	0,004	19,3	0,001	75,1	0,00	45,9	0,44	27,4	0,002	42,5	0,00	87,5
134,9		61,5		168,2		89,6		47,2		56,7		29,6		105,5		206,4		149,0		197,2		53,2		100,3	
0,002	63,8	0,002	71,5	0,000	77,5	0,007	14,1	0,002	46,2	0,060	6,1	0,07	2,3	0,004	19,3	0,001	75,1	0,00	45,9	0,44	27,4	0,002	42,5	0,00	87,5
134,9		61,5		168,2		89,6		47,2		56,7		29,6		105,5		206,4		149,0		197,2		53,2		100,3	
5	5	5	5	5	5	5	5	5	5	5	5	5	5	5	5	5	5	5	5	5	5	5	5	5	5

Pr141(MR)		Sm147(MR)		Lu175(MR)		W182(MR)		Au197(MR)		Tl205(MR)		Pb208(MR)		Th232(MR)		U238(MR)		As75(HR)		Zr90(HR)		Nb93(HR)		Pt195(HR)	
Conc. µg/g	RSD, %	Conc. µg/g	RSD, %	Conc. µg/g	RSD, %	Conc. µg/g	RSD, %	Conc. µg/g	RSD, %	Conc. µg/g	RSD, %	Conc. µg/g	RSD, %	Conc. µg/g	RSD, %	Conc. µg/g	RSD, %	Conc. µg/g	RSD, %	Conc. µg/g	RSD, %	Conc. µg/g	RSD, %	Conc. µg/g	RSD, %
0,009	86,6	0,027	91,7	0,012	86,7	0,028	43,3	0,016	110,2	1,644	6,9	2,78	11,0	0,031	44,1	0,000	0,0	0,10	71,3	0,24	68,0	0,045	93,9	0,05	173,2
0,012	137,8	0,046	114,6	0,000	0,0	0,112	52,9	0,051	15,7	1,589	11,5	3,01	6,0	0,041	75,1	0,000	0,0	-0,03	0,0	0,41	76,1	0,036	86,6	0,08	173,2
0,006	114,6	0,000	0,0	0,000	0,0	0,069	32,8	0,039	81,7	1,579	10,9	3,23	11,2	0,021	70,5	0,002	173,2	0,04	26,6	0,47	48,0	0,066	20,4	0,00	0,0
0,004	173,2	0,056	173,2	0,000	0,0	0,038	61,9	0,031	121,2	1,528	16,2	3,54	7,7	0,015	52,0	0,000	0,0	0,07	113,5	0,15	28,9	0,030	97,2	0,11	114,6
0,047	4,3	0,035	173,2	0,003	173,2	0,173	27,7	0,047	34,6	0,000	0,0	0,93	10,1	0,103	28,0	0,019	33,2	0,00	86,6	8,59	9,8	0,073	10,8	0,00	0,0
0,016	103,3	0,033	110,5	0,003	52,0	0,084	43,7	0,037	72,7	1,268	9,1	2,70	9,2	0,042	53,9	0,004	41,3	0,04	59,6	1,97	46,2	0,050	61,8	0,05	92,2
0,004	4,3	0,000	0,0	0,000	0,0	0,028	27,7	0,016	15,7	0,000	0,0	0,93	6,0	0,015	28,0	0,000	0,0	-0,03	0,0	0,15	9,8	0,030	10,8	0,00	0,0
0,047	173,2	0,056	173,2	0,012	173,2	0,173	61,9	0,051	121,2	1,644	16,2	3,54	11,2	0,103	75,1	0,019	173,2	0,10	113,5	8,59	76,1	0,073	97,2	0,11	173,2
0,018	63,8	0,021	71,5	0,005	77,5	0,060	14,1	0,014	46,2	0,710	6,1	1,02	2,3	0,035	19,3	0,008	75,1	0,05	45,9	3,70	27,4	0,019	42,5	0,05	87,5
114,0		65,2		178,1		70,8		37,8		56,0		38,0		83,4		200,4		146,4		188,0		37,3		103,7	
0,018	63,8	0,021	71,5	0,005	77,5	0,060	14,1	0,014	46,2	0,710	6,1	1,02	2,3	0,035	19,3	0,008	75,1	0,05	45,9	3,70	27,4	0,019	42,5	0,05	87,5
114,0		65,2		178,1		70,8		37,8		56,0		38,0		83,4		200,4		146,4		188,0		37,3		103,7	
5	5	5	5	5	5	5	5	5	5	5	5	5	5	5	5	5	5	5	5	5	5	5	5	5	5

Results calculated back to solid material, and corrected for blanks

Reanalyzes procedure: Ultrasonic bath 80C approx 30 minutes with 1.5 ml kons HNO3 + 0.5 ml conc. HF, the diluted to 216 ml. All samples was completly disolved, as far visula check could tell.

Date of analyses: 21.02.14 sekvens 14

Counting digits = 3

Sample received	UltraClave Date	Serial nr.	25 ml PFA via	Smp.weight (mg)	Final vol. ml	Project-Inr	ID-1	Elements	Al	Na	Si	Pfa-16 ml	Isotope Parameteres / Sample ID
				mg	ml								
Start formulas								Start formulas					Start statistical calculations
17.12.2013	**24.01.2014**	room temper	56	16,4	216,00	6	H-ZSM-5 Zeolite	2	1		1	356	Farbod-dagar-pfa-356 feil i sekvens
17.12.2013	**24.01.2014**	room temper	57	44,8	216,00	7	NaH-ZSM-5	3	1	1	1	357	Farbod-dagar-pfa-357
17.12.2013	**24.01.2014**	room temper	58	17,0	216,00	8	H-ZSM-5 Zeolite	2	1		1	358	Farbod-dagar-pfa-358
17.12.2013	**24.01.2014**	room temper	59	29,0	216,00	9	NaH-ZSM-5	3	1	1	1	359	Farbod-dagar-pfa-359
													Stop statistical calculations
Stop formulas								Stop formulas					Average
number	4	4	4			4	4	4	4	2	4		Min
Average								10					Max
													Std
													Rsd % <5, 5-10, >10
													Confidence interval 95%
													Confidence interval 95% (%) <5, 5-10, >10
													Number

Results calculated back to solid material, and corrected for blank values

First analyzes: UltraClave 245 C, total time 2.5 hours 20-245-20C with 1.5 ml kons HNO3 + 0.5 ml conc. HF, the diluted to 216 ml. All samples was completly disolved, as far visula check could tell.

Date of analyses: 05.02.14 sekvens 7

Counting digits = 3

Sample received	UltraClave Date	Serial nr.	Vessel-nr	Smp.weight (mg)	Final vol. ml	Project-Inr	ID-1	Elements	Al	Na	Si	Pfa-16 ml	Isotope Parameteres / Sample ID
				mg	ml								
Start formulas								Start formulas					Start statistical calculations
17.12.2013	**24.01.2014**	793	37	31,5	216,00	6	H-ZSM-5 Zeolite	2	1		1	194	Dagar-pfaror-396-399-396
17.12.2013	**24.01.2014**	793	38	45,4	216,00	7	NaH-ZSM-5	3	1	1	1	195	Dagar-pfaror-396-399-397
17.12.2013	**24.01.2014**	793	39	23,2	216,00	8	H-ZSM-5 Zeolite	2	1		1	196	Dagar-pfaror-396-399-398
17.12.2013	**24.01.2014**	793	40	21,1	216,00	9	NaH-ZSM-5	3	1	1	1	197	Dagar-pfaror-396-399-399
Stop formulas								Stop formulas					Stop statistical calculations
number	4	4	4			4	4	4	4	2	4		Average
Average								10					Min
													Max
													Std
													Rsd % <5, 5-10, >10
													Confidence interval 95%
													Confidence interval 95% (%) <5, 5-10, >10
													Number

Operator : Syverin Lierhagen

Statistics Sum %	µg/g	Al27(MR) Conc. µg/g	Na23(MR) Conc. µg/g	Si29(MR) Conc. µg/g	U238(LR) Conc. µg/g
75,4	754 045	32 501	39	721 505	0,209
42,9	429 475	9 440	1 048	418 986	0,136
48,3	482 792	27 536	61	455 194	0,207
44,3	443 247	24 521	3 112	415 614	0,177
53	527 390	23 499	1 065	502 825	0,182
43	429 475	9 440	39	415 614	0,136
75	754 045	32 501	3 112	721 505	0,209
15	152 784	9 934	1 443	146 884	0,034
29,0	29,0	42,3	135,5	29,2	18,7
18	176 420	11 470	1 667	169 606	0,039
33,5	33,5	48,8	156,5	33,7	21,6
4	4	4	4	4	4

Statistics Sum %	µg/g	Al27(MR) Conc. µg/g	Na23(MR) Conc. µg/g	Si29(MR) Conc. µg/g	U238(LR) Conc. µg/g
33,4	334 485	9 709	17	324 758	0,173
33,3	333 197	3 747	1 034	328 416	0,143
21,4	213 713	8 197	26	205 489	0,172
35,7	356 507	11 312	3 830	341 366	0,171
31	309 475	8 241,3	1 226,8	300 007	0,1649
21	213 713	3 747,2	17,2	205 489	0,1431
36	356 507	11 311,6	3 830,1	341 366	0,1730
6	64 732	3 254,8	1 799,9	63 414	0,0146
20,9	20,9	39,5	146,7	21,1	8,8
7	74 746	3 758,3	2 078,3	73 224	0,0168
24,2	24,2	45,6	169,4	24,4	10,2
4	4	4	4	4	4

Operator : Syverin Lierhagen

Appendix C

Copper Dispersion

To calculate the dispersion of copper in the methanol catalysts, the amount of copper in the sample and on the surface was estimated. The total amount of copper was calculated based on the weight loss during reduction, while the amount of copper on the surface was found by linear regression.

Table C.1 below gives the mass of the catalyst samples at the start of the temperature program, and at the end of the pretreatment and the end of the reduction.

Table C.1: *Sample mass changes during N_2O titration experiment*

Comment	**Homemade (1)** mg	**Homemade (2)** mg
start	15.7	16.9
end of pretreatment	14.1	15.5
end of reduction	13.3	14.3
intercept	0.0069	0.0052

The mass change during reduction is due to copper atoms being reduced. It is assumed that prior to the reduction, all copper atoms are present as Cu^{2+}. By converting the mass reduction to a reduction of oxygen atoms, the number of copper atoms is found:

$$\frac{\Delta m}{m_O} = n_{Cu} \tag{C.1}$$

The amount of copper on the surface of the catalyst sample is found by linear regression (see section 4.2.3). The weight change due to oxidation of copper atoms on the surface is taken as the intercept on the y-axis and is given in table C.1. This weight change is assumed to the partial oxidation of copper atoms as given below:

$$N_2O + 2Cu \rightarrow Cu - O - Cu + N_2 \tag{C.2}$$

For the second the amount of copper atoms on the surface is then: $^{0.0052[mg]}/_{16[^{mg}/_{mmol}]} \cdot 2 = 0.0015[mmol]$. The dispersion is calculated as the percentage of copper atoms on the surface relative to the total amount of copper atoms in the sample:

$$D = \frac{n_{Cu_s}}{n_{Cu_t}} \tag{C.3}$$

To evaluate the calculations for the homemade catalyst, the amount of copper in the samples were calculated from the copper loading. The copper loading was determined by ICP to be 22.4 wt%. The amount of copper in the sample based on the loading is then (trial 2) $15.5[mg] \cdot 0.2235 = 3.46[mg]$. The amount of copper from the calculation above however is 4.57 [mg]. The amount of copper in the catalyst sample is overestimated by about $^{4.57 - 3.46}/_{3.46} \cdot 100\% = 31.8\%$.

For the first trial, the calculated amount is in more agreement with the copper loading. The calculated amount of copper in this sample is about 8 % higher than the loading suggests. The fact that amount of copper is more overestimated in the first sample explains why the dispersion was calculated to be lower for this sample.

The reason why the amount of copper is overestimated is probably due to the assumption that all the copper is present as Cu^{2+} and possibly measurement errors. The reason why the overestimation is larger for the first sample however is unclear.

The raw data for the reduction is given in figure C.1 for the homemade catalyst (both trials).

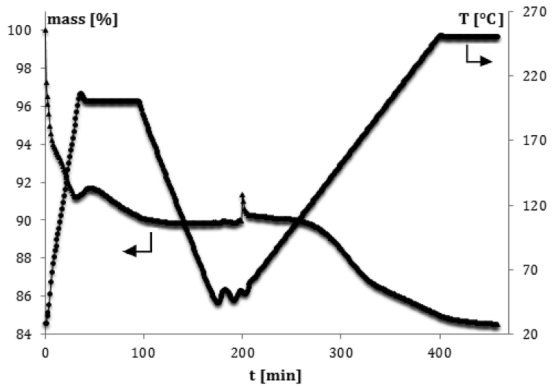

(a) *Homemade methanol catalyst, 1. trial*

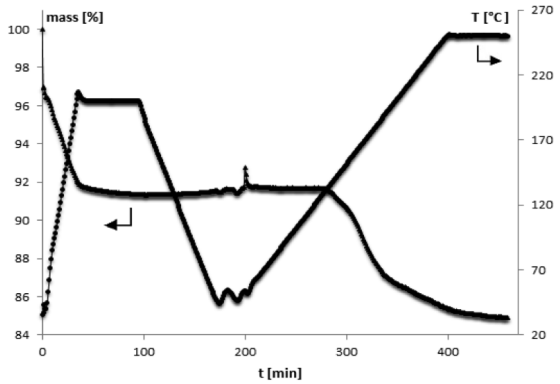

(b) *Homemade methanol catalyst, 2. trial*

Figure C.1: *Reduction raw data for homemade methanol catalyst.*

Appendix D

NH_3 TPD

Two different temperature programs were used for the ammonia temperature-programmed desorption experiments. The main difference between the two temperature programs is the pretreatment temperature. Pretreatment temperature may affect the acidity of the zeolites, as mentioned in section 2.4.5. To check if the pretreatment temperature had any effect on the TPD results, H-ZSM-5 80 were tested with both programs. Figure D.1 shows the mass variation as a function of temperature for the H-ZSM-5 80 zeolite for both temperature programs.

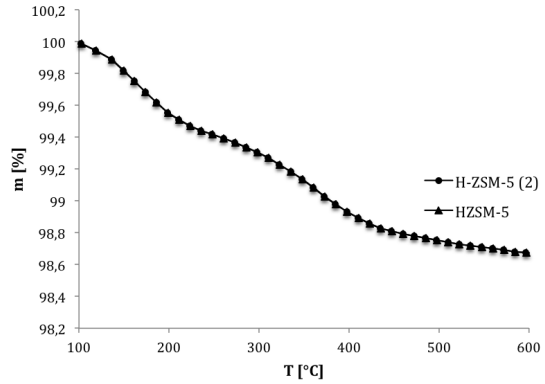

(a) *Mass change*

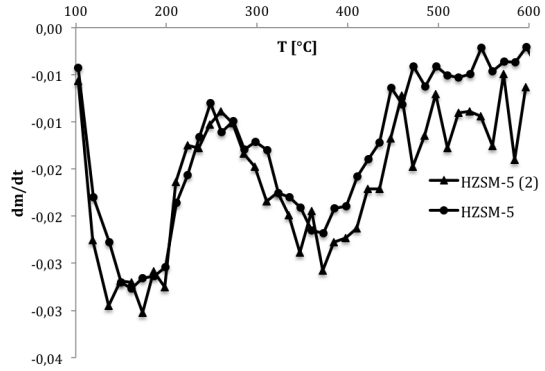

(b) *Differential mass change*

Figure D.1: *Variation in sample mass during ammonia TPD for H-ZSM-5 80 with pretreatment temperature of 600 °C and 250 °C*

As seen in figure D.1, the effect of the pretreatment temperature is hardly noticed for H-ZSM-5 80. Figure D.1a shows the variation in sample mass as a function of temperature for both temperature programs. The two curves are indistinguishable. Figure D.1b shows the differential mass change as a function of temperature. The two curves are very similar at low temperature. At high temperature, there is a small difference between the two curves, but this difference is assumed to be small enough to be negligible.

Figure D.2 shows the raw data for the two ammonia TPD experiments on H-ZSM-5 80.

The raw data for the other acidic catalysts is not shown, as they were very similar to the curves shown in figure D.2a and D.2b.

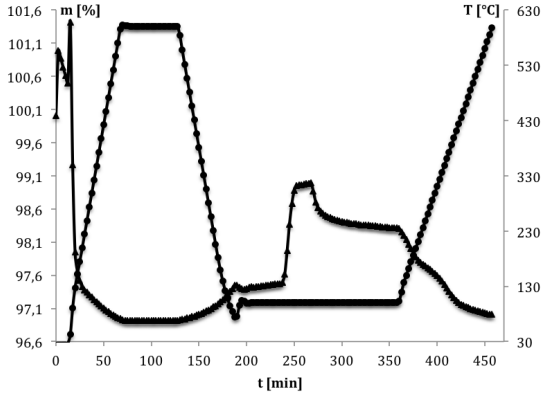

(a) *600 °C*

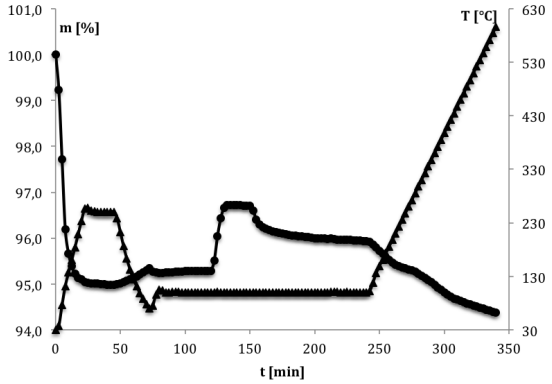

(b) *250 °C*

Figure D.2: *Temperature and mass change as a function of time for for H-ZSM-5 80 with pretreatment temperature of 600 °C (a) and 250 °C (b)*

Appendix E

Calorimetry

Volume Calibration

The volume calibrations were carried out as described in section 3.3.5. Table E.1 shows the recorded pressures, p_i and p_f and the calculated volume of V_0.

Table E.1: *Raw data for volume calibration of* V_0

measurement	$\mathbf{p_i}$	$\mathbf{p_f}$	$\mathbf{V_0}$
number	[torr]	[torr]	[ml]
1	7.394	4.614	334.7
2	9.783	6.120	333.8
3	8.017	5.008	334.3
4	8.280	5.170	334.4
5	7.532	4.701	334.6

The second measurement was assumed to be a measurement error and was not included in further calculations. The average value for the volume of V_0 is then 334.5 with a standard deviation of 0.156. The next measurement performed was the volume of V_x. Table E.2 shows the recorded pressures, p_i and p_f and the calculated volume.

Table E.2: *Raw data for volume calibration of V_x*

measurement	$\mathbf{p_i}$	$\mathbf{p_f}$	$\mathbf{V_x}$
number	[torr]	[torr]	[ml]
1	5.797	0.854	18.51
2	8.029	1.205	18.86
3	8.598	1.305	19.07
4	8.595	1.309	19.14
5	8.376	1.279	19.19
6	8.040	1.225	19.15

The first measurement was assumed to be a measurement error and was not included in further calculations. The average value for the volume of V_x is then 19.08 with a standard deviation of 0.131. Volume V_1 was then calculated as:

$$V_1 = V_0 - V_{fl} - V_x = 334.5 - 208.8 - 19.08[ml] = 106.6[ml] \tag{E.1}$$

The next measurement performed was V_{dose}. Table E.3 shows the recorded pressures, p_i and p_f and the calculated volume.

Table E.3: *Raw data for volume calibration of V_{dose}*

measurement	$\mathbf{p_i}$	$\mathbf{p_f}$	$\mathbf{V_{dose}}$
number	[torr]	[torr]	[ml]
1	9.515	9.039	5.61
2	9.345	8.875	5.64
3	9.168	8.705	5.67

The average value for this volume was then 5.64 [ml] with a standard deviation of 0.028. The final measurement performed was the volume called V_2. Table E.4 shows the recorded pressures, p_i and p_f and the calculated volume.

Table E.4: *Raw data for volume calibration of V_2*

measurement	$\mathbf{p_i}$	$\mathbf{p_f}$	$\mathbf{V_2}$
number	[torr]	[torr]	[ml]
1	6.524	1.032	673.80
2	6.230	1.049	633.01
3	6.488	1.104	626.38
4	6.149	1.014	646.34
5	6.117	1.031	632.38
6	6.229	1.060	626.34
7	6.593	1.073	654.91
8	6.295	1.062	631.78
9	6.327	1.059	636.79
10	6.262	1.038	643.00

The horizontal line in the table divides the measurements of the first day from the second day. As seen in table E.4, the calculated volume of V_2 varies considerably between measurements. The reason for this variation is uncertain, as both the gas used for the measurement and the temperature of the calorimeter had not been used previously for this setup. Most likely, the time needed to fully evacuate the system between the measurements was a factor, as the two highest recorded volumes were in the start of the day. The time used to evacuate between measurement varied somewhat, and the calculated volume reflects this. The 4. measurement was performed after evacuating 1.5 hours, while most of the other measurements that day was performed after evacuating about 20 minutes.

Based on these measurements, the volume of V_2 cannot be determined with satisfactorily accuracy. However, it was decided that the best course of action was to try some calorimetric experiments even though the uncertainty of the results would be fairly high. Two average values were calculated; one based on the measurements 2,3,5,6,8 and 9, and one based on measurement 4, 7 and 10. The reason for this was that the evacuation time preceding the measurements were similar, i.e. about 20 minutes for the first group, and more than 1.5 hours for the second group. The adsorbed amounts were then calculated twice, one with each average value.

The average value for the first group of measurements, i.e. 2, 3, 5, 5, 8 and 9, was determined to be 631,1 [ml], and the second average value was determined to be 648.1 [ml].

Calculations

The amount of adsorbed ammonia was calculated as explained in section 3.3.5. The adsorbed amount was related to the amount of unit cells (u.c.) in the catalyst. The unit cell of ZSM-5 is $C_nAl_nSi_{96-n}O_{192}$, where C represents the charge-

compensating cation. For the H-ZSM-5 with molar silica to alumina ratio, the charge-compensating cation is a proton, and n is equal to 6. The molecular mass of the unit cell is therefore 5767.52 g/mol.

The number of unit cells in the catalyst mass was then calculated as:

$$n_{u.c.} = \frac{m_{cat}}{5767.52} \tag{E.2}$$

where $n_{u.c.}$ is the number of unit cells in the catalyst and m_{cat} is the mass of the catalyst sample.

Thermographs

The figures below, figure E.1 -E.4, shows the raw data obtained from the Calisto software of the calorimeter. The Calisto software allows for baseline integration of the heat signal peaks. Each peak is associated with a single dose of probe gas. The text boxes connected to the peaks shows the calculated heat for each peak. This heat value was divided by the adsorbed amount in calculations.

The peaks shown in figure E.2 and E.3 are all well defined. Baseline integration was performed and is shown as yellow areas.

The first peaks shown in figure E.1 and E.4 are less sharply defined compared to the other peaks. The shape of these peaks makes baseline integration more difficult than for the others. The calculated heats of adsorption associated with these peaks are therefore uncertain.

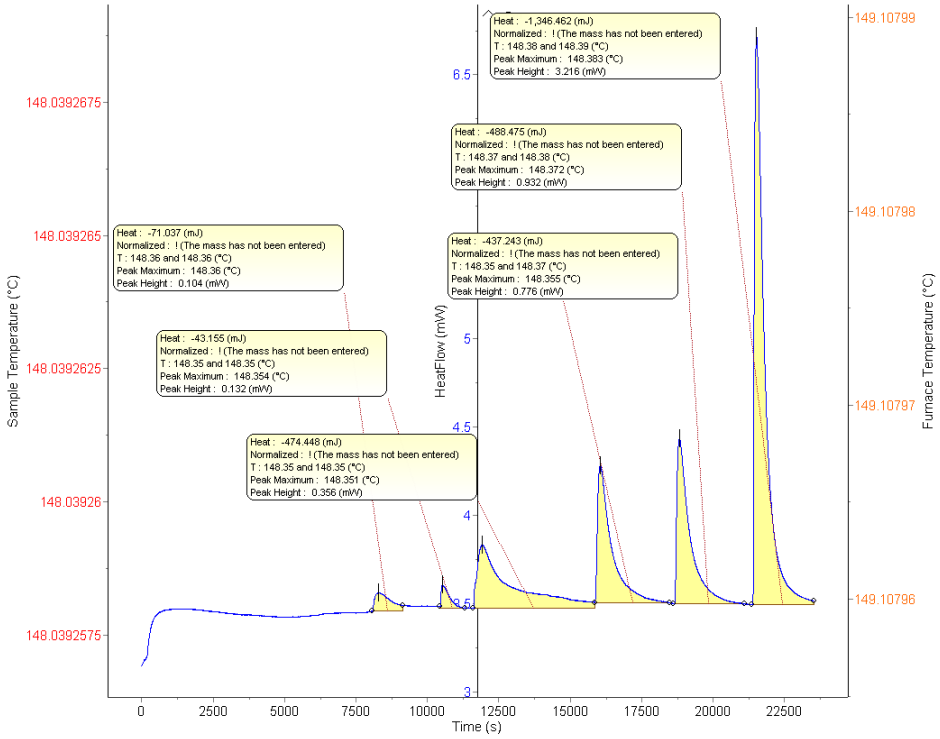

Figure E.1: *Baseline integration of heat signal, 1. trial of NH_3 calorimetry. The areas of the peaks are shown in yellow and the text boxes shows the calculated heat for each peak.*

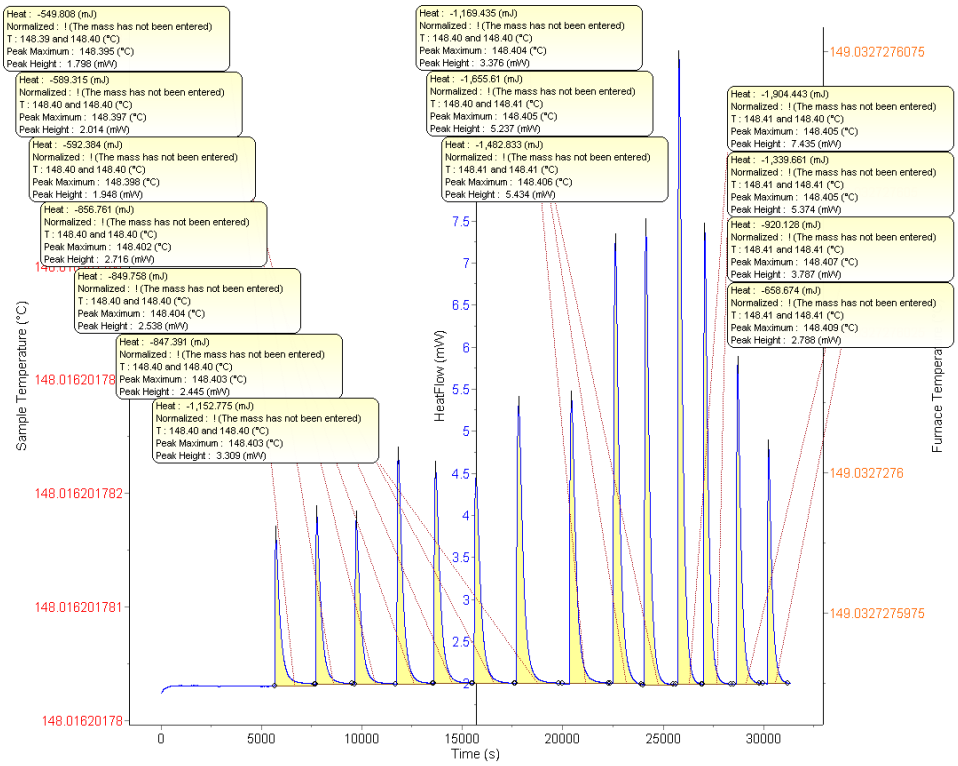

Figure E.2: *Baseline integration of heat signal, 2. trial of NH_3 calorimetry. The areas of the peaks are shown in yellow and the text boxes shows the calculated heat for each peak.*

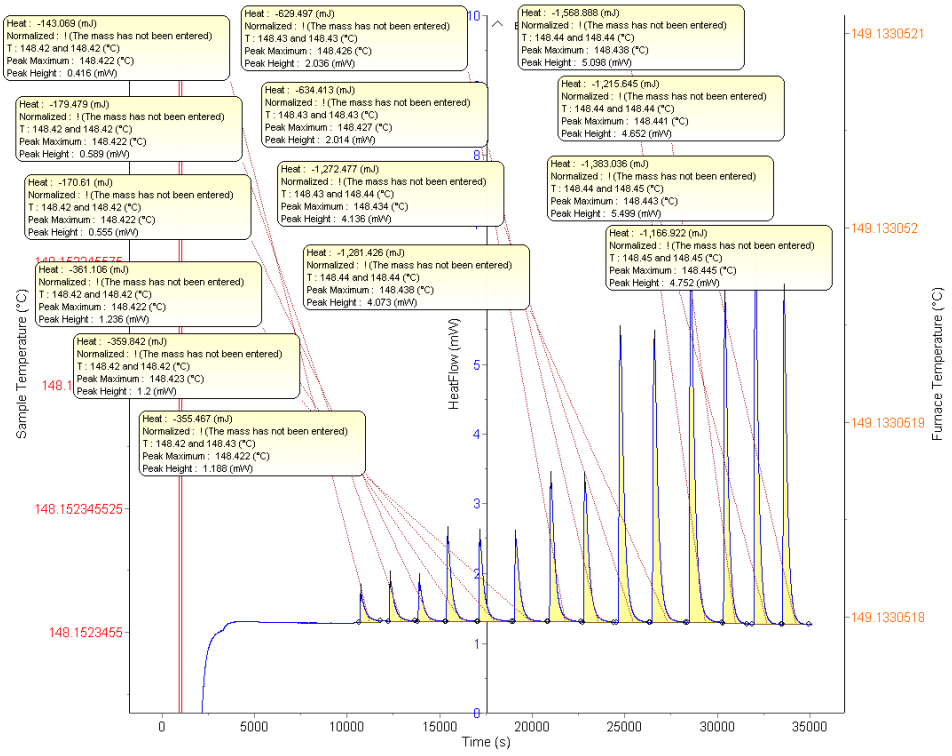

Figure E.3: *Baseline integration of heat signal, 3. trial of NH_3 calorimetry. The areas of the peaks are shown in yellow and the text boxes shows the calculated heat for each peak.*

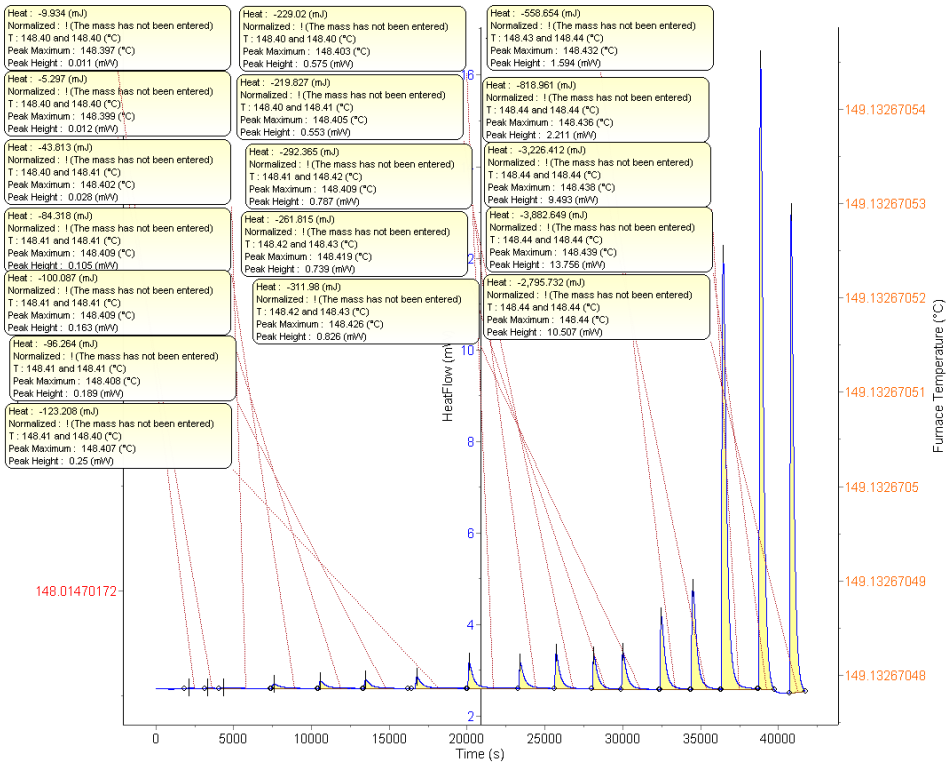

Figure E.4: *Baseline integration of heat signal, 4. trial of NH_3 calorimetry. The areas of the peaks are shown in yellow and the text boxes shows the calculated heat for each peak.*

Appendix F

Calibration of Mass Flow Controllers

The mass flow controllers (MFC) which were used in the set-up was calibrated for different gases and pressures. This was done by A. Montebelli in the fall of 2013 [44]. The calibration was performed with hydrogen gas at 1 bar (F.1), with nitrogen gas at 1 bar (F.2) and for synthesis gas at 50 bar (F.3). The synthesis gas used for the calibration was of a different composition than the synthesis gas used for activity measurements. The composition of the synthesis gas is assumed to not influence the MFC significantly.

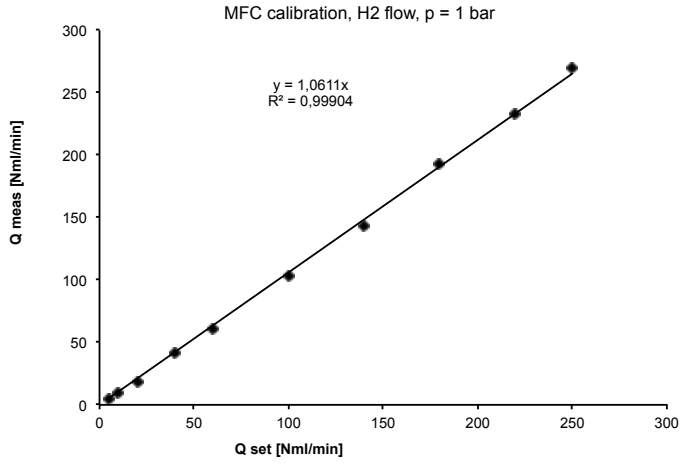

Figure F.1: *Calibration of mass flow controller for hydrogen gas at 1 bar. The calibration was performed in june 2013.*

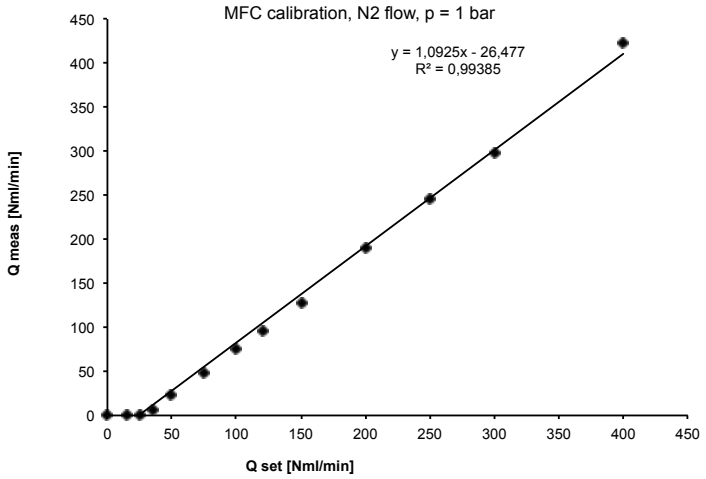

Figure F.2: *Calibration of mass flow controller for nitrogen gas at 1 bar. The calibration was performed in june 2013.*

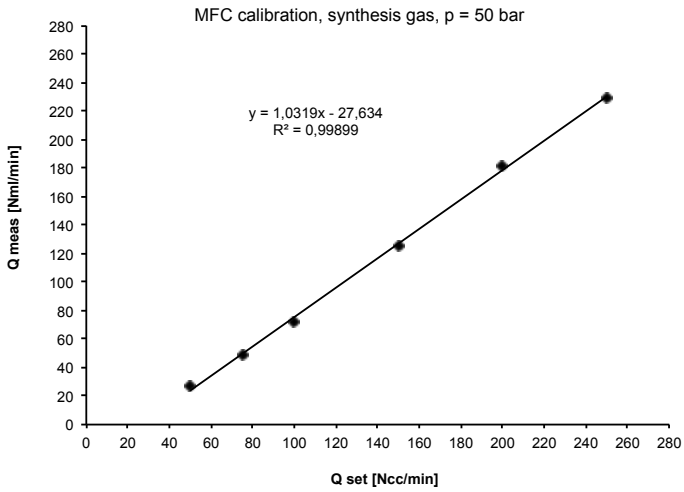

Figure F.3: *Calibration of mass flow controller for synthesis gas at 50 bar. The calibration was performed in july 2013.*

Appendix G

Feed Analysis and Mass Balance

The feed gas was analyzed prior to the methanol synthesis experiments. The ratio of the area under the CO peak to the area under the N_2 peak is given as a function of time in figure G.1.The dashed line represents the average area ratio used in calculations.

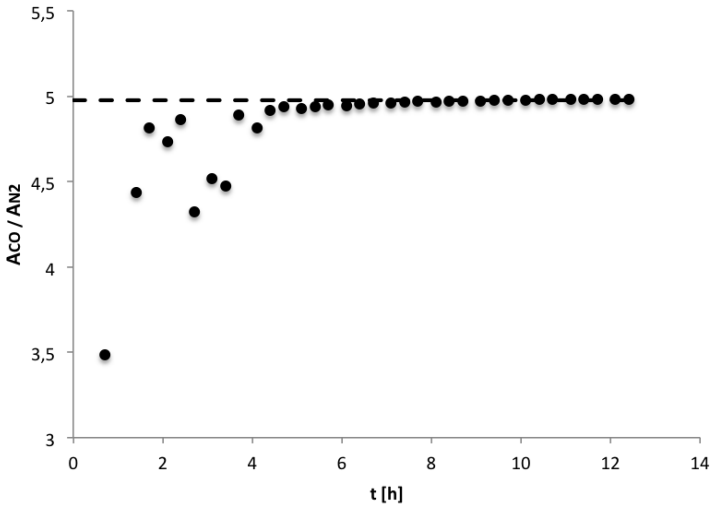

Figure G.1: *Feed gas analysis for CO as a function of time. The dashed line represent the average value used for calculations.*

A mass balance with respect to carbon was calculated for the methanol synthesis experiment with homemade catalyst. The carbon balance was calculated as described in section 3.4.3. The amount of methanol was calculated from the density analysis of the liquid product, assuming that the liquid product consisted of only methanol and water. The liquid product was collected over a time period of 16 hours. The rate of methanol formation was assumed to be constant in this time period.

The amount of carbon coming in to the system was assumed constant and was calculated based on the feed analysis and the molar feed rate. The molar feed rate was calculated using the ideal gas law.

The error in the mass balance was then calculated for each data point, as shown in section 3.4.3, and the result is shown graphically in figure G.2.

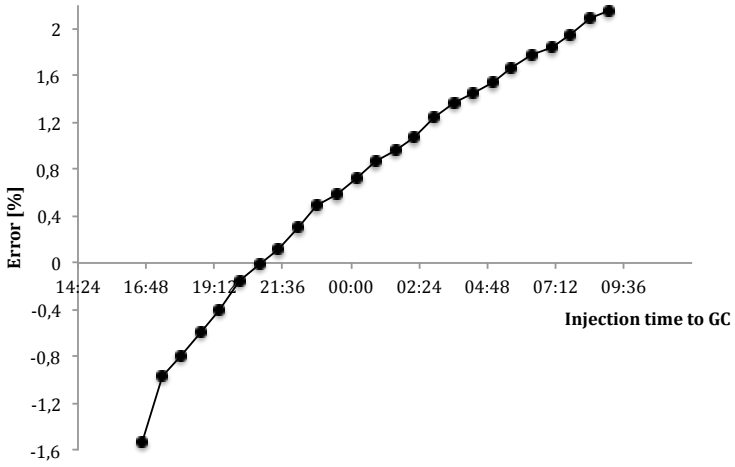

Figure G.2: *Error in carbon mass balance for the time period when the liquid methanol product was collected. Note that the error in the carbon balance never exceeds 2.2 %.*

As seen in figure G.2, the error in carbon mass balance never exceeds 2.2 %. The error is negative at the start, and then increases with time and becomes positive. A negative error means that the amount of carbon coming out is greater than the amount of carbon going in. This is not surprising as the amount of methanol coming into the system is assumed to be constant over this time period, while the total carbon conversion is shown to decrease in the same time period.

Nevertheless, a maximum error of 2.2 % is well within what is acceptable for these types of experiments.

Appendix H

GC Analysis of Liquid Product

The original report for the gas chromatographic analysis of the liquid product is included here.

Data File D:\CHEM32\1\DATA\20131028\SIG1000034.D
Sample Name: Calibration I

```
==========================================================================
Acq. Operator    : Kamilla
Acq. Instrument : Instrument 1                    Location : Vial 1
Injection Date  : 21-Nov-13, 15:44:06                 Inj :   1
                                                 Inj Volume : Manually
Acq. Method     : D:\CHEM32\1\METHODS\METHANOL_JIA1.M
Last changed    : 10/28/2013 6:38:52 PM by Jia
Analysis Method : D:\CHEM32\1\METHODS\METHANOL_JIA1.M
Last changed    : 11/21/2013 4:25:06 PM by Kamilla
```

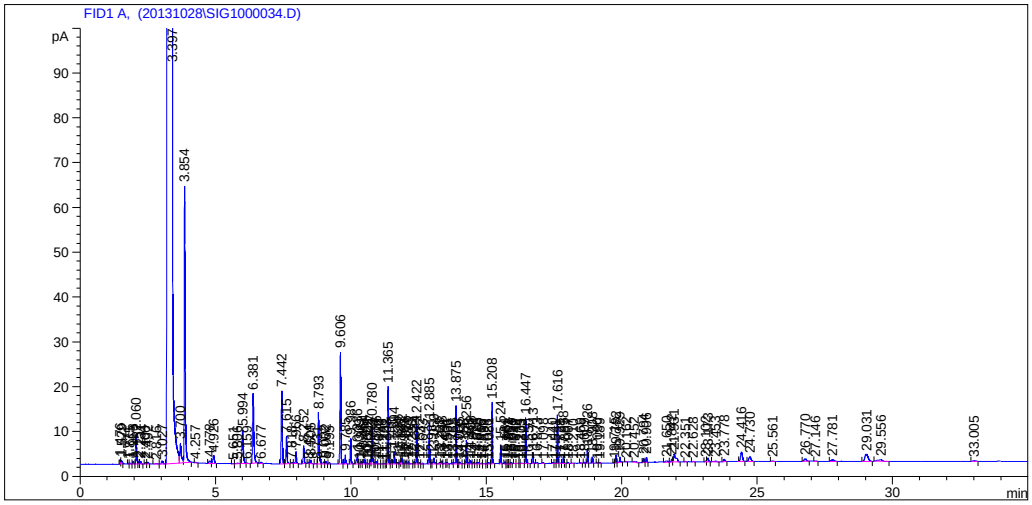


```
==========================================================================
                        External Standard Report
==========================================================================

Sorted By             :      Signal
Multiplier:                   :      1.0000
Dilution:                     :      1.0000
Use Multiplier & Dilution Factor with ISTDs

Signal 1: FID1 A,

==========================================================================
```

Data File D:\CHEM32\1\DATA\20131028\SIG1000034.D
Sample Name: Calibration I

Area Percent Report

Sorted By : Signal
Multiplier: : 1.0000
Dilution: : 1.0000
Use Multiplier & Dilution Factor with ISTDs

Signal 1: FID1 A,

Peak #	RetTime [min]	Type	Width [min]	Area [pA*s]	Height [pA]	Area %
1	1.476	BV	0.0300	2.08301	9.91965e-1	0.00267
2	1.529	VV	0.0420	2.26350	7.44346e-1	0.00290
3	1.771	BV	0.0235	3.77474e-1	2.51086e-1	0.00048
4	1.835	VB	0.0347	6.49338e-1	2.63695e-1	0.00083
5	1.953	BB	0.0300	1.22942	6.10954e-1	0.00157
6	2.060	BV	0.0279	12.61468	6.57979	0.01614
7	2.157	VV	0.0304	1.17276	5.49773e-1	0.00150
8	2.231	VB	0.0386	1.53957	6.16366e-1	0.00197
9	2.406	BV	0.0320	7.80114e-1	3.24656e-1	0.00100
10	2.492	VB	0.0388	1.04368	3.77035e-1	0.00134
11	2.816	VV	0.0576	6.85112e-1	1.43795e-1	0.00088
12	3.027	VV	0.0563	2.97632	7.18570e-1	0.00381
13	3.397	VV	0.0912	7.73315e4	1.02848e4	98.96193
14	3.700	VV	0.0535	16.94114	4.44344	0.02168
15	3.854	VB	0.0335	142.82726	61.68847	0.18278
16	4.257	BB	0.0425	2.78985e-1	7.93647e-2	0.00036
17	4.778	BV	0.0588	2.57705	5.75088e-1	0.00330
18	4.926	VB	0.0599	6.90096	1.79148	0.00883
19	5.651	BV	0.0423	2.68653e-1	8.50698e-2	0.00034
20	5.806	VV	0.0556	7.51234e-1	1.71548e-1	0.00096
21	5.994	VV	0.0491	24.56155	7.52351	0.03143
22	6.159	VB	0.0472	5.04377e-1	1.58118e-1	0.00065
23	6.381	BB	0.0473	49.97187	15.62423	0.06395
24	6.677	BV	0.0503	1.00867	3.20189e-1	0.00129
25	7.442	BV	0.0442	46.97404	16.26795	0.06011
26	7.615	VB	0.0384	15.46976	6.12889	0.01980
27	7.818	BV	0.0430	6.72535e-1	2.41590e-1	0.00086
28	7.966	VB	0.0359	6.33054	2.64480	0.00810
29	8.252	BB	0.0356	9.44935	3.99344	0.01209
30	8.424	BV	0.0366	7.63099e-1	3.28544e-1	0.00098
31	8.505	VB	0.0413	2.25007	8.38238e-1	0.00288
32	8.731	BV	0.0407	3.97978e-1	1.35905e-1	0.00051
33	8.793	VV	0.0348	26.79356	11.43214	0.03429
34	9.002	VV	0.0535	1.84534	4.68007e-1	0.00236
35	9.072	VB	0.0411	1.48725	5.57212e-1	0.00190
36	9.195	BB	0.0321	5.05792e-1	2.39801e-1	0.00065
37	9.606	BB	0.0387	61.43195	24.99949	0.07862
38	9.785	BB	0.0338	4.46683	1.98238	0.00572

Data File D:\CHEM32\1\DATA\20131028\SIG1000034.D
Sample Name: Calibration I

Peak #	RetTime [min]	Type	Width [min]	Area [pA*s]	Height [pA]	Area %
39	9.986	BB	0.0314	11.38719	5.68057	0.01457
40	10.236	BV	0.0402	6.62087	2.29222	0.00847
41	10.309	VV	0.0344	3.95983e-1	1.78540e-1	0.00051
42	10.381	VV	0.0340	1.31312	5.89498e-1	0.00168
43	10.464	VV	0.0390	2.60198	1.06445	0.00333
44	10.582	VV	0.0304	5.18759e-1	2.63722e-1	0.00066
45	10.625	VV	0.0317	2.36702e-1	1.13981e-1	0.00030
46	10.727	VV	0.0308	2.02012	1.03293	0.00259
47	10.780	VV	0.0285	15.40389	8.15034	0.01971
48	10.874	VV	0.0292	3.46282e-1	1.77980e-1	0.00044
49	10.936	VV	0.0333	1.40194	6.46956e-1	0.00179
50	11.020	VB	0.0385	2.24121e-1	8.30187e-2	0.00029
51	11.146	BV	0.0336	1.84119e-1	8.06613e-2	0.00024
52	11.221	VV	0.0357	2.84884e-1	1.11854e-1	0.00036
53	11.303	VV	0.0240	2.09692e-1	1.32365e-1	0.00027
54	11.365	VV	0.0311	34.94281	17.24416	0.04472
55	11.491	VV	0.0316	2.12744	1.02926	0.00272
56	11.594	VB	0.0312	5.52926	2.66547	0.00708
57	11.724	BV	0.0290	7.15516e-1	3.62488e-1	0.00092
58	11.822	VV	0.0307	1.31626	6.47136e-1	0.00168
59	11.882	VV	0.0324	2.78052	1.27819	0.00356
60	11.969	VV	0.0260	2.14504e-1	1.19292e-1	0.00027
61	12.026	VV	0.0300	1.27121	6.58506e-1	0.00163
62	12.113	VV	0.0357	1.07813	4.79928e-1	0.00138
63	12.238	VV	0.0461	4.58203e-1	1.38556e-1	0.00059
64	12.334	VV	0.0312	1.20330	6.05581e-1	0.00154
65	12.422	VV	0.0260	14.81981	8.85200	0.01897
66	12.532	VV	0.0328	6.86059e-1	3.16917e-1	0.00088
67	12.643	VV	0.0296	3.55482e-1	1.76095e-1	0.00045
68	12.885	VV	0.0301	17.84348	9.20763	0.02283
69	12.981	VV	0.0255	5.63890e-1	3.37177e-1	0.00072
70	13.059	VV	0.0356	3.34769	1.31980	0.00428
71	13.268	VV	0.0446	9.70270e-1	3.01019e-1	0.00124
72	13.348	VV	0.0350	1.51146	6.19389e-1	0.00193
73	13.454	VV	0.0462	6.75179e-1	1.82249e-1	0.00086
74	13.531	VV	0.0280	5.00550e-1	2.71258e-1	0.00064
75	13.566	VV	0.0319	3.90894e-1	1.76398e-1	0.00050
76	13.765	BV	0.0303	5.03625e-1	2.57933e-1	0.00064
77	13.875	VV	0.0265	21.60638	12.90515	0.02765
78	13.956	VV	0.0304	3.06245e-1	1.49583e-1	0.00039
79	14.005	VV	0.0368	1.12798	4.34423e-1	0.00144
80	14.156	VV	0.0429	2.23990e-1	6.79799e-2	0.00029
81	14.256	VV	0.0301	10.28760	5.32065	0.01317
82	14.338	VV	0.0350	5.83245e-1	2.38708e-1	0.00075
83	14.408	VV	0.0291	1.52108	8.01554e-1	0.00195
84	14.524	VV	0.0360	8.64411e-1	3.60298e-1	0.00111
85	14.626	VV	0.0394	7.18467e-1	2.50900e-1	0.00092
86	14.685	VV	0.0374	8.20536e-1	3.10287e-1	0.00105
87	14.816	VV	0.0474	5.93353e-1	1.77953e-1	0.00076
88	14.899	VV	0.0461	4.04227e-1	1.13291e-1	0.00052

Data File D:\CHEM32\1\DATA\20131028\SIG1000034.D
Sample Name: Calibration I

Peak #	RetTime [min]	Type	Width [min]	Area [pA*s]	Height [pA]	Area %
89	15.026	VV	0.0269	2.86036e-1	1.59635e-1	0.00037
90	15.081	VV	0.0384	6.39062e-1	2.53353e-1	0.00082
91	15.208	VB	0.0251	21.80178	13.65786	0.02790
92	15.524	BV	0.0308	8.12197	4.15244	0.01039
93	15.681	VV	0.0272	7.35158e-1	4.35607e-1	0.00094
94	15.761	VV	0.0239	2.33304e-1	1.47711e-1	0.00030
95	15.801	VV	0.0303	2.70182e-1	1.24576e-1	0.00035
96	15.857	VV	0.0336	4.55951e-1	2.00284e-1	0.00058
97	15.919	VV	0.0452	6.29694e-1	2.21420e-1	0.00081
98	16.049	VV	0.0404	2.97377e-1	9.14460e-2	0.00038
99	16.174	VV	0.0374	3.91413e-1	1.47825e-1	0.00050
100	16.235	VV	0.0257	2.45839e-1	1.49018e-1	0.00031
101	16.303	VV	0.0542	5.15999e-1	1.22244e-1	0.00066
102	16.447	VB	0.0262	17.00546	10.31324	0.02176
103	16.550	BB	0.0342	1.76278e-1	7.43538e-2	0.00023
104	16.713	BB	0.0304	4.78853	2.44432	0.00613
105	16.873	BB	0.0259	4.04382e-1	2.43263e-1	0.00052
106	17.098	BB	0.0382	5.13965e-1	2.05632e-1	0.00066
107	17.440	BV	0.0379	6.33184e-1	2.24593e-1	0.00081
108	17.541	VV	0.0397	2.11185e-1	7.43196e-2	0.00027
109	17.616	VB	0.0269	18.53623	10.87913	0.02372
110	17.728	BV	0.0364	2.30793e-1	9.01588e-2	0.00030
111	17.838	VV	0.0323	3.71191	1.85514	0.00475
112	17.891	VB	0.0270	1.89107e-1	1.00433e-1	0.00024
113	18.007	BB	0.0262	2.08328e-1	1.23119e-1	0.00027
114	18.210	BV	0.0426	2.14482e-1	6.56718e-2	0.00027
115	18.469	VB	0.0249	1.68557e-1	1.01590e-1	0.00022
116	18.609	BB	0.0266	4.31104e-1	2.50122e-1	0.00055
117	18.726	BB	0.0269	5.70905	3.27192	0.00731
118	18.908	BB	0.0320	2.77978	1.37908	0.00356
119	19.090	BB	0.0297	3.70205e-1	1.86041e-1	0.00047
120	19.189	BB	0.0324	2.48903e-1	1.21359e-1	0.00032
121	19.715	BV	0.0249	3.40852e-1	2.16012e-1	0.00044
122	19.782	VV	0.0276	3.03324	1.71524	0.00388
123	19.929	VB	0.0384	3.16470	1.21463	0.00405
124	20.162	BB	0.0356	3.21892e-1	1.22655e-1	0.00041
125	20.452	BB	0.0737	1.02623	1.72971e-1	0.00131
126	20.794	BB	0.0323	2.00126	9.41923e-1	0.00256
127	20.906	BB	0.0323	2.12514	1.01910	0.00272
128	21.650	BV	0.0865	1.62621	2.25831e-1	0.00208
129	21.842	VV	0.0393	1.71278	6.60269e-1	0.00219
130	21.931	VB	0.0829	10.77306	1.75942	0.01379
131	22.351	BB	0.0488	3.04749e-1	8.50079e-2	0.00039
132	22.628	BB	0.0409	3.18411e-1	9.80565e-2	0.00041
133	23.102	BV	0.0368	5.21540e-1	1.97708e-1	0.00067
134	23.173	VB	0.0526	2.92574	8.72390e-1	0.00374
135	23.453	BB	0.0680	8.34068e-1	1.52091e-1	0.00107
136	23.778	BB	0.0532	1.99461	4.92909e-1	0.00255
137	24.416	BB	0.0675	10.26913	2.08395	0.01314
138	24.730	BB	0.0716	5.68448	1.05911	0.00727

Data File D:\CHEM32\1\DATA\20131028\SIG1000034.D
Sample Name: Calibration I

Peak #	RetTime [min]	Type	Width [min]	Area [pA*s]	Height [pA]	Area %
139	25.561	BB	0.0593	4.97440e-1	1.03114e-1	0.00064
140	26.770	BB	0.0768	3.23979	5.66157e-1	0.00415
141	27.146	BB	0.0537	3.79591e-1	8.64539e-2	0.00049
142	27.781	BB	0.0870	2.50229	3.58167e-1	0.00320
143	29.031	BB	0.1054	13.21542	1.56706	0.01691
144	29.556	BB	0.1373	4.29706	3.73248e-1	0.00550
145	33.005	BB	0.1069	1.36018	1.51343e-1	0.00174
146	38.605	BB	0.2101	16.69014	9.63244e-1	0.02136
Totals :				7.81427e4	1.06178e4	

*** End of Report ***

Appendix I

Deactivation of Methanol Catalyst

Deactivation Rate

Figure I.1a, I.1b, I.2a, I.2b and I.3 below shows the CO conversion as a function of time on stream (TOS). Each plot shows CO conversion at the chosen standard conditions; 50 bar pressure, Weighted Average Bed Temperature (WABT) = 255 °C and a contact time of 300 $^{ms \cdot g_{cat}}/_{ml}$. The standard conditions were applied after changes in the conditions to measure the effect of those conditions on the deactivation. Linear regression were performed to assess the deactivation where appropriate.

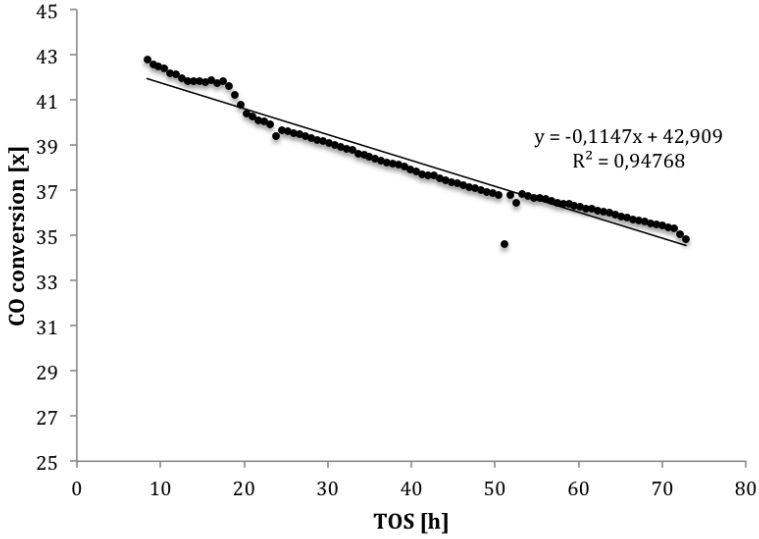

(a) *1. measurement*

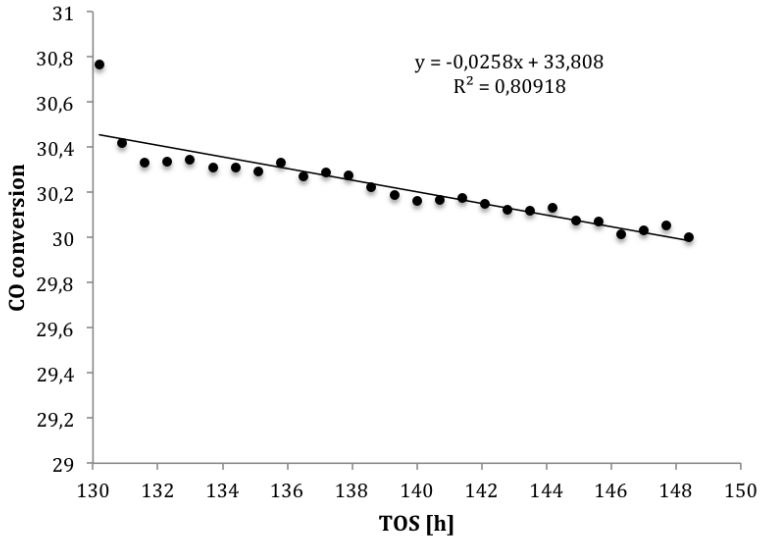

(b) *2. measurement*

Figure I.1: *CO conversion as a function of time on stream (TOS) for methanol synthesis in a fixed bed reactor with diluted commercial catalyst at 50 bar, WABT = 255 °C and contact time 300* $^{ms \cdot g_{cat}}/_{ml}$

As seen from figure I.1a, the activity of the catalyst is decreasing nearly linearly. This behavior is assumed to be caused by deactivation of the catalyst. The deactivation mechanism is assumed to be sintering. The measured CO conversion shown in figure I.1a is for the first time the standard conditions were applied. The time omitted is the time needed to establish the standard conditions when the experiment was started.

As seen from figure I.1b, the activity of the catalyst is decreasing nearly linearly also this time. The measured CO conversion shown in figure I.1b is for the second time the standard conditions were applied. In between the first and second time the standard conditions were applied, the WABT was measured to be 240 °C and then 220 °C. When comparing figure I.1a and I.1b, the slope of the line is somewhat lower, indicating that the deactivation was proceeding faster the first time the standard conditions were applied compared to the second time.

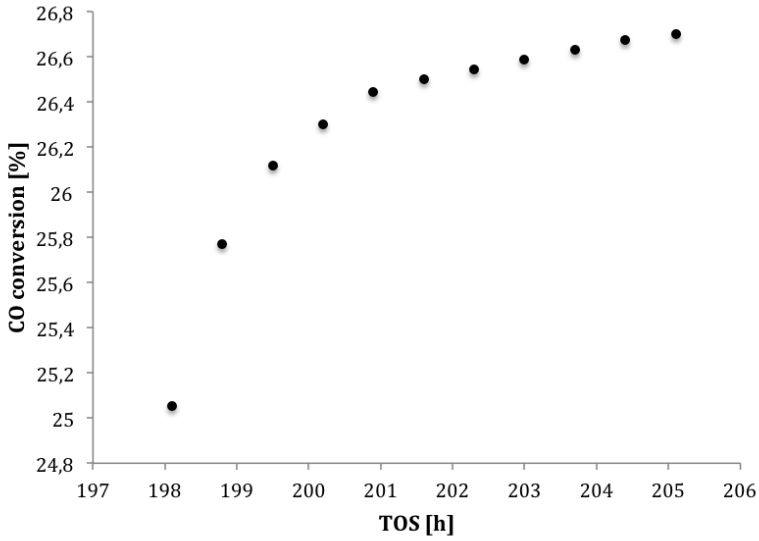

(a) *3. measurement*

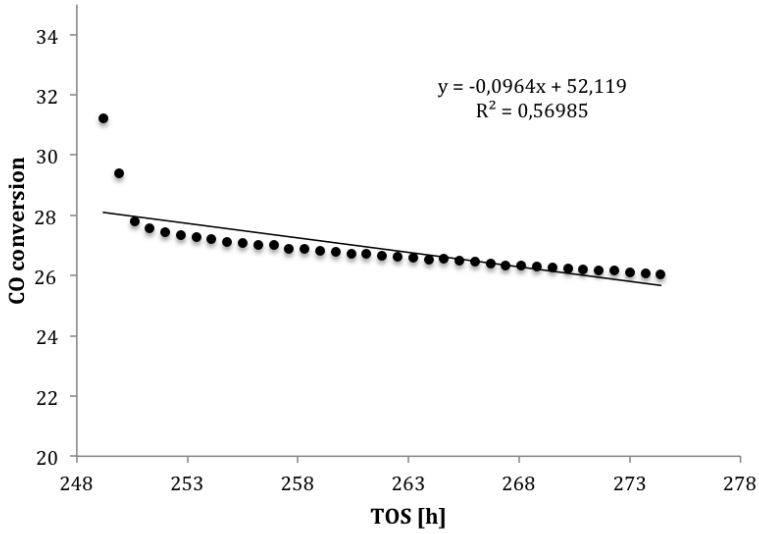

(b) *4. measurement*

Figure I.2: *CO conversion as a function of time on stream (TOS) for methanol synthesis in a fixed bed reactor with diluted commercial catalyst at 50 bar, WABT = 255 °C and contact time 300* $^{ms \cdot g_{cat}}/_{ml}$

As seen from figure I.2a, the activity of the catalyst is increasing in the beginning before it seems to level out. The measured CO conversion shown in figure I.2a is for the third time the standard conditions were applied. In between the second and third time the standard conditions were applied, the WABT was measured to be 240 °C and then 230 °C. From the shape of the curve in figure I.2a, it seems likely that the standard conditions were not completely established before the conditions were again changed. It is therefore not possibly to say anything about the deactivation during this time.

As seen from figure I.2b, the activity of the catalyst is decreasing nearly linearly also this time. The measured CO conversion shown in figure I.2b is for the fourth time the standard conditions were applied. In between the third and fourth time the standard conditions were applied, the WABT was measured to be 265 °C and then 275 °C. The slope of the line for this plot is somewhat lower than for the first plot, and somewhat higher than for the second plot. This indicates that the deactivation is decreasing with time, and also that the deactivation is increasing when the catalyst is subjected to higher temperature. This supports the claim that the deactivation mechanism is sintering.

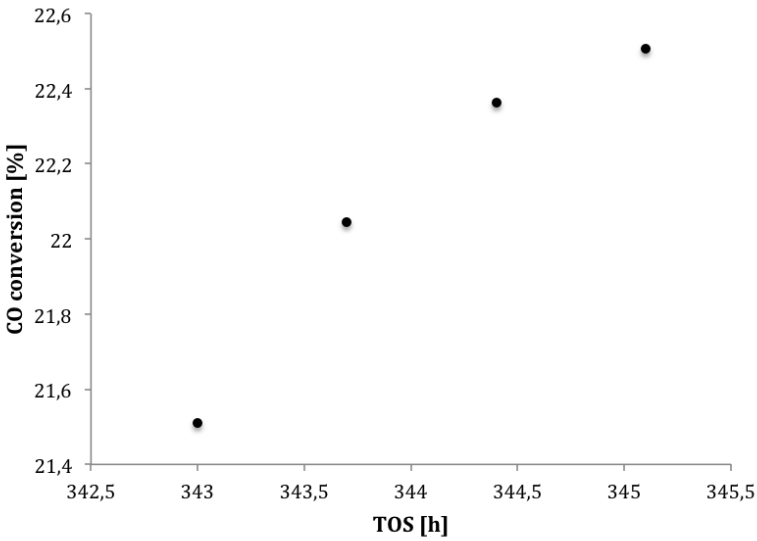

Figure I.3: *CO conversion as a function of time on stream (TOS) for methanol synthesis in a fixed bed reactor with diluted commercial catalyst at 50 bar, WABT = 255 °C and contact time 300* $^{ms \cdot g_{cat}}/_{ml}$*, 5. measurement.*

As seen from figure I.3, the activity of the catalyst is increasing in the beginning before it seems to level out. The measured CO conversion shown in figure I.3 is for the last time the standard conditions were applied. Between the last measurement at standard conditions and this measurement, the temperature and the contact

time were changed multiple times. From the shape of the curve in figure I.2a, it seems likely that the standard conditions were not completely established before the conditions were again changed. It is therefore not possibly to say anything about the deactivation during this time.

Adjusting Activity for Deactivation

In order to plot initial activity as a function of temperature, the initial activity should be adjusted to account for the fact that the catalyst is deactivating continuously. This is not a straightforward calculation, as the deactivation rate is not constant throughout the experiment. As seen from the plots in section I, the temperature may affect the deactivation rate. Additionally, it is not always clear if the observed effect on the activity is due to deactivation or due to the establishment of steady state conditions in the reactor.

To account for deactivation, when measuring the CO conversion at low contact time, the plot in figure 4.15 was used. To account for deactivation when measuring the CO conversion at high contact time, the plot in figure 4.18 was used.

The measured CO conversion is fitted to an equation as : $x_{CO} = a \cdot t + b$. The measured CO conversion, $x_{CO,m}$, at time $t = t_m$, was then calculated back to time 0 as shown below:

$$\frac{\Delta x_{CO}}{\Delta t} = a \tag{I.1}$$

Where a is the slope of the line given in figure 4.15 or 4.18. Expanding the equation above gives:

$$\frac{x_{CO,a} - x_{CO,m}}{t_a - t_m} = a \tag{I.2}$$

Where $x_{CO,a}$ is the adjusted CO conversion at time 0 (t_a). The adjusted CO conversion is then calculated as:

$$x_{CO,a} = x_{CO,m} - a \cdot t_m \tag{I.3}$$

Appendix J

Reaction Rate Calculation

For fixed bed reactors at low conversion, the reaction rate may be calculated as follows:

$$r_A = \frac{F_0 \cdot (C_{A,in} - C_{A,out})}{m_{cat}} \tag{J.1}$$

Where r_A is the rate of consumption of A, m_{cat} is the catalyst mass, F_0 is the flow to the reactor and $C_{A,in}$ is the concentration of A in F_0. As the activity is calculated based on GC data, the rate of CO consumption is:

$$r_{CO} = \frac{N_{in}}{m_{cat}} \cdot \frac{k_{CO}}{k_{N2}} \cdot \left(\frac{A_{CO,in}}{A_{N2,in}} - \frac{A_{CO,out}}{A_{N2,out}} \right) \tag{J.2}$$

Where N_{in} is the total molar feed [mol/s], and k_i is a constant from the GC calibration which relates the measured area under a peak to the concentration of the component.

To account for deactivation when calculating the reaction rate, the measured ratio of the area under the CO peak to the area under the N_2 peak was plotted as a function of time on stream (TOS), as shown in figure J.1.

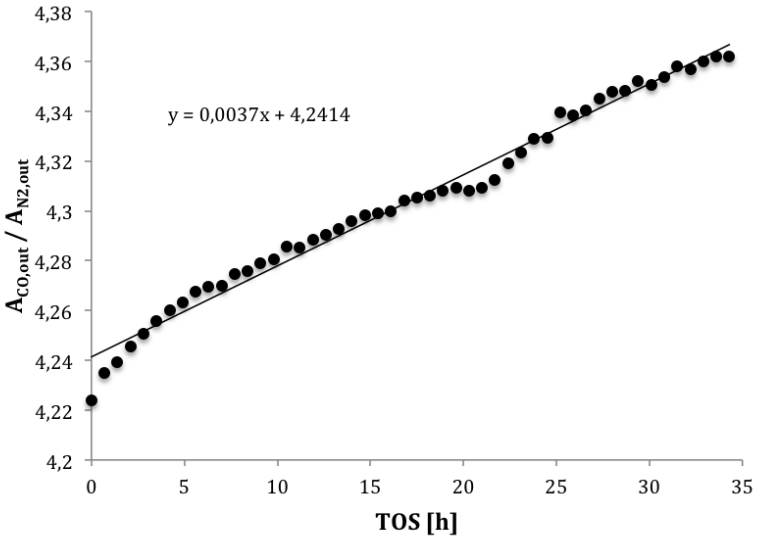

Figure J.1: *Raw data for methanol synthesis at differential conditions. The ratio of the area under the CO peak to the area under the N_2 peak as a function of time. Linear regression was performed using Excel.*

The concentration of CO in the outlet was then adjusted by using the regression line in figure J.1, as shown below:

$$\frac{y_a - y_m}{t_a - t_m} = a \tag{J.3}$$

Where y_a is the adjusted ratio of ${}^{A_{CO,out}}/_{A_{N2,out}}$ at time 0 (t_a), and y_m is the measured ratio of ${}^{A_{CO,out}}/_{A_{N2,out}}$ at time t_m. Rearranging:

$$y_a = y_m - a \cdot t_m \tag{J.4}$$